Synthesis, Morphology, and Dynamics of Microgels with Different Architectures

Von der Fakultät für Mathematik, Informatik und Naturwissenschaften der RWTH Aachen University zur Erlangung des akademischen Grades einer Doktorin der Naturwissenschaften

vorgelegt von

M.Sc. Andreea Cristina Bălăceanu

aus Piteşti, Argeş, România

Berichter: Universitätsprofessor Prof. Dr. Andrij Pich

Universitätsprofessor korr. Mitgl. der rumänischen Akademie der Wissenschaften Prof. Dr. Dan Demco

Universitätsprofessor Prof. Dr. Wolfgang Stahl

Tag der mündlichen Prüfung: 19.12.2013

‘The Answer to the Great Question... Of Life, the Universe and Everything... Is... Forty-two’, said Deep Thought, with infinite majesty and calm.

Douglas Adams, *The Hitchhiker's Guide to the Galaxy*

To my mother…

Content

1 Introduction

Microgels are a subclass of polymer colloids that gained a lot of attention in the scientific community in the last years due to a wide range of possible applications. Based on their special characteristics, they can be defined as crosslinked polymeric particles with a hairy morphology, which respond to environmental stimuli by adjusting their size, density and related properties [1(1)]. Microgels are spherical particles with dimensions in the range of hundreds of nm to µm; they are composed of polymer chains chemically or physically crosslinked into a network; they form stable dispersions in different solvents; their most important property is the capacity to respond to external stimuli, such as temperature, pH, electromagnetic radiation, etc., with a change in dimension. Due to the properties described, microgels have a wide range of possible applications, for example: as superabsorbant materials; in biomedicine as control-release carriers; in industry as valves; in organic chemistry as microreactors, etc.[1(2)]

The studies presented in this work characterise different novel microgel systems concentrating on the structure, morphology, dynamics, and phase transition behaviour. I am using experimental and theoretical methods for determining the properties of microgels that were synthesised with various morphological architectures. The introductory chapter of the thesis presents a definition of microgels and an overlook over the content of each subsequent chapter.

The second chapter gives a literature overlook of the synthesis of thermosensitive microgels, and presents the synthesised samples and the measurement conditions of the experimental methods employed for their characterisation. The synthesis procedure is described for the microgels with different morphology, and the recipe for the preparation is

presented. References that provide a clear and comprehensive description of the basic principles of the analytical methods are suggested for each experimental technique used.

The third chapter aims to explain the Flory-Rehner swelling theory for microgels, and to present the modifications, extrapolations and generalisations that I introduced in this theory in order to better characterise different microgel morphologies.

In chapters four and five I am presenting results of different studies. Chapter four is composed of three studies that combine Flory swelling theory generalised for different microgel morphologies with NMR transverse relaxation results to characterise a logical sequence of morphologically different microgel systems (starting from homopolymer microgels, to copolymer and core-shell structures). The results of each of these studies were published in peer reviewed journals.

The last results chapter is a more heterogeneous mixture of four studies. I am presenting the synthesis of copolymer (results that were also published), and of core-shell microgels, for each encompassing a general characterisation of the particles. The third study concentrates on the interactions between polymer chains and solvent, leading to a phase transition of the microgel particles in water/alcohol mixtures. The last study takes a closer look into the observation of the temperature phase transition of microgels by NMR, and presents the possible theoretical reasons governing the disappearance of the spectrum lines corresponding to functional groups of the microgel in a ^{1}H NMR spectrum with increase of temperature.

The general conclusions at the end of this work emphasise the novelties in each study presented, therefore presenting the value of the investigations undertaken and the results obtained.

Most of the studies I present in this thesis are peer reviewed and published as first author papers in high ranking journals. All measurements, theoretical work, results, their analysis and description that I use in this thesis were done and written by me or by students under my supervision. My publications are cited at the end of the thesis, and are referenced throughout the thesis using the corresponding letters (from *a* to *g*) ascribed to them in the list of publications.

References

1(1) Pich, A.Z.;Adler, H-J. P. *Polym Int*, **2007**, *56*, 291-307.

1(2) Nayak, S.; Lyon, L.A. *Angew. Chem. Int.*, **2005**, *44*, 7686-7708.

2 Samples and experimental conditions

My research work consists of characterising microgel particles with different morphologies. For this purpose I have synthesised homopolymer, statistical copolymer, and core-shell microgels using the precipitation polymerization technique. The microgels created for my investigations are thermoresponsive, being based on poly (*N*-vinylcaprolactam) (PVCL), which is a biocompatible polymer[2(1)-2(3)]with a lower critical solution temperature (the temperature at which the polymer experiences the coil to globule transition, abbreviated LCST) in the physiological range, around 32°C[2(4)].

The synthesis technique is based on radical polymerization, and it is the method of choice for creating thermoresponsive microgels, giving the opportunity to control the size, size distribution, density, morphology, and desired functionalization of the particles formed[2(5),2(6)]. The fundamental requirement is that the synthesis is performed at temperatures above the LCST of the constituent polymers, in order for the particles to form in collapsed state. The water soluble monomers form insoluble collapsed polymers which are intra and intermolecularly crosslinked to form microgel particles. A comprehensive didactic description of the precipitation polymerisation technique used for microgel synthesis is presented by Pich and Richtering[2(7)].

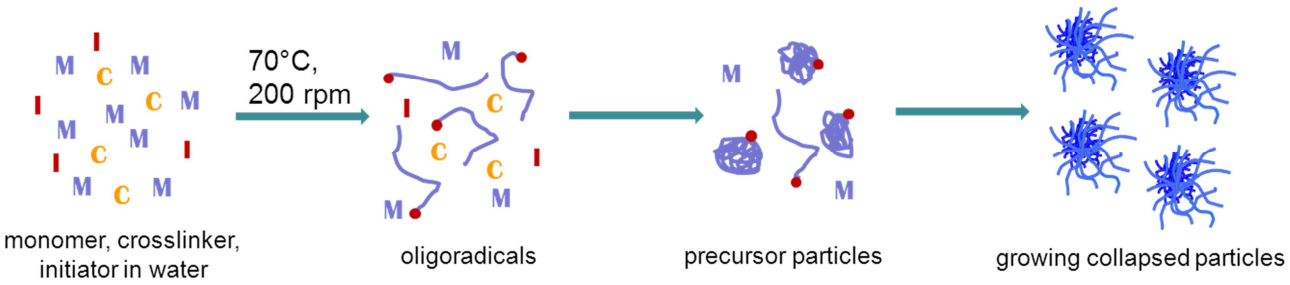

Figure 2.1 The precipitation polymerization mechanism

Most of the procedures and the descriptions in this chapter were presented by Balaceanu *et al.*[c,d,e,f,g]

The resulting microgel particles have the property of changing the size, density and related morphological and surface properties as response to a change in temperature. The critical temperature for the coil to globule transition of the constituent polymers, the LCST, is reflected into the volume phase transition temperature (VPTT) for the microgel particles.

The synthesis of homopolymer thermosensitive microgels without the use of surfactant was presented in the pioneer work of Pelton's group[2(8)]. They showed that the microgel size decreases with increasing the stirring rate during the reaction. The group also showed that the size of the particles decreases drastically if sodium dodecyl sulfate (SDS) surfactant is used in the reaction mixture[2(9)].

For copolymer microgels, the use of surfactant is not necessary to obtain small particles, because the reactive co-monomers can improve colloidal stability and help regulate the size of the particles. Moreover, co-monomers can be used to incorporate desired functional groups in the microgels. Richtering's group synthesized microgels combining *N*-isoproplyacrylamide (NIPAAm) and *N*,*N*-diethylacrylamide (DEAAm), or *N*-isopropylmethaacrylamide (NIPMAAm) and DEAAm[2(10),2(11)]. Boyko *et al.*[2(12)] synthesized copolymer microgels based on poly(*N*-vinylcaprolactam-*co*-*N*-vinylpyrrolidone). Pich's group synthesized copolymer microgels by combining *N*-vinylcaprolactam (VCL) and acetoacetoxyethyl methacrylate (AAEM) in the presence of methoxy-caped PEGMA macromonomers.[2(13)]

Microgels with a core-shell morphology can be synthesized by using monomers of different reactivity[b], or by a two-step polymerization technique, where the core is used as seeds for the growth of the shell[2(14), 2(15)].

In order to determine the characteristics and proprieties of the microgels synthesised with different morphologies, they were analysed using a variety of analytical techniques. The dimension of the particles can be determined using dynamic light scattering (DLS), which

estimates the hydrodynamic radius through the translational diffusion coefficient[2(16),2(17)]. The CONTIN[2(18)] analysis relays on an inverse Laplace transform of the autocorrelation function, and provides the size distribution of the particles. Microscopy methods (such as atomic force microscopy AFM[2(19)] and transmission electron microscopy TEM[2(20)]) can help in the size estimation and visualisation of the quality and uniform distribution of the sample. TEM can be used to reveal guest particles inside the microgels, and to distinguish core-shell structures depending on the materials used. AFM provides a three dimensional surface profile, and gives information about the morphology and surface proprieties of the particles. The phase shift signal measured in intermittent-contact AFM (phase imaging) was shown[2(21)] to be sensitive to the viscoelastic proprieties, adhesion and contact surface of the material.

By estimating the hydrodynamic radius at different temperatures DLS can also be used to determine the temperature volume phase transition of thermoresponsive microgels. Nuclear magnetic resonance (NMR) spectroscopy[2(22),2(23)] and differential scanning calorimetry (DSC)[2(24)]are two other methods that show the temperature transition behaviour in thermoresponsive microges[2(25)]. NMR shows the temperature transition of microgels through a shrinking of the spectrum lines as the temperature increases[f, 2(25) and references therein]. The explanation is thought to be related to a broadening of the spectrum lines caused by restraining the motions of the polymer subchains with increasing temperature. DSC shows an energetic response of the microgel sample at the transition temperature, associated with the breaking of hydrogen bonds between water and the polymer chains. Recently, the swelling and deswelling of microgels could also be visualised by measuring AFM with a wet-cell. These techniques function on very different theoretical principles, and a good understanding of the differences could lead to the explanation of different aspects of the phase transition.

^{1}H and ^{13}C liquid-state NMR spectroscopy were also used to determine the ratio of monomers in copolymer microgel samples. Solid-state MAS NMR[2(26)]spectroscopy and transverse relaxation techniques[2(27),2(28)]were employed to analyse the morphology and structure of microgel particles. By analysing the high resolution distribution of transverse relaxation times of the microgel particle, I have succeeded in developing a method perfectly suited for microgel structure analysis[c,f].

The references mentioned for the different analytical techniques were found to provide a clear and comprehensive description of the classical theoretical principles that they are based on.

2.1 Preparation of microgel samples

2.1.1 PVCL, PNIPAAm and PNIPMAAm homopolymer microgels

The monomers *N*-vinylcaprolactam (VCL), *N*-isopropylacrylamide (NIPAAm) and *N*-isopropylmethaacrylamide (NIPMAAm) were purchased from Aldrich and purified by distillation under vacuum. The cationic surfactant *N*-cetyl-*N*,*N*,*N*-trimethylammoniumbromide (CTAB), the initiator 2,2'-azobis(2-methylpropion amidine) dihydrochloride (AMPA), the crosslinker *N*,*N'*-methylenebisacrylamide (BIS) (Aldrich) were used as received. Deionized water was used as the polymerization medium.

The series of PVCL microgels with increasing amount of crosslinker were prepared as described by Balaceanu *et al.*[c] (see Table 2.1): the VCL monomer; appropriate amounts of CTAB and BIS were dissolved in 145 g of deionized water and then placed into a double-wall glass reactor equipped with a mechanical stirrer. After 1 hour of the incubation at 70°C and nitrogen purging, the initiator AMPA dissolved in 5 g water was added under continuous stirring to initiate the reaction. The reactions were carried out for 8 hours. Stable microgel

dispersions were obtained and were purified by membrane dialysis (using the Millipore Labscale TFF System). The PVCL microgels with three different amounts of crosslinker will be referred to in the text as PVCL 0.04 BIS, PVCL 0.1 BIS, and PVCL 0.15 BIS.

PVCL 0.06, PNIPAAm 0.06 and PNIPMAAm 0.06 microgel samples (see Table 2.1) were prepared as described by Balaceanu *et al.* to serve as reference samples in the studies conducted on copolymer and core-shell system of the same polymers[e,f,g]. Their synthesis method is similar, with the difference that for the PNIPMAAm microgel the reaction is carried out at 80 °C, because the LCST of the polymer (45 °C) is higher than for the other two.

Table 2.1 Homopolymer microgel synthesis recipe

Sample	Monomer [g]	CTAB [g]	BIS [g]	AMPA [g]	H_2O [g]	T [°C]
PVCL 0.04	2.215	0.022	0.04	0.05	150	70
PVCL 0.1	2.215	0.022	0.1	0.05	150	70
PVCL 0.15	2.215	0.022	0.15	0.05	150	70
PVCL 0.06	2.215	0.022	0.06	0.05	150	70
PNIPAAm 0.06	2.02	0.02	0.06	0.05	150	70
PNIPMAAm 0.06	2.02	0.02	0.06	0.05	150	80

2.1.2 PVCL-PNIPAAm, PVCL-PNIPMAAm copolymer microgels

The monomers *N*-vinylcaprolactam (VCL), *N*-isopropylacrylamide (NIPAAm) and *N*-isopropylmethaacrylamide (NIPMAAm) (Aldrich) were purified by high vacuum distillation under nitrogen, at 80°C. The initiator 2.2'-azobis(2-methylpropionamidine) dihydrochloride (AMPA) and the crosslinker *N.N*'-methylenebisacrylamide (MBA) were obtained from Aldrich and used as received. Deionized water was employed as the polymerization medium.

Appropriate amounts of VCL, NIPAAm and NIPMAAm (see Tables 2.2 and 2.3) and 0.06 g BIS (3 mol%) crosslinker were added to 145 mL deionized water. A double-wall glass

reactor equipped with stirrer and reflux condenser was purged with nitrogen. The solution of the monomers was placed into the reactor and stirred for 1 h at 70°C with purging with nitrogen. After that the 5 mL water solution of initiator (5 g/L) was added under continuous stirring. The reaction was carried out for 8 hours. Samples were purified for 72 hours by dialysis (Millipore Labscale TFF System).

Two series of microgel samples were synthesized by varying the molar ratios between VCL and NIPAAm, and VCL and NIPMAAm, respectively (Tables 2.2 and 2.3) as described by Balaceanu *et al.*[f]. Although no surfactant was used for the synthesis of copolymer microgels, controlled size and stability of the particles in dispersion was achieved. The samples will be referred to in the text as PVCL-PNIPAAm (or PNIPMAAm) and the monomers' theoretical molar ratios, for example PVCL-PNIPAAm 1:1.

Table 2.2 PVCL-PNIPAAm copolymer microgel synthesis recipe[f]

Sample	VCL [g]	NIPAAm [g]	VCL/NIPAAm [mol:mol]^{theor}
1	1.905	0.309	5:1
2	1.742	0.472	3:1
3	1.57	0.65	2:1
4	1.220	0.993	1:1
5	0.84	1.37	1:2
6	0.644	1.571	1:3
7	0.437	1.770	1:5

Table 2.3 PVCL-PNIPMAAm copolymer microgel synthesis recipe[f]

Sample	VCL [g]	NIPMAAm [g]	VCL/NIPMAAm [mol:mol]^{theor}
1	1.872	0.342	5:1
2	1.697	0.519	3:1
3	1.52	0.69	2:1
4	1.16	1.06	1:1
5	0.78	1.43	1:2
6	0.592	1.623	1:3
7	0.397	1.820	1:5

2.1.3 PVCL/PNIPAAm and PVCL/PNIPMAAm core-shell microgels

The monomers *N*-vinylcaprolactam (VCL), *N*-isopropylmethacrylamide (NIPMAAm) and *N*-isopropylacrylamide (NIPMAAm) were purified by distillation under high vacuum (between $2x10^{-2}$ and $9x10^{-2}$ mbar) at 80 °C. The cationic surfactant *N*-cetyl-*N*,*N*,*N*-trimethylammoniumbromide (CTAB), the initiator 2,2'-azobis(2-methylpropionamidine) dihydrochloride (AMPA), and the crosslinker *N*,*N'*-methylenebisacrylamide (BIS) (Aldrich), were used as received.

The core-shell crosslinked microgels were prepared using a two steps synthesis method[2(14)]. First, the core, following the recipe described in previous studies for homopolymer microgels prepared by precipitation polymerization[c], was synthesised. The appropriate amounts of monomer, CTAB, BIS and deionized water (Table 2.4) were placed in a double-wall glass reactor equipped with mechanical stirrer. After one hour of the incubation at 80 °C and nitrogen purging, the initiator AMPA dissolved in 5 g water was added under continuous stirring to start the polymerization reaction. This reaction was carried out for 8 hours. During the second step the appropriate amount of the second monomer and the crosslinker BIS were added to the seed dispersion of the core, followed by nitrogen purging. Finally, AMPA solution in water was added to start the polymerization of the shell (Table 2.4). The reaction was continued for another 8 hours. Colloidally stable microgel dispersions were obtained and were purified by dialysis (Millipore Labscale TFF System). The synthesised core-shell microgels will be referred to in the text as PVCL-core/ PNIPMAAm-shell and PNIPMAAm-core/ PVCL-shell. The synthesis of these microgel samples was presented by Balaceanu *et al.*[g].

Table 2.4 PVCL/PNIPMAAm and PNIPMAAm/PVCL core-shell microgels synthesis recipe[g]

Sample		Monomer [g]	CTAB [g]	BIS [g]	AMPA [g]	H_2O [g]
PVCL-core/	Core	2.215	0.022	0.06	0.05	150
PNIPMAAm-shell	Shell	2.023	-	0.06	0.05	-
PNIPMAAm-core/	Core	2.023	0.022	0.06	0.05	150
PVCL-shell	Shell	2.215	-	0.06	0.05	-

Furthermore, four series of PVCL-core/ PNIPAAm-shell, PVCL-core/PNIPMAAm-shell, PNIPAAm-shell/ PVCL-core and PNIPMAAm-shell/ PVCL-core microgels were synthesised, where the thickness of the shell was varied. The synthesis method is similar to the one described above, a double step synthesis. For these series, I have divided the initial amount of core sample in two and for the shell I have added an equivalent amount of water, apart from the second monomer and the appropriate crosslinker amount (See Tables 2.5 – 2.8). These samples will be referred to in the text as for example PVCL-core/ PNIPAAm-shell, and the respective theoretical monomer molar ratios.

Table 2.5 Synthesis recipe of core-shell PVCL/PNIPAAm microgel systems

Synthesis of the core (double amount used for two core-shell microgel sythesis)					
VCL [g]	CTAB [g]	BIS [g]	AMPA [g]	H_2O [g]	
2.725	0.021	0.06	0.05	150	
Synthesis of core-shell microgel					
Core:Shell [mol:mol]	NIPAAm [g]	BIS [g]	AMPA [g]	H_2O [g]	Core microgel [mL]
1:0.5	0.554	0.03	0.025	37.5	68
1:1	1.108	0.03	0.025	75	68
1:2	2.215	0.03	0.025	150	68
1:3	3.323	0.03	0.025	225	68

Table 2.6 Synthesis recipe of core-shell PNIPAAm/PVCL microgel systems

Synthesis of the core (double amount used for two core-shell microgel sythesis)					
NIPAAm [g]	CTAB [g]	BIS [g]	AMPA [g]	H_2O [g]	
2.215	0.021	0.06	0.05	150	
Synthesis of core-shell microgel					
Core:Shell [mol:mol]	VCL [g]	BIS [g]	AMPA [g]	H_2O [g]	Core microgel [mL]
1:0.5	0.681	0.03	0.025	37.5	68
1:1	1.362	0.03	0.025	75	68
1:2	2.725	0.03	0.025	150	68
1:3	4.087	0.03	0.025	225	68

Table 2.7 Synthesis recipe of core-shell PVCL/PNIPMAAm microgel systems

Synthesis of the core (double amount used for two core-shell microgel sythesis)					
VCL [g]	CTAB [g]	BIS [g]	AMPA [g]	H_2O [g]	
2.725	0.021	0.06	0.05	150	
Synthesis of core-shell microgel					
Core:Shell [mol:mol]	NIPMAAm [g]	BIS [g]	AMPA [g]	H_2O [g]	Core microgel [mL]
1:0.5	0.622	0.03	0.025	37.5	68
1:1	1.245	0.03	0.025	75	68
1:2	2.489	0.03	0.025	150	68
1:3	3.734	0.03	0.025	225	68

Table 2.8 Synthesis recipe of core-shell PNIPMAAm/PVCL microgel systems

Synthesis of the core (double amount used for two core-shell microgel sythesis)						
NIPMAAm [g]	CTAB [g]	BIS [g]	AMPA [g]	H_2O [g]		
2.489	0.021	0.06	0.05	150		
Synthesis of core-shell microgel						
Core:Shell [mol:mol]	VCL [g]	BIS [g]	AMPA [g]	H_2O [g]	Core microgel [mL]	T [°C]
1:0.5	0.681	0.03	0.025	37.5	68	70
1:1	1.362	0.03	0.025	75	68	70
1:2	2.725	0.03	0.025	150	68	70
1:3	4.087	0.03	0.025	225	68	70
1:2 (80°C)	2.725	0.03	0.025	150	68	80
1:2 (2·MBA)	2.725	0.06	0.025	150	68	70
1:2 (2·MBA, 80 °C)	2.725	0.06	0.025	150	68	80
1:2 (slow)	1.3625/ 1.3625	0.015/ 0.015	0.025	120/ 30	68	70
1:2 (direct)	2.725	0.03	0.025	150	70	70
1:2 (direct, 80 °C)	2.725	0.03	0.025	150	70	70
1:0.5 (direct, no H_2O)	0.681	0.03	0.025	0	68	70
1:1 (direct, no H_2O)	1.362	0.03	0.025	0	68	70
1:2 (direct, no H_2O)	2.725	0.03	0.025	0	68	70
1:3 (direct, no H_2O)	4.087	0.03	0.025	0	68	70

The synthesis of PNIPMAAm-core/ PVCL-shell microgel was initially planned very similar to the PNIPAAm-core/ PVCL-shell synthesis described in Table 2.6, just replacing the NIPAAm monomer with NIPMAAm. Because of unsatisfying results a series of optimizing experiments was undertaken for the 1:2 core:shell molar ratio:

1. The same starting materials were used, but the temperature of the experiment was increased from 70 to 80 °C because of the higher LCST of PNIPMAAm;

2. Double amount of crosslinker BIS was used for the second step of the synthesis, and the temperature varied between 70 and 80 °C.
3. Slow addition of monomer was also attempted. For this, half of the entire core microgel was mixed with half of the foreseen VCL and BIS amounts. The mixture was stirred for 30 min under nitrogen purging. At the same time 1 mL increments of the remaining 30 mL solution of VCL/BIS and AMPA was added to the reaction under nitrogen purging;
4. The second step of the reaction was carried out immediately after the first. Variation at 70 and 80 °C.
5. The same amounts were used, but the second step of synthesis was continued directly after the first and no additional water was added.

The best results were obtained using the method described at point 5, where the synthesis of the shell in carried on directly after the core, and no supplementary water is added to the mixture.

2.2 Experimental measurement conditions

2.2.1 Dynamic Light Scattering (DLS)

The size of the microgel particles was measured using an ALV/LSE-5004 Light Scattering Multiple Tau Digital Correlator with the scattering angle set at 90°. The samples were drastically diluted with doubly distilled water (or water/alcohol mixture for the cononsolvency studies in Chapter 5.3) to avoid multiple scattering errors. 0.2 µm filters were used for the solvent and 5 µm filters were used for the microgel dispersion to avoid dust, aggregation and impurities. Test measurements were performed for each sample at different angles to validate the accuracy of the method.

For temperature dependent measurements, samples were measured between 10 and 58 °C, keeping the temperature fluctuations below 0.1°C. Three runs of 120 s where performed at each temperature in order to calculate the standard deviation.

2.2.2 Differential Scanning Calorimetry (DSC)

DSC measurements were carried out with a DSC Netzsch F1 Pheonix® differential calorimeter. Aluminium pans were used as sample holders, and no holes were made, keeping the holders sealed, so no evaporation of the solvent can occur. The sample environment was rinsed with a nitrogen flow during measurement. Deuterated solvents (water or water/methanol mixtures) were used for the microgel solution and as the reference. Approximately 40 mg of 10 wt.% microgel solution in deuterated solvent was used per measurement. The measurements were carried out over a temperature range from 15 to 60 °C with a constant heating rate of 2 K/min. For all samples at least two heating runs and one cooling run were performed; all transitions were fully reversible and appeared in each heating-cooling cycle.

2.2.3 Nuclear magnetic resonance spectroscopy and relaxometry

Proton and ^{13}C high-resolution Liquid – State NMR spectra were measured using an AV600 Bruker® NMR spectrometer. The microgel ^{1}H NMR spectra under magic-angle sample spinning (MAS) conditions were measured on a widebore AV700 Bruker® NMR spectrometer operating at 700 MHz with a cross-polarization magic-angle sample spinning (MAS) probe head. The rotor frequency and the sample temperature were ν_R=7 kHz or 5 kHz, and 22 ^{0}C, respectively. The temperature was maintained within ± 0.5 K, following a standard

calibration. For all measurements the recycle delay was 5 s, the radio-frequency pulse length was 3.2 µs, and a dwell time of 10 µs was used.

The high-resolution MAS transverse relaxation (T_2) NMR measurements[2(29)]were made at 700.2378 MHz proton frequency of the Bruker AV700® NMR spectrometer. The same rotor frequency, recycle delay, dwell time, and temperature as for ^{1}H spectra were employed. The decay of transverse magnetization relaxation was measured using the Hahn-echo pulse sequence: 90^0_x – t - 180^0_x – t – Hahn echo - (acquisition), where *t* is the echo time[2(29)]. Half of the Hahn echo decay was detected and Fourier transformed. The normalized integral intensity of various resonances was fitted by two-exponential decay functions using the Origin® 6.0 program. The errors of the fits were smaller than 10%.

For all measurements either 2 wt.% or 5 wt.% microgel in deuterated solvent was used. The spectra were calibrated to the water peak. The processing of the spectra was performed using TopSpin®. All spectra were phase corrected and a manual baseline was employed.

2.2.4 Microscopy techniques

A) Atomic Force Microscopy (AFM)

AFM images were recorded with a Dimension Atomic Force Microscope icon ScanAsyst. Nanoscope 8.10 (Build R1.60476) software. OTESPA cantilevers with resonance frequencies of 284–338 kHz and spring constants of ~12–103 N/m in tapping mode were used. The microgels were uniformly deposited by spin coating on a silicon wafer, and dried at room temperature for 24h prior to measurement.

B) Transmission Electron Microscopy (TEM)

The samples were analysed with transmission electron microscopy on a Zeiss Libra 120 device. The accelerating voltage was adjusted to 120 kV. The pressure within the TEM

column was around $5x10^{-7}$ bar in the sample stage and the beam stage, and in the camera stage was around 10^{-4} bar. Microgels were diluted with distilled water and dried on the carbon-coated copper grids at room temperature for 24h prior to measurement.

References

2(1) Lau, A. C. W. ; Wu, C. *Macromolecules*, **1999**, *32* (3), 581.

2(2) Naha, P. ; Casey, A.; Tenuta, T.; Lynch, I.; Dawson, K.,A. *Aquatic Toxicology*, **2009**, *92*, 146-154.

2(3) Dimitrov, I.; Trzebicka, B.; Müller, A. H. E.; Dworak, A.; Tsvetanov, C. B. *Prog. Polym. Sci.*, **2007,** *32*, 1275.

2(4) Boyko, V.; Richter, S.; Burchard, W.; Arndt, K.F. *Langmuir*, **2007**, *23*, 776.

2(5) Park, T.G.; Hoffman, A.S. *J. Polym. Sci.* **1992**, 30, 505.

2(6) Pelton, R. *Adv. Colloid Interface Sci.* **2000**, 85, 1.

2(7) Pich, A.; Richtering, W. *Advances in Polymer Science*, **2011**, *234*, 1-37.

2(8) Pelton, R.H.; Chibante, *P. Colloids, Surf.* **1986**, *20*, 247.

2(9) McPhee, W.; Tam, K.C.; Pelton, R. *J. Colloid Interface Sci.* **1993**, *156*, 24.

2(10) Keerl, M.; Smirnovas, V.; Winter, R.; Richtering, W. *Macromolecules*, **2008**, *41*, 6830.

2(11) Keerl, M.; Richtering, W. *Colloid Polym. Sci.* **2007**, *285*, 471.

2(12) Boyko, V.; Richter, S.; Burchard, W.; Arndt, K.F. *Lagmuir*, **2007**, *23*, 776.

2(13) Pich, A.; Berger, S.; Ornatsky, O.; Baranov, V.; Winnik, M.A. *Colloid Polym. Sci.* **2009**, *287*, 269.

2(14) Berndt, I.; Richtering, W. *Macromolecules*, **2003**, *36*, 8780.

2(15) Berndt, I.; Popescu, C.; Wortmann, F.J.; Richtering, W. *Angew. Chem. Int. Edit. Engl.* **2006**, *45*, 1081.

2(16) Koppel, D.E. *J. Chem. Phys*. **1972**,*57*(11), 4814.

2(17) Frisken, B.J. *Appl. Opt.* **2001**, *40* (24), 4087–91.

2(18) Provencher, S. *Comp. Phys. Commun.* **1982**, *27* (3), 229.

2(19) Eaton, P.; West, P. *Atomic Force Microscopy*, Oxford University Press, New York, 2010.

2(20) Williams, D.B.; Carter, C.B. *Transmission electron microscopy*, Springer US, 2009.

2(21) Tamayo, J.; García, R. *Langmuir*, **1996**, *12*, 4430.

2(22) Blümich, B. *Essential NMR*, Springer, Berlin, 2005.

2(23) Levitt, M.H. *Spin Dynamics*, John Wiley and Sons Ltd., West Sussex, 2008.

2(24) Höhne, G. *Differential scanning calorimetry : an introduction for practitioners*, Springer, Berlin, 1996.

2(25) Spěváček, J. *Curr. Opin.Colloid & Interf. Sci*., **2009**, *14*, 184-191.

2(26) Duer, M.J. *Introduction to Solid-State NMR Spectroscopy*, Blackwell Publishing Ltd, Oxford, 2004.

2(27) Abragam, A. *The Principles of Nuclear Magnetism*, Oxford University Press, Oxford, 1983.

2(28) Callaghan, P.T. *Principles of Nuclear Magnetic Resonance Microscopy*, Clarendon Press, Oxford, 1991.

2(29) Ernst, R.R.; Bodenhausen, G.; Wokaun, A. *Principles of Nuclear Magnetic Resonance in One and Two Dimensions*, Clarendon Press, Oxford, 1987.

3 Flory-Rehner temperature transition theory for microgels

Theoretical descriptions of different aspects of microgel characterisation such as structure, dynamics, synthesis kinetics, critical phenomena, have recently attracted attention[3(1)]. My work is concentrated on the most important property of these systems: their capacity to swell as response to external stimuli, in particular temperature change. The theory of gel swelling/deswelling was developed by Flory and Rehner in 1943[3(2)]. There are several reasons for considering this theory. First, the mathematical description and the physical concept are very straight forward, which makes it very friendly, and thus preferred in comparison to other more sophisticated approaches. In addition, most of the more recent gel swelling theories[3(3) and references therein] are based on the classical principles described by Flory and Rehner.

In the last three decades, the swelling theory of bulk gels is repeatedly used and described in many studies. The group of Tanaka[3(4)] studied continuous and discontinuous volume changes undergone by NIPAAm-based gels in response to temperature change. Hirotsu measured the static bulk modulus of PNIPAAm hydrogels as a function of temperature[3(5)]. In 1980 the same group showed[3(6)] that for poly(acrylamide)-based gels immersed in acetone–water mixtures, the ionization of the polymer network plays an important role in the discrete transition which occurs with increasing amount of acetone. The same authors also demonstrate that the degree of ionization increased with time (due to hydrolysis) and estimate the number of ionized groups per polymer chain. Shibayama *et al.* investigated the effect of the monomer concentration[3(7)], and concluded that it is necessary to introduce an effective crosslinker density parameter in the Flory-Rehner gel swelling theory.

More recent studies were undertaken for microgel systems. Fernandez-Nieves and co-workers have thoroughly studied the microgels' swelling behaviour induced by different stimuli (pH, charge distribution, temperature and amount of salt in the solvent) using the Flory-Rehner theoretical approach[3(8)-3(11)]. They have shown that the theory can explain certain behaviours at the limit conditions, but didn't specify parameter values. Lietor-Santos *et al.*[3(12)] have shown how an additional stimulus, the hydrostatic pressure, can induce the phase transition in thermo-responsive PNIPAAm based microgels. Extrapolating from temperature swelling curves, and using the classical Flory theory for polymer gels, they have obtained the pressure dependence of the Flory parameter. Bae *et al.* have used an extended Flory-Huggins model for polymer-solvent mixing combined with a modified Flory-Rehner theory for elastic contribution, and fitted the equations to the experimental data obtained for microgel particles and bulk gels[3(13)]. The same authors also generalised the model for homopolymer particles to the copolymer gel particle/solvent systems by modifying the Flory interaction parameter[3(14)]. Eichenbaum *et al.*[3(15)]investigated the swelling behaviour of particles based on poly(methacrylic acid-co-acrylic acid) with different degrees of crosslink, by changing the pH and salt concentration. Bromberg *et al.* studied the swelling-deswelling of polyether-modified poly(acrylic acid) microgels [3(16)], considering the enthalpy (ΔH) and entropy (ΔS) values estimated from differential scanning calorimetry experiments as initial parameters. More recently, Hertle *et al.*[3(17)] have worked on the Flory swelling theory for thermoresponsive gels developed by Shibayama, modifying the power expansion for the Flory parameter.

In this work I am extending the classical Flory-Rehner swelling/deswelling volume transition theory applied to homopolymer[c] and copolymer microgels[e] in order to account for the bimodal internal structural heterogeneities of the crosslink density observed in PVCL based microgels. Moreover, by using an extended Flory volume transition theory for core-

shell microgels, I analyse the correlated changes in the core-shell morphology[g] during the volume phase transition temperature.

3.1 Flory theory for homopolymer microgels with homogeneous distribution of crosslinking

The Flory-Rehner gel swelling theory[3(2)] is based upon the assumption that the free energy change on swelling has two contributions that are separable and additive. These are the free energy of mixing and the free energy of elastic deformation. There is some controversy regarding the existence of a third contribution. Neuburger and Eichinger[3(18)] described the necessity of using a mixing-elastic cross-term to explain the solvent dependence in studies performed on two non-ionized poly(dimethylsiloxane) networks swollen in benzene and cyclohexane. On the other hand, Mann *et al.* [3(19)] have performed computer simulations on the swelling of salt-free hydrogels, and have concluded that the violation of separability does not play a significant role in the description because of a lucky cancellation of two cross-terms that involve electrostatic interactions. An alternative to separability for the theoretical description of swelling was not yet found, thus I consider that for a neutral microgel, the osmotic pressure arises from two major contributions, the mixing of the polymer and the solvent, and the elasticity resulting from crosslinking the polymer to form the polymer network.

According to Flory's theory for the swelling of polymer gels, the equilibrium is achieved when the chemical potential of the solvent inside and outside the microgel become equal, or equivalently, when the net osmotic pressure is equal to zero, i.e.,

$$\Pi = \Pi_{mix} + \Pi_{elastic} = 0\,, \qquad (3.1)$$

where,

$$\Pi_{mix} = -\frac{N_A k_B T}{\nu_S}[\phi + \ln(1-\phi) + \chi\phi^2], \tag{3.2}$$

and

$$\Pi_{elastic} = \frac{N k_B T}{V_0}\left[\left(\frac{\phi}{2\phi_0}\right) - \left(\frac{\phi}{\phi_0}\right)^{1/3}\right]. \tag{3.3}$$

In the above equations N_A is the Avogadro number, k_B is the Boltzmann constant, $\nu_S = 1.81\times10^{-5}\ \mathrm{m}^3$ is the molar volume of water, which is the solvent, χ is the Flory parameter that accounts for the monomer-monomer and monomer-solvent interactions, and for the quality of the solvent, ϕ is the polymer volume fraction in the particle, N is the number of subchains in a microgel particle (defined as the polymer chain between two subsequent crosslink points) and $V_0 = 4\pi R_{H0}{}^3/3$ is the volume of the particle in deswollen state.

For a microgel that swells isotropically, it can be written[3(12)],

$$\frac{\phi}{\phi_0} = \left(\frac{R_{H0}}{R_H}\right)^3, \tag{3.4}$$

where R_H (R_{H0}) and ϕ (ϕ_0) are chosen as the particle size and volume fraction in the swollen (deswollen) state.

In order to account for the steep or discrete volume transition, the polymer-solvent interaction parameter, χ, is assumed to be concentration dependent and has the approximate form,[3(20)]

$$\chi \approx \chi_0 + \phi\chi_1, \tag{3.5}$$

with

$$\chi_0 = \frac{\Delta H - T\Delta S}{k_B T} = \frac{1}{2} - A\left(1 - \frac{\Theta}{T}\right), \tag{3.6}$$

where ΔS and ΔH are the corresponding entropic and enthalpic energy changes, $A=(2\Delta S + k_B)/2k_B$ is the second virial coefficient and $\Theta=2\Delta H/(2\Delta S + k_B)$ is the Θ-temperature of the

polymer-solvent system (for T=Θ, χ=0.5 and the second virial coefficient of the mixture becomes zero).

The temperature dependence of the microgel size is accounted for through the temperature dependence of χ. By introducing Eq. (3.4) and (3.5) into Eq. (3.1), an explicit equation of state relating the temperature and the hydrodynamic radius R_H is obtained,[3(12)]

$$T_{\Pi=0} = \frac{A\Theta\phi_0^2\left(\frac{R_{H0}}{R_H}\right)^6}{\frac{\nu_S N}{N_A V_0}\left[\frac{1}{2}\left(\frac{R_{H0}}{R_H}\right)^3 - \left(\frac{R_{H0}}{R_H}\right)\right] - \phi_0\left(\frac{R_{H0}}{R_H}\right)^3 - \ln\left(1-\phi_0\left(\frac{R_{H0}}{R_H}\right)^3\right) + \left(A-\frac{1}{2}\right)\phi_0{}^2\left(\frac{R_{H0}}{R_H}\right)^6 - \chi_1\phi_0^3\left(\frac{R_{H0}}{R_H}\right)^9} \quad .(3.7)$$

A similar deduction for the swelling-deswelling of homopolymer homogeneous microgels was presented by Lietor-Santos *et al.*[3(12)]. One major assumption employed in the derivation of the above equation of state is the uniform distribution of crosslink density throughout the microgel particle.

3.2 Flory theory for copolymer microgels with homogeneous distribution of crosslinking

The parameter which accounts for the monomer-monomer and solvent-monomer interactions in Eq. (3.7) is the Flory parameter, χ, which is responsible for the collapse of the microgel particle. This is why in order to account for the net interaction of a copolymer and solvent, the Flory interaction parameter was modified following the work of Oh and Bae[3(13)] by separating the interaction into χ_{AC} of *A*-type polymer segment and solvent *C* and χ_{BC} between *B*-type polymer segment and solvent *C*. The microgel system is considered in the following to consist of a statistical distribution of *A* and *B* monomers in the copolymer network. The interaction between *A* and *B* segments is neglected, considering that their

interaction with the solvent is predominant. Therefore, the copolymer interaction parameter has the following form[3(13)],

$$\chi_{copol} = w\chi_{AC} + (1-w)\chi_{BC}\,, \tag{3.8}$$

where

$$\chi_{XC} = \frac{1}{2} - A_{XC}\left(1-\frac{\Theta_{XC}}{T}\right) + \phi\chi_{1XC}\,, \tag{3.9}$$

with X=A or B, A_{XC} is the second virial coefficient and w is the mole fraction of the A polymer (which is 0.5 for both our systems). The Θ-temperatures of the polymer-solvent system are denoted by Θ_{XC}; for T=Θ_{XC}, χ_{XC}=0.5 and the second virial coefficient A_{XC} becomes zero. The temperature dependence of the microgel size is accounted for through the temperature dependence of χ. By introducing Eq. (3.8) into the state equation developed for a homopolymer microgel (Eq. (3.7)), an explicit equation of state relating the temperature and the hydrodynamic radius for the copolymer microgel in the homogeneous approximation is obtained, i.e[3(13)].

$$T_{\Pi=0} = \frac{\phi_0^2\left(\frac{R_{H0}}{R_H}\right)^6\left[wA_{AC}\Theta_{AC} + (1-w)A_{BC}\Theta_{BC}\right]}{\frac{v_S N}{N_A V_0}\left[\frac{1}{2}\left(\frac{R_{H0}}{R_H}\right)^3 - \left(\frac{R_{H0}}{R_H}\right)\right] - \phi_0\left(\frac{R_{H0}}{R_H}\right)^3 - \ln\left(1-\phi_0\left(\frac{R_{H0}}{R_H}\right)^3\right) + \left[wA_{AC} + (1-w)A_{BC} - \frac{1}{2}\right]\phi_0^2\left(\frac{R_{H0}}{R_H}\right)^6 - \left[w\chi_{AC} + (1-w)\chi_{BC}\right]\phi_0^3\left(\frac{R_{H0}}{R_H}\right)^9} \tag{3.10}$$

A similar equation was reported by Bae *et al*..[3(13),3(14)] For a microgel made of only one component polymer, i.e., $\chi_{AC} = \chi_{BC}$ and w=1, Eq. (3.10) becomes Eq. (3.7) for the homopolymer microgel.

3.3 Flory theory for homopolymer microgels with heterogeneous distribution of crosslinking

Previous studies[3(21)-3(28)] on microgel systems synthesised by precipitation polymerization processes have shown proof of heterogeneous internal structure due to the difference in crosslinking density from core to shell. Our ^{1}H high-resolution NMR transverse relaxation measurements made on different PVCL based microgel systems[b,c,e,f] reveal a heterogeneous crosslink density from core to corona that can be described in a good approximation by a bimodal model. Figure 3.1 depicts schematically a homopolymer microgel with heterogeneous crosslink morphology.

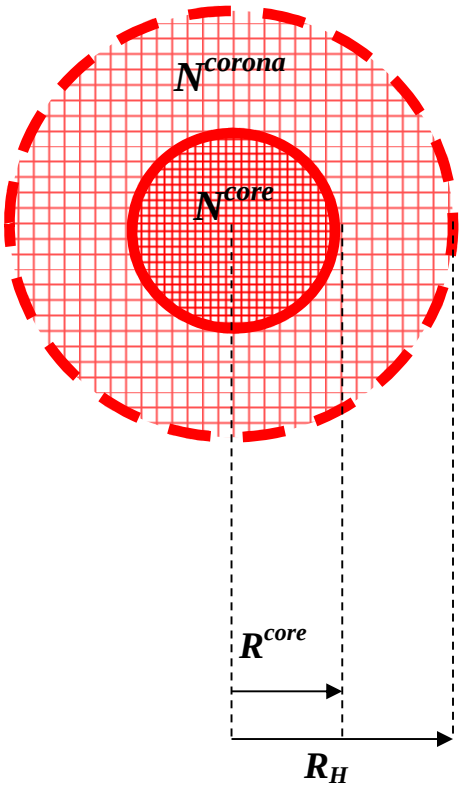

Figure 3.1 Representation of the bimodal heterogeneous morphology of homopolymer microgel particles. The crosslink density is different in the core and corona.[c]

In order to describe the behaviour of the bimodal heterogeneous microgel system in the Flory-Rehner formalism the mixing and elastic contributions for the core and the corona of the microgel are considered separate and additive,

$$\Pi_{mix} = \Pi_{mix}^{core} + \Pi_{mix}^{corona}, \tag{3.11}$$

and

$$\Pi_{elastic} = \Pi_{elastic}^{core} + \Pi_{elastic}^{corona}. \tag{3.12}$$

The heterogeneous morphology model discussed here is based on the following assumptions: (i) The core radius shrinks with the temperature proportionally with the measured hydrodynamic radius of the entire particle: $R^{core}(T) = \rho R_H(T)$, which means that in the deswollen state $R_0^{core} = \rho R_{H0}$. The scaling quantity ρ is assumed independent of temperature. That results in the equality of the ratios,

$$\frac{\phi^{core}}{\phi_0^{core}} = \frac{\phi^{corona}}{\phi_0^{corona}} = \left(\frac{R_{H0}}{R_H}\right)^3. \tag{3.13}$$

The validity of this assumption will be discussed below. On the other hand, for a PNIPAAm microgel it was shown using SANS that the corona size evolution with temperature is different from that of the core.[3(23)] This effect was not reported, though, by the results of Ref. 3(26). (ii) The temperature dependent part of the Flory-Huggins interaction parameter is not influenced by the change in crosslink density from core to corona, whereas the concentration dependent part is different for the core and corona, i.e.,

$$\chi^{core} = \frac{1}{2} - A\left(1 - \frac{\Theta}{T}\right) + \chi_1 \phi^{core}, \tag{3.14}$$

and

$$\chi^{corona} = \frac{1}{2} - A(1-\frac{\Theta}{T}) + \chi_1 \phi^{corona} . \qquad (3.15)$$

(iii) The number of subchains for the core and corona are N^{core} and N^{corona}, respectively, corresponding to the bimodal crosslinking density model. (iv) Any elastic force of interaction between core and corona is neglected. (v) Any defects of the polymer network such as the dangling chains and loops are not taken into account.

Considering the above assumptions the mixing and the elastic osmotic pressures can be written as,

$$\Pi_{mix} = -\frac{N_A k_B T}{\nu_S}\left\{ X + \ln\left(\left[1-\phi_0^{core}\left(\frac{R_{H0}}{R_H}\right)^3\right]\left[1-\phi_0^{corona}\left(\frac{R_{H0}}{R_H}\right)^3\right]\right) + Y\left[\frac{1}{2} - A(1-\frac{\Theta}{T})\right] + Z\chi_1 \right\}, \qquad (3.16)$$

and

$$\Pi_{elastic} = \frac{k_B T}{V_0}\left[\frac{1}{2}\left(\frac{R_{H0}}{R_H}\right)^3 - \frac{R_{H0}}{R_H}\right]\left[\frac{N^{core}}{\rho^3} + \frac{N^{corona}}{1-\rho^3}\right], \qquad (3.17)$$

where X,Y and Z are defined as,

$$X = \left(\frac{R_{H0}}{R_H}\right)^3 \left(\phi_0^{core} + \phi_0^{corona}\right),$$

$$Y = \left(\frac{R_{H0}}{R_H}\right)^6 \left[\left(\phi_0^{core}\right)^2 + \left(\phi_0^{corona}\right)^2\right], \qquad (3.18)$$

and

$$Z = \left(\frac{R_{H0}}{R_H}\right)^9 \left[\left(\phi_0^{core}\right)^3 + \left(\phi_0^{corona}\right)^3\right].$$

By matching these two terms (Eqs. (3.16) and (3.17)) in the equation of state the hydrodynamic radius temperature dependence ($R_H(T)$) is deduced, i.e.,

$$T_{\Pi=0}=\frac{YA\Theta}{\frac{v_S}{V_0N_A}\left[\frac{1}{2}\left(\frac{R_{H0}}{R_H}\right)^3-\left(\frac{R_{H0}}{R_H}\right)\right]\left[\frac{N^{core}}{\rho^3}+\frac{N^{corona}}{1-\rho^3}\right]-X-\ln\left(\left[1-\phi_0^{core}\left(\frac{R_{H0}}{R_H}\right)^3\right]\left[1-\phi_0^{corona}\left(\frac{R_{H0}}{R_H}\right)^3\right]\right)+Y\left(A-\frac{1}{2}\right)-Z\chi_1} \quad ,(3.19)$$

Finally, we can note that the equation of state for a homopolymer microgel with bimodal heterogeneity given by Eq. (3.19) in the limit of $N^{corona}\to 0$, $\phi_0^{corona}\to 0$ and $\rho\to 1$ agrees with the equation of state derived for the homogeneous morphology (Eq. (3.7)).

The formalism of Flory temperature transition for homopolymer heterogeneous microgels is described by Balaceanu *et al.*[c]

3.4 Flory theory for copolymer microgels with heterogeneous distribution of crosslinking

After describing the heterogeneous morphology for a homopolymer microgel system made of the temperature sensitive polymer PVCL, it is of interest now to see how the heterogeneity changes when copolymer systems of PVCL and PNIPAAm or PNIPMAAm, all of them being temperature sensitive, are investigated. Figure 3.2 shows a representation of a statistical copolymer microgel with a bimodal crosslink density.

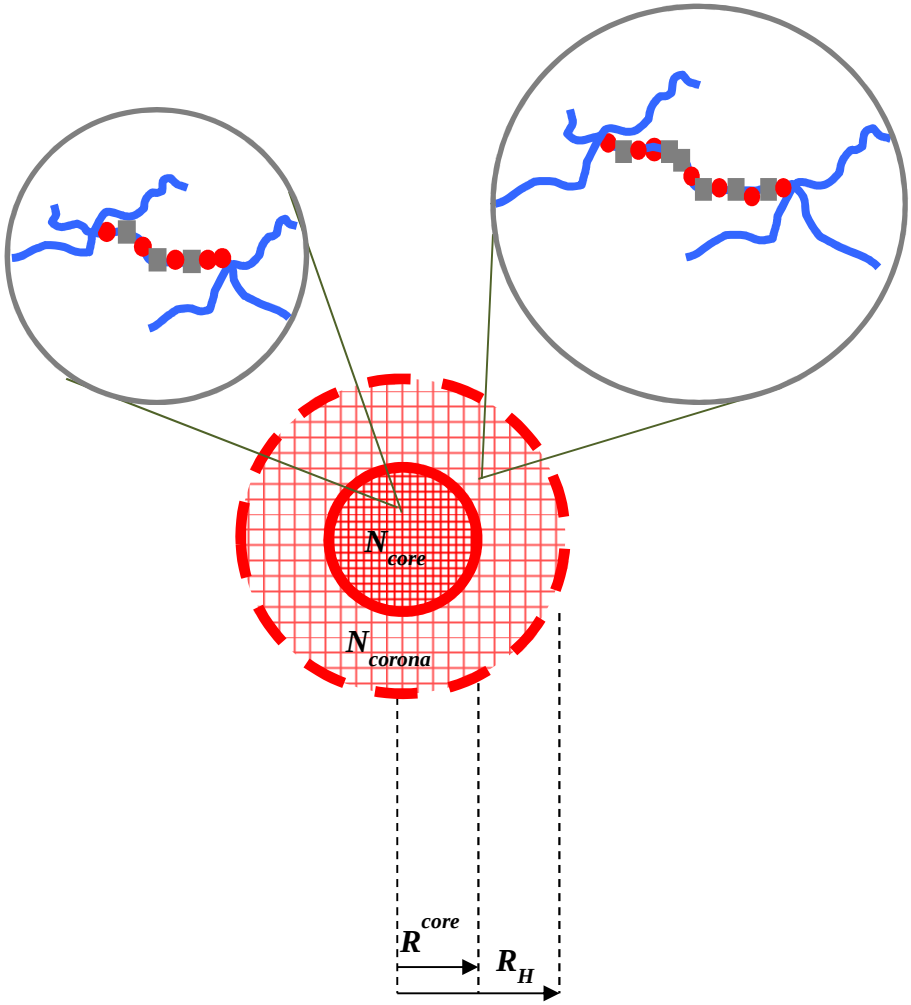

Figure 3.2 Representation of the bimodal heterogeneous morphology of copolymer microgel particles. The crosslink density is different in the core and corona.[e]

When combining the Eqs. (3.11) - (3.15) from the previous section with the equations for copolymer system from section 3.3 (Eqs. (3.8) and (3.9)) and introduce them into the state equation Eq. (3.10), we yield for a copolymer microgel with heterogeneous morphology,

(3.20)

$$T_{\Pi=0} = \frac{Y\left[wA_{AC}\Theta_{AC} + (1-w)A_{BC}\Theta_{BC}\right]}{\frac{\nu_S}{N_A V_0}\left[\frac{1}{2}\left(\frac{R_{H0}}{R_H}\right)^3 - \left(\frac{R_{H0}}{R_H}\right)\right]\left[\frac{N^{core}}{\rho^3} + \frac{N^{corona}}{1-\rho^3}\right] - X - \ln\left[\left(1-\phi_0^{core}\left(\frac{R_{H0}}{R_H}\right)^3\right)\left(1-\phi_0^{corona}\left(\frac{R_{H0}}{R_H}\right)^3\right)\right] + \left[wA_{AC} + (1-w)A_{BC} - \frac{1}{2}\right]Y - \left[w\chi_{AC} + (1-w)\chi_{BC}\right]Z}$$

where

$$X = \left(\frac{R_{H0}}{R_H} \right)^3 \left(\phi_0^{core} + \phi_0^{corona} \right),$$

$$Y = \left(\frac{R_{H0}}{R_H} \right)^6 \left[\left(\phi_0^{core} \right)^2 + \left(\phi_0^{corona} \right)^2 \right], \qquad (3.21)$$

and

$$Z = \left(\frac{R_{H0}}{R_H} \right)^9 \left[\left(\phi_0^{core} \right)^3 + \left(\phi_0^{corona} \right)^3 \right].$$

The equation of state for a copolymer microgel with bimodal heterogeneity given by Eq. (3.20) in the limit of $N^{corona} \to 0$, $\phi_0^{corona} \to 0$ and $\rho \to 1$ agrees with the equation of state derived for the homogeneous morphology (Eq. (3.10)).

The formalism of Flory temperature transition for copolymer heterogeneous microgels is described by Balaceanu *et al.*[e]

3.5 Flory theory for core-shell microgel systems considering a homogeneous distribution of crosslinking

Microgel systems having a bimodal morphology, such as core-shell microgels (with a core consisting of a polymer and the shell consisting of a different polymer) exhibit a complex swelling-deswelling behaviour, which comes from constraining interactions between core and shell due to different volume transition temperatures of the two components. I assume that the core and shell components are homogeneous in respect to crosslink density in order to simplify the state equations. Figure 3.3 depicts the morphology of a core-shell microgel particle, having different polymeric components in the core and shell.

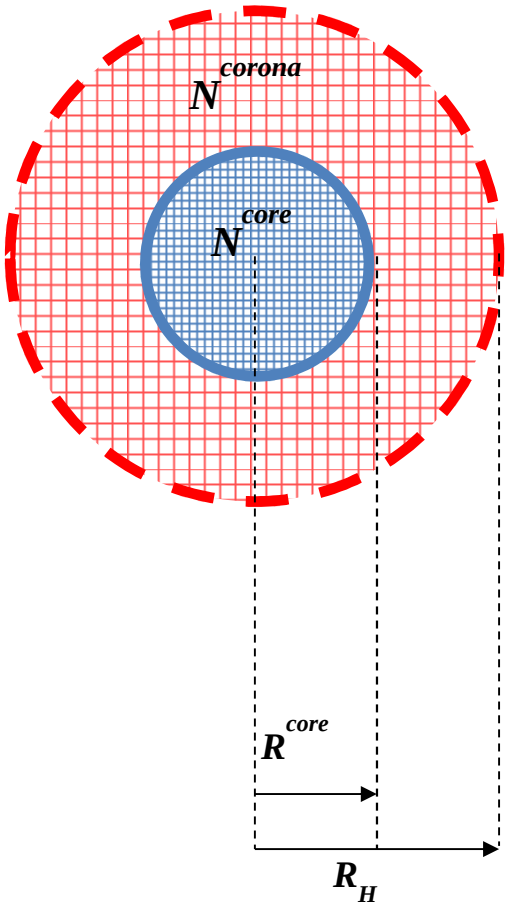

Figure 3.3 Representation of core-shell microgel particles. The crosslink density in core and shell components is assumed to be homogeneous.

In order to describe the behaviour of the bimodal morphology microgel system in the Flory-Rehner formalism, I consider that the contributions of the core and shell are volume weighted:

$$\Pi_{total} = \frac{V^{core}}{V^{total}}\Pi^{core} + \frac{V^{shell}}{V^{total}}\Pi^{shell}, \qquad (3.22)$$

where

$$\Pi^{core} = \Pi^{core}_{mix} + \Pi^{core}_{elastic}, \qquad (3.23)$$

and

$$\Pi^{shell} = \Pi^{shell}_{mix} + \Pi^{shell}_{elastic}. \qquad (3.24)$$

At thermodynamic equilibrium of the system $\Pi_{total} = 0$.

The radius of the core is expected not to have the same temperature dependence as the total particle radius, since the swelling/deswelling of the core and shell have different behaviours. In general it can be written: $R^{core}(T) = \rho(T) R_H(T)$ where, $R^{core}(T)$ is the radius of the core, $R_H(T)$ is the total hydrodynamic radius of the particle and $\rho(T)$ is the temperature dependent radial scale factor. An exact definition of the radius of the core and the hydrodynamic radius is not possible because of the fuzziness of the interface between core and shell and at the exterior of the particle, especially considering the dangling chains.

Nevertheless, in order to simplify the Flory transition state equation, I introduce a coarse-grained assumption that the radius of the core has a constant proportionality to the radius of the microgel particle on different temperature intervals along the volume temperature transition curve, i.e.,

$$R^{core}(T) = \rho_i R_H(T), \tag{3.25}$$

where $i \in [1, n]$ and n is the number of intervals dividing the temperature range. The Flory equation of state for core-shell microgel particles using the ratio between the radius of the core and shell can be written,

$$\Pi_{total} = \rho_i^3 \Pi^{core} + (1 - \rho_i^3) \Pi^{shell}, \tag{3.26}$$

and $\Pi_{total} = 0$.

In order to account for the shift in transition temperature of the components of the core-shell microgel compared to the homopolymer microgels of the same chemical components I assume that the core and shell are connected by an interpenetrating network layer. The temperature shift may be understood as being caused by an elastic force developed in the shell and acting on the core, which for the PVCL-core/ PNIPMAAm-shell system

decreases the shrinking force in the core, while for the PNIPMAAm-core/ PVCL-shell system increases the shrinking force in the core.

Using DSC measurements it was shown[3(29)] that the total elastic force interaction taking place at the interface between core and shell is temperature dependent,

$$F = kT \,. \tag{3.27}$$

where*k* is an interfacial parameter.

The elastic osmotic pressure of both the core and shell has to account for this elastic force, which influences the swelling/deswelling behaviour of the microgel. Because the total osmotic pressure is volume weighted, the effect of the force will still be present in the equation of state. The total osmotic pressures in core or shell have similar expressions, i.e.,

$$\Pi^{core/shell} = \Pi_{mix}^{core/shell} + \Pi_{elastic}^{core/shell} + \frac{k\ T}{S^{core}}, \tag{3.28}$$

where S^{core} is the surface of the core in contact with the shell. I shall note that at the interface the same force is acting on the core and shell but in opposite directions.

Taking into account that the ratio of the core is considered proportional to the radius of the particle on certain temperature intervals, the volume ratios can be written,

$$\frac{\phi^{core}}{\phi_0^{core}} = \left(\frac{\rho_0}{\rho_i}\right)^3 \left(\frac{R_{H0}}{R_H}\right)^3, \tag{3.29}$$

and,

$$\frac{\phi^{shell}}{\phi_0^{shell}} = \left(\frac{1-\rho_0{}^3}{1-\rho_i{}^3}\right)\left(\frac{R_{H0}}{R_H}\right)^3, \tag{3.30}$$

where ρ_0 is the ratio between the radius of the core and the hydrodynamic radius of the microgel particle in the deswollen state, in the last temperature interval; while ρ_i corresponds to each chosen temperature interval.

Considering the above assumptions the equation of state for a core-shell microgel system can be written as,

$$T = \frac{\left[A^{core}\Theta^{core}(\phi^{core})^2\rho_i^3 + A^{shell}\Theta^{shell}(\phi^{shell})^2(1-\rho_i^3)\right]}{-\left[M^{core}\rho_i^3 + M^{shell}(1-\rho_i^3)\right] + \frac{\nu_S}{N_A}\left[\frac{N^{core}}{V_0^{core}}E^{core}\rho_i^3 + \frac{N^{shell}}{V_0^{shell}}E^{shell}(1-\rho_i^3)\right] + \frac{\nu_S k}{N_A k_B S^{core}}}, \quad (3.31)$$

where

$$M^{core/shell} = \phi^{core/shell} + \ln(1-\phi^{core/shell}) + (\phi^{core/shell})^2\left(\frac{1}{2} - A^{core/shell}\right) + \chi_1^{core/shell}(\phi^{core/shell})^3 \quad (3.32)$$

and

$$E^{core/shell} = \frac{\phi^{core/shell}}{2\phi_0^{core/shell}} - \left(\frac{\phi^{core/shell}}{\phi_0^{core/shell}}\right)^{1/3}, \quad (3.33)$$

are mixing and elastic terms, which have the same form for core and shell and are used to simplify the expression of the equation of state. The connection between the temperature and the measured hydrodynamic radius is made through Eqs. (3.29) and (3.30).

Finally, I can note that the equation of state for core shell microgel, given by Eq. (3.31), in the limit of $\rho^{core} \to 1, N^{shell} \to 0$ and $k \to 0$, when the microgel consists only of the core region, agrees with the equation of state derived for the homopolymer microgel Eq. (3.7).

It must be noted that, due to the complexity of the equation of state for core-shell microgels, I have only considered the homogeneous approximation. However, it is most likely that the real microgel particle contains a distribution of crosslink density both in the core and in the shell of the microgel. The theoretical treatment would be too lengthy and would introduce significant errors in fitting the experimental data by considering too many free parameters.

The formalism of Flory temperature transition for core-shell microgels is described by Balaceanu *et al.*[g]

3.6 Conclusions

As a concluding section the strengths and the weaknesses of the Flory-Rehner swelling theory for microgels will be discussed[3(3)]. Firstly, the theory is applicable to a large variety of situations and phenomena; it is a simple, straight-forward description that does not require a great number of parameters, which gives it a clear advantage. Secondly, it gives the possibility of extension to different situations and stimuli. Although in my work I have only considered the effect of temperature in detail, the effect of other parameters (solvent composition, charge, pH, salt concentration, etc.) can be discussed with the help of this classical swelling theory. For example, this formalism was applied to predict the swelling behaviour depending on the salt concentration and pHs in some pioneer works.[3(30),3(31)]Thirdly, it successfully describes both continuous and discontinuous volume phase transitions.

On the other hand, this theory has some weaknesses and limitations[3(3)], mainly due to the assumptions used. As mentioned above, the theory assumes the principle of separability of the mixing, elastic deformation and if the case, ionic contributions. Secondly, an ideal chain conformation entropy is assumed, overestimating the elastic energy[3(32)]. The underlying model also does not consider the effects of defects, loops, dangling chains or their polydispersity. It should also be considered that the number of subchains that the theory provides is related to the number of elastically active chains, not to the entire network[3(33)]. Thirdly, the parameters characterizing χ (ΔH, ΔS, χ_1) are phenomenological, and theoretical considerations can only estimate roughly their values for particular cases. Finally, it should be

stressed that the theories were developed for macroscopical gels, and they are usually applied to microgel particles, without significant modifications related to their size or surface effects, although recent simulations and experiments demonstrate that the dimensions of the polymer network can have a significant influence on certain parameters.[3(34),3(35)]

References

3(1) Dusek, K. *Responsive gels: Volume transitions I,* Springer-Verlag, Berlin, 1993.

3(2) Flory, P.J.; Rehner, J. *J. Chem. Phys* .**1943**, *11*, 521.

3(3) Quesada-Perez, M.; Maroto-Centeno, J.A.; Forcadab, J.; Hidalgo-Alvarez, R. *Soft Matter*, **2011**, *7*, 10536.

3(4) Hirotsu, S.; Hirokawa, Y.; Tanaka, J. *Chem. Phys.*, **1987**, *87*, 1392–1395.

3(5) Hirotsu, S. *J. Chem. Phys.*, **1991**, *94*, 3949–3957.

3(6) Tanaka, T.; Fillmore, D.; Sun, S.T; Nishio, I.; Swislow, G.; Shah, A. *Phys. Rev. Lett.*, **1980**, *45*, 1636–1639.

3(7) Shibayama, M.; Shirotani, Y.; Hirose, H.; Nomura, S. *Macromolecules*, **1997**, *30*, 7307–7312.

3(8) Fernandez-Nieves, A.; Fernandez-Barbero, A.; Vincent, B.; de las Nieves, F.J. *Macromolecules*, **2000**, *33*, 2114–2118.

3(9) Fernandez-Nieves, A.; Fernandez-Barbero A.; de las Nieves, F.J. *J. Chem. Phys.*, **2001**, *115*, 7644–7649.

3(10) Fernandez-Nieves, A.; Fernandez-Barbero, A.; Vincent, B.; de las Nieves, F.J. *J. Chem. Phys.*, **2003**, *119*, 10383–10388.

3(11) Capriles-Gonzalez, D.; Sierra-Martin, B.; Fernandez-Nieves, A.; A. Fernandez-Barbero, A. *J. Phys. Chem. B*, **2008**, *112*, 12195–12200.

3(12) Lietor-Santos, J.J.; Sierra-Martin, V.; Vavrin, R.; Hu, Z.; Gasser U.; Fernandez-Nieves, A. *Macromolecules*, **2009**, *42*, 6225–6230.

3(13) Oh, K.S.; Bae, Y.C. *Euro.Polym. J.* **1999**, *35*, 1653.

3(14) Oh, K.S.; Bae, Y.C. *J. Appl. Polym.Sci.* **1998**, *69*, 109.

3(15) Eichenbaum, G.M.; Kiser, P.F.; Dobrynin, A.V.; Simon, S.A.; Needham, D. *Macromolecules*, **1999**, *32*, 4867–4878.

3(16) Bromberg, L.; Temchenko, M.; Moeser, G.D.; Hatton, T.A.*Langmuir*, **2004**, *20*, 5683–5692.

3(17) Hashmi, S.M.; Dufresne, E.R. *Soft Matter*, **2009**, *5*, 3682–3688.

3(18) Neuburger, N.A.; Eichinger, B.E. *Macromolecules*, **1988**, *21*, 3060–3070.

3(19) Mann, B.A.; Holm, C.; Kremer, K. *J. Chem. Phys.*, **2005**, *122*, 154903.

3(20) Moerkerke, R.; Koningsveld, R.; Berghmans, H.; Dusek, K.; Solc, K. *Macromolecules*, **1995**, *28*, 1103.

3(21) Wu, X.; Pelton, R.H.; Hamielec, A.E.; Woods D.R.; McPhee W. *Colloid Polym.Sci.* **1994**, *272*, 467.

3(22) Varga, I.; Gilanyi, T.; Meszaros, R.; Filipcsei, G.; Zrinyi, M. *J. Phys. Chem. B* **2001**, *105*, 9071.

3(23) Fernández-Barbero A.; Fernández-Nieves A.; Grillo I.; López-Cabarcos E. *Phys. Rev. E*, **2002**, *66*, 051803.

3(24) Saunders, B.R. *Langmuir* **2004**,*20*, 3925.

3(25) Mason, T.G.; Lin, M.Y. *Phys. Rev. E*, **2005**, *71*, 040801 (R).

3(26) Stieger, M.; Richtering, W.; Pedersen, J.S.; Linder, P. *J. Chem. Phys.***2004**, *120*, 6197.

3(27) Guillermo, A.; Cohen Addad, P.J.; Bazile, J.P.; Duracher, D.; Elaissari, A.; Pichot,C. *J. Polym. Sci.: Part B: Polym. Phys.* **1999**, *38*, 889.

3(28) Ru, G.; Wang, N.; Huang, S.; Feng, J. *Macromolecules*, **2009**, *42*, 2074.

3(29) Berndt, I.; Popescu, C.; Wortmann, F.Z.; Richtering, W. *Angew. Chem. Int. Ed.*, **2006**, *45*, 1081-1085.

3(30) Khokhlov, A.R. *Polymer*, **1980**, *21*, 376–380.

3(31) Brannon-Peppas, L.; Peppas, N.A. *Chem. Eng. Sci.*, **1991**, *15*, 715–722.

3(32) Rubinstein, M.; Colby, R.H. *Polymer Physics*, Oxford University Press, New York 2003.

3(33) Dusek K.; Duskova-Smrckova, M. *Prog.Polym. Sci.*, **2000**, *25*, 1215–1260.

3(34) Claudio, G.C.; Kremer K.; Holm, C. *J. Chem. Phys.*, **2009**, *131*, 094903.

3(35) Ikkai, F.; Shibayama, M. *Polymer*, **2007**, *48*, 2387–2394.

4 Morphology of microgel particles by NMR and Flory theory

The Flory Rehner swelling theory was extended for different microgel morphologies, including internal crosslinking heterogeneity of homopolymer microgels[c], copolymer microgels[e] and core-shell microgels[g]. All of the studies presented in this chapter are published in pier reviewed journals (see the list of publications at the end of the manuscript).

4.1 Homopolymer PVCL microgels with heterogeneous morphology

The formation of a heterogeneous internal structure, determined by a difference in crosslinking density from core to corona, of microgel particles formed by precipitation polymerization was reported in previous studies[4(1)-4(8)]. ^{1}H high-resolution NMR transverse relaxation measurements made on copolymer systems based on PVCL[b,e,f] and on the system under investigation (see below) reveal a heterogeneous crosslinking density from core to corona that can be described in a good approximation by a bimodal morphological model.

In this study[c] I am extending the classical Flory swelling temperature transition theory for homopolymer microgels in order to account for the bimodal internal structural heterogeneities of the crosslinking density observed in PVCL microgels. I also used ^{1}H transverse relaxation NMR results to select the best fitting parameters for the Flory state equation. This approach allows for the quantitative characterisation of the core-corona morphology of a series of PVCL microgels with different amounts of crosslinker. The series of PVCL microgels will be referred to in the text according to the amount of crosslinker (see Chapter 2, synthesis section 2.1.1) as: PVCL 0.04 BIS, PVCL 0.1 BIS, and PVCL 0.15 BIS.

The results and the descriptions in this chapter were presented by Balaceanu *et al.*[c,e,g]

4.1.1 Dynamic light scattering study on the effect of crosslinker amount

Dynamic light scattering measurements (Figure 4.1a) show that the radius of the microgel particles increases with the increase in crosslinker amount. This is an unexpected result, since studies performed on PNIPAAm microgels show that the size decreases with more crosslinker[4(9)]. The explanation for this behaviour could be that for PVCL microgels, with a higher crosslinker amount, more polymer chains participate in the particle formation, and thus the particles are larger.

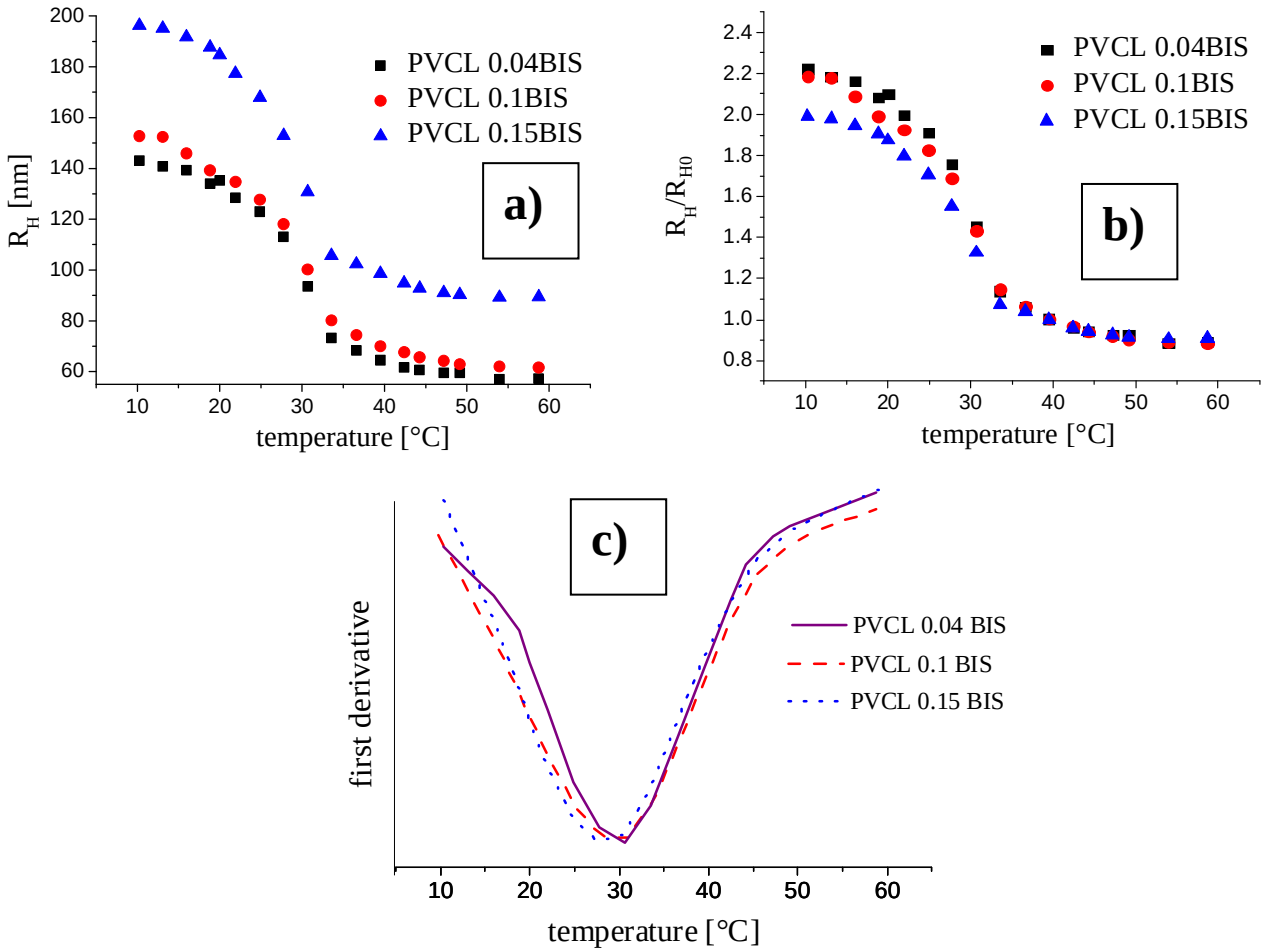

Figure 4.1 a) Hydrodynamic radius as a function of temperature; b) normalized hydrodynamic radius of the PVCL microgels (0.04 BIS, 0.1 BIS and 0.15 BIS) versus temperature. c) First-order derivatives of the volume size-temperature curves presented in subfigure a) showing the volume transition temperature.[c]

The swelling degree of PVCL microgel particles with different amounts of crosslinker was also analysed (Figure 4.1b). In order to compare the swelling behaviour of the three samples, the measured hydrodynamic radius (R_H) is normalized by the value in the deswollen state (R_{H0} at 40°C). The crosslinking density has an effect on the swelling behaviour of the particles, the relative swelling of the microgel particles decreases with the increase of crosslinker amount used in the synthesis, which means that the microgel particles become more compact, the network loses elasticity and permits less uptake of water. This result would be in accordance with previous studies performed on PNIPAAm microgels[4(9)]. Nevertheless, this decrease of the swelling of the microgel particles is not drastic, and for the first two microgel systems (PVCL 0.04 BIS and 0.1 BIS), although the crosslinker amount is double, the swelling remains almost constant. Figure 4.1c shows the first-order derivative of the temperature transition curves measured by DLS. As it can be seen, the volume phase transition temperature shows only a slight dependence on the amount of crosslinker of the PVCL microgels, in accordance with previous studies on PNIPAAm microgels[4(10)].

4.1.2 Structure and dynamic heterogeneity of microgels by ^{1}H transverse magnetization relaxation.

To confirm the bimodal heterogeneous structure of the homopolymer microgels of PVCL, I performed an NMR study using ^{1}H high-resolution spectroscopy and relaxometry. Proton high-resolution NMR spectrum of VCL monomer measured at 600 MHz is shown in Fig. 4.2a.

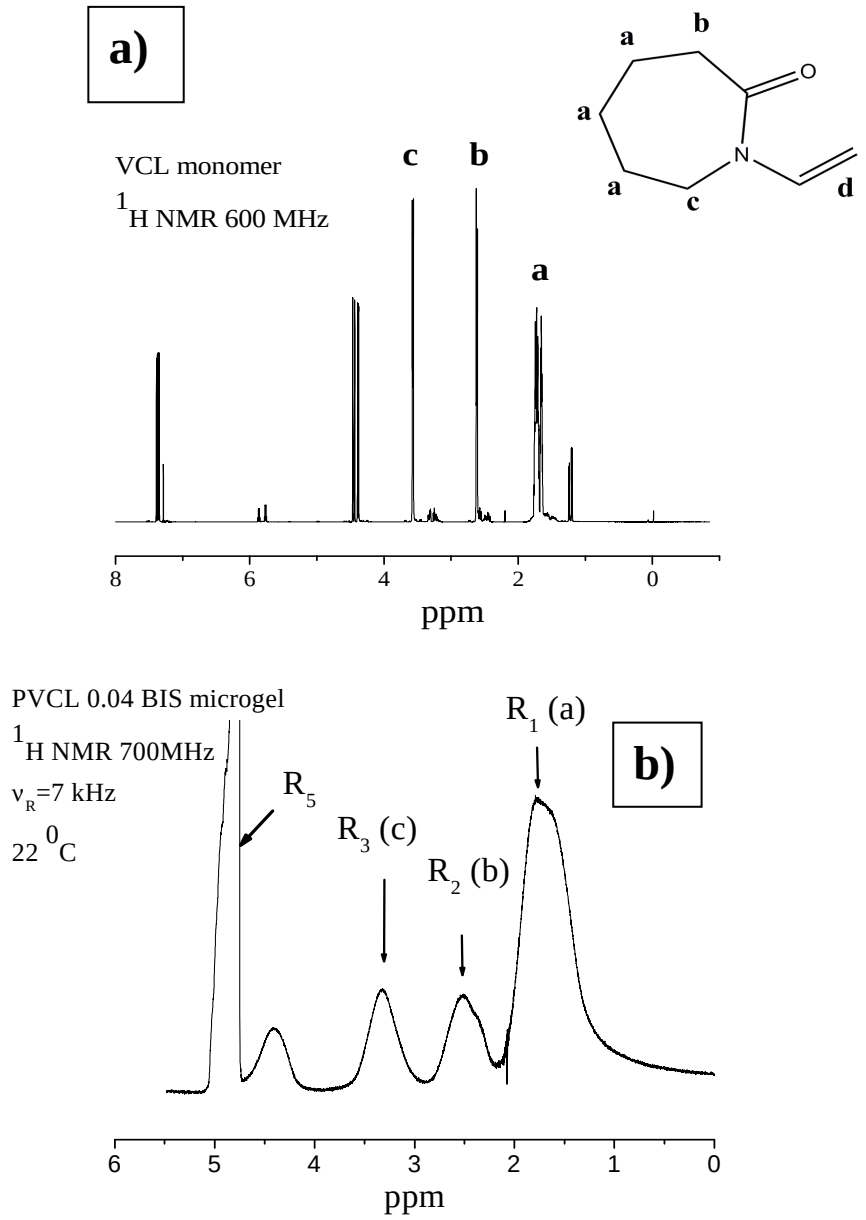

Figure 4.2 a) Proton high-resolution spectrum of VCL monomer in D_2O measured at 600 MHz. b) Proton high-resolution spectrum of PVCL 0.04 BIS microgel (2% wt. in D_2O) at 22 ^{0}C. The spectrum was measured at 700 MHz NMR spectrometer under MAS conditions (ν_R= 7 kHz).[c]

The assignment of these peaks (see Scheme in Fig. 4.2a) was made by comparison with simulated NMR spectra obtained using the ChemDraw® and Gaussian03® programs. Proton high-resolution spectrum of PVCL 0.04 BIS microgel measured in D_2O at 22 ^{0}C with an AV700 Bruker NMR spectrometer under MAS condition (rotor frequency of 7 kHz) is shown in Fig. 4.2b. In the resulting NMR spectrum the resonances with the following chemical shifts were identified: R_1= 1.8 ppm; R_2= 2.5 ppm; R_3= 3.3 ppm; R_5= 4.8 ppm. The

R_5 resonance corresponds to HDO, while the others are assigned to different proton groups in the microgel (Fig. 4.2a). In the limit of experimental errors the amount of crosslinking will not modify the resonances assignment. Resonance R_1 of methylene protons was used in the following measurements to investigate the heterogeneity of the PVCL microgels (see below).

The heterogeneity in the microgel particles morphology would be reflected in the ^1H transverse magnetization relaxation due to different degree of local molecular motions correlated to the distribution in crosslinking density inside the particle.[b,c,e] Using transverse magnetization (T_2) decays it can be shown that a bimodal distribution of molecular dynamics is present inside the microgel particle from which the morphological model of core-corona could be derived. The proton Hahn-echo decays for the individual resonances assigned in the NMR spectrum and for the ensemble of microgel resonances were calculated (Fig. 4.2b). Because the results are identical in the limit of experimental errors (see Table 4.1), I chose to use in subsequent calculations the transverse relaxation decays of the R_1 resonance of VCL microgels because its high intensity makes it less sensitive to noise interference.

Table 4.1 Proton transverse relaxation rates measured using different NMR resonances R_1, R_2 and R_3(Fig. 5.2b) for PVCL microgels with 0.04 BIS. The errors are of the order of 10%.[c]

	R_1	R_2	R_3
T_{2S} [ms]	0.42	0.34	0.32
T_{2L} [ms]	5.8	6.2	5

The transverse relaxation decay of the PVCL 0.04 BIS microgel is shown in Figure 4.3a. A biexponential decay for the integral intensity of the R_1 resonance can be assumed (Fig. 4.3a), i.e.,

$$\frac{S(t)}{S(0)} = C_S \exp\left\{-\frac{t}{T_{2S}}\right\} + C_L \exp\left\{-\frac{t}{T_{2L}}\right\}, \qquad (4.1)$$

where $S(t)/S(0)$ is the normalized NMR signal integral as a function of spin-echo time t, C_i (i=S and L) are the relative contributions of the decays characterised by short (T_{2S}) and long (T_{2L}) transverse relaxation times. The coefficients C_S and C_L are related to the number of protons in the methylene fragments of PVCL describing quantitatively the bimodal heterogeneity of the polymer network in microgel.

The fit with two exponentials (Eq. (4.1)) has the Chi^2 = 0.00112 and a coefficient of correlation of R^2 = 0.99112. Moreover, to prove the existence of two decay components an inverse Laplace transform was performed on the NMR decay curves (Fig. 4.3b) that reveals a bimodal T_2 distribution.

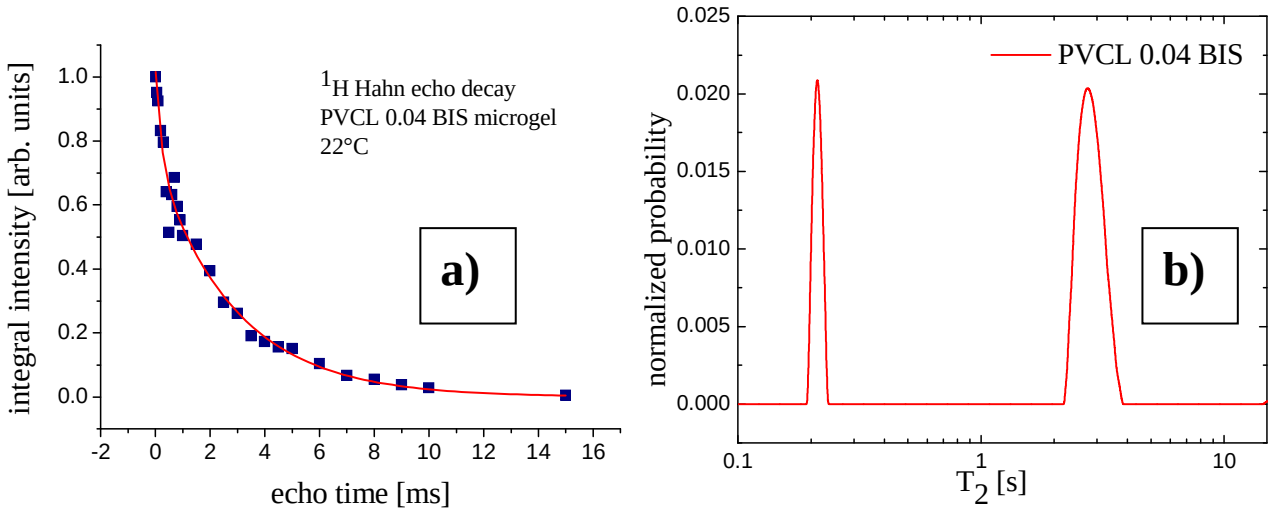

Figure 4.3 a) Proton NMR transverse relaxation decay by Hahn echo for PVCL 0.04 BIS microgel at 22 ^{0}C with concentration of 2% wt. in D_2O fitted with biexponential decay function (solid line). b) Inverse Laplace transformation of the NMR experimental data from a) shows the existence of two decay components.[c]

The values of the ^{1}H transverse relaxation times and the relative concentration of methylene protons given by $C_{S,L}$ coefficients for the three microgel systems are shown in Table 4.2. The values are similar for the PVCL microgel systems with different crosslinker amounts, which means that the ratio between core and corona in terms of mobility does not change substantially with the increase of crosslinker amount in the investigated range.

Therefore, I will use the average values of these parameters (Table 4.2) in the subsequent calculations.

Table 4.2 Proton transverse relaxation rates measured using the NMR resonance R_1 (Fig. 4.2b) and relative weights coefficients (C_S and C_L) for the series of PVCL microgels with different crosslinker amounts.[c]

	0.04 BIS	0.1 BIS	0.15 BIS	average
T_{2S} [ms]	0.42	0.48	0.48	0.46
C_S	0.28	0.28	0.25	0.27
T_{2L} [ms]	5.8	5.68	5.72	5.74
C_L	0.74	0.75	0.77	0.75

It is known from the NMR relaxometry of polymer networks[4(11)-4(13)] that the transverse relaxation is strongly affected by the degree of the crosslinking density via residual dipolar couplings and their fluctuations. Therefore, the value of $T_{2S} \approx 0.46$ ms corresponds to a network with a larger value of the crosslinking density as compared to $T_{2L} \approx 5.74$ ms.

Scale invariant theory of polymer networks shows that ^{1}H transverse relaxation rate ($1/T_2$) is proportional to the averaged square of the residual dipolar Hamiltonian $\left\langle (\overline{H}_d)^2 \right\rangle$, i.e.,

$$\frac{1}{T_2} \propto \left\langle \left(\overline{H}_d\right)^2 \right\rangle, \qquad (4.2)$$

where the average is taken over the orientation and size of the end-to-end vector[4(13),4(14)]. In the approximation of Gaussian distribution of the end-to-end vectors it can be written,[4(14)]

$$\frac{1}{T_2} \propto \frac{1}{(N_{stat})^2}, \qquad (4.3)$$

where the number of statistical segments of a subchain (strand) is denoted by N_{stat}. The crosslinking density can be defined as $CLD \equiv 1/N_{stat}$ (see Ref. 4(14)) and finally we yield

$1/T_2 \propto (CLD)^2$. Hence, the ratio of the crosslinking density of the microgel in core and corona can be obtained from the following relationship,

$$\frac{CLD^{core}}{CLD^{corona}} = \left(\frac{T_2^{corona}}{T_2^{core}} \right)^{1/2} . \qquad (4.4)$$

Therefore, the bimodal morphology of PVCL microgel particles is characterised from Eq. (4.4), and the data shown in Table 4.2 by the ratio of the averaged crosslinking density of $CLD^{core} / CLD^{corona} \approx 3.5$.

In conclusion, the biexponential fit of the decay of the R_1 resonance of PVCL microgels can be interpreted as probing the heterogeneity of the PVCL distribution and allows the evaluation of crosslinking density distribution in the microgel particle.

4.1.3 Structural parameters for PVCL microgels using the homogeneous Flory model.

In order to estimate the temperature transition parameters for the PVCL microgels with different crosslinking density I have used experimental data measured with DLS (Figure 4.1a) and fitted them with the equation of state Eq. (3.7) presented in Chapter 3, theory section 3.1. Since the volume fraction in the deswollen state for this polymeric microgels is unknown, different fits for different values of ϕ_0 were performed, leaving N, A, Θ and χ_1 as free parameters as previously discussed in Ref. 4(15). Figure 4.4 shows the homogeneous model fit of the DLS data for PVCL 0.04 BIS, using the equation of state Eq. (3.7). The quality of the different fits is comparable, the chi-square values obtained are similar, but the resultant values for the free parameters vary considerably, as shown in Table 4.3 for PVCL 0.04 BIS microgel.

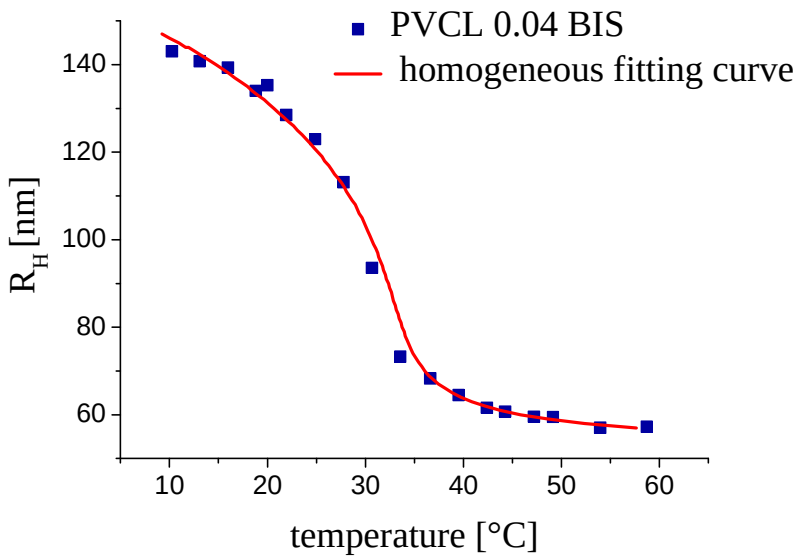

Figure 4.4 Size-temperature data from DLS for PVCL 0.04 BIS microgel fitted with equation of state (Eq. (3.7)) in the homogeneous morphology approximation (solid line).[c]

Table 4.3 Results for the size-temperature fit with different ϕ_0 by the homogeneous Flory theory morphology approximation for PVCL 0.04 BIS microgel. The bold entries correspond to the best fit.[c]

ϕ_0	0.7	0.75	**0.8**	**0.85**	0.9
N	3.5×10^4	5.6×10^4	$\mathbf{8.8\times10^4}$	$\mathbf{1.44\times10^5}$	2.48×10^5
Θ	308.6	308.1	**307.41**	**306.7**	305.7
A	-3.22	-4.5	**-6.44**	**-9.59**	-15.38
χ_1	0.45	0.43	**0.39**	**0.3**	0.07

In order to choose the best set of values, these results can be compared with known values of the microgel parameters. The number of subchains in the microgel particle can be estimated by considering that each crosslinker molecule connects two subchains. As a result $N=2N_A V_0 c$, with c the molar concentration of the crosslinker used in the synthesis process, resulting in $N = 1.12 \times 10^5$ for PVCL 0.04 BIS. The parameters set that agrees best with this assumption are the ones for $\phi_0 = 0.8$ and $\phi_0 = 0.85$ (bold entries in Table 4.3).

The best fit parameters obtained for the series of crosslinked microgels are shown in Table 4.4. The polymer volume fraction in deswollen state (ϕ_0), *A*, Θ and χ_1 shouldn't change with the increase of crosslinker amount, being related to the PVCL homopolymer used for the synthesis of microgels. Therefore an average value of these parameters should be considered as standard for this type of microgels. On the other hand, the number of subchains increases drastically with the increase of crosslinker amount.

Table 4.4 Results for the size-temperature fit by the homogeneous Flory theory morphology approximation for the series of PVCL microgels with different crosslinker amounts. The entries correspond to the best fit.[c]

Parameters	0.04 BIS	0.1 BIS	0.15 BIS	average
ϕ_0	0.8	0.85	0.85	0.83
N	8.8×10^4	1.85×10^5	8.2×10^5	-
Θ	307.41	305.6	308.3	307.1
A	-6.44	-9.3	-7.05	-7.6
χ_1	0.39	0.23	0.49	0.37

Figure 4.5 shows the temperature dependence of the Flory parameter χ for the PVCL 0.04 BIS microgel, using the experimental DLS measurements, Eqs. (3.5) and (3.6) from Chapter 3, theory section 3.2, together with the values of the best-fit parameters that I considered most accurate for ϕ_0=0.8 (Table 4.4). Below the LCST the Flory interaction parameter scales linearly with 1/T, but above this temperature the microgel particles deswell, and the polymer concentration dependence of the Flory interaction parameters becomes relevant, influencing the temperature dependence. As expected for a system with LCST, χ increases with the temperature. Moreover, this result is in good accordance with previous literature[4(16)], where the value for the Flory interaction parameter for PVCL networks

considering only the temperature dependence was calculated at the transition temperature of 32 ^{0}C as χ =0.522.

Considering the averaged best-fit parameters shown in Table 4.4 the parameters of interest for the PVCL polymeric microgel temperature transition could be calculated using Eq. (3.6). The entropic and enthalpic energies are $\Delta S = -11.18\times10^{-23}$ J/K and $\Delta H = -3.22\times10^{-20}$ J, respectively.

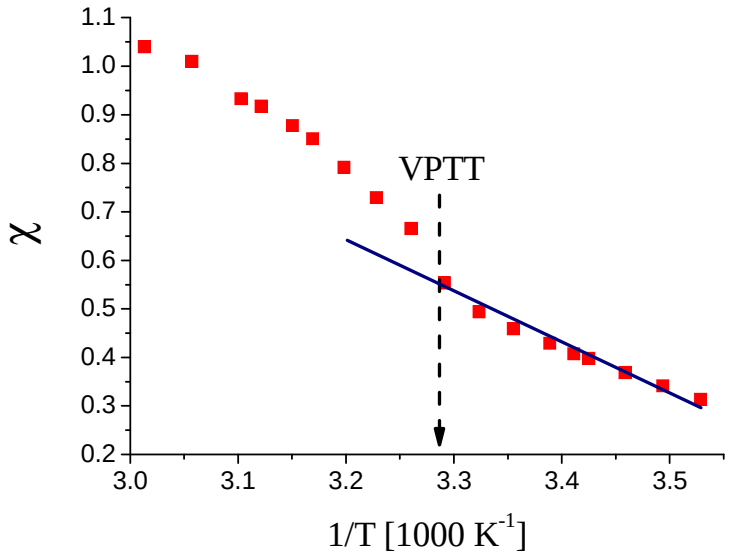

Figure 4.5 Temperature dependence of the Flory interaction parameter χ for the 0.04 BIS PVCL/water system using *A*, Θ, and χ_1 parameters from Table 4.4. The behaviour of the interaction parameter is no longer linear above the VPTT.[c]

4.1.4 Structural parameters for PVCL microgels using the heterogeneous model fit

In order to describe the heterogeneous morphology of a microgel system I have modified the Flory-Rehner state equation for the swelling/deswelling of microgels resulting in temperature dependence of the hydrodynamic radius given by Eq. (3.19) presented in Chapter 3, theory section 3.3. This equation was used to fit the data obtained by dynamic light scattering with the purpose of finding relevant microgel structural parameters (Fig. 4.6). NMR transverse

relaxation results (Table 4.2) were used to select the most physically correct set of fitting parameters. Moreover, some of the microgel parameters obtained above for the homogeneous model were useful for calculating the structural parameters for the heterogeneous morphology. For instance, the quantities A, Θ and χ_1 determined before can be used in good approximation, because the system is a homopolymer microgel. Hence, the free parameters of the fit are ϕ_0^{core}, ϕ_0^{corona}, N^{core}, N^{corona} and ρ (see Eq. (3.19)).

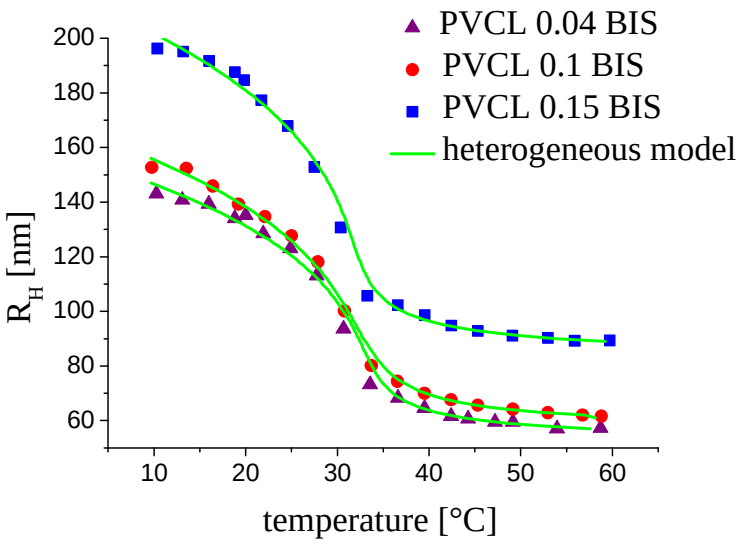

Figure 4.6 Size-temperature data from DLS for the series of PVCL microgels with different crosslinker amounts fitted with equation of state (Eq. (3.19)) in the bimodal heterogeneous morphology approximation (solid lines).[c]

The best-fit set of parameters was obtained by comparing the fit quality and by comparison with the best result obtained for the homogeneous morphology model (Table 4.4). The best fit parameters satisfy the following conditions that relates them to the homogeneous model, i.e.,

$$\frac{1}{2}\left(\frac{N^{core}}{\rho^3}+\frac{N^{corona}}{1-\rho^3}\right)=N \qquad (4.5)$$

$$\rho^3\phi_0^{core}+(1-\rho^3)\phi_0^{corona}=\phi_0, \qquad (4.6)$$

where N and ϕ_0 are the number of subchains, and volume fraction of gel in the deswollen state, respectively, in the homogeneous approximation.

Furthermore, NMR relaxation results can be used to impose additional constraints and to obtain the best-fit parameter set for the heterogeneous model. The total number of monomers (N_{mono}) in the microgel particles can be evaluated by,

$$N_{mono} = m\, N_{stat}\, N\,, \tag{4.7}$$

where m is the number of monomers in a statistical segment. If assumed that the number of monomers in a statistical segment will not differ in core and corona it can be written,

$$\frac{N_{mono}^{corona}}{N_{mono}^{core}} = \frac{N_{stat}^{corona}}{N_{stat}^{core}}\,\frac{N^{corona}}{N^{core}}\,. \tag{4.8}$$

The ratio of the number of monomers is proportional to the concentration of protons measured by the quantities C_{i} in the T_2 NMR experiment. Furthermore, from Eq. (4.3) we yield,

$$\frac{C_L}{C_S}\left(\frac{T_{2S}}{T_{2L}}\right)^{1/2} = \frac{N^{corona}}{N^{core}}\,. \tag{4.9}$$

The left-hand side term of the above equation can be calculated from averaged results (Table 4.2) of the T_2 NMR experiment (Section 4.1.2) and has the value of approximately 0.8. By taking into account all these macroscopic and microscopic constraints the best-fit parameters for the heterogeneous model that describes the structural heterogeneity inside the microgel particles were obtained. The results are shown in Table 4.5 for the series of PVCL microgels with different amount of crosslinker.

Table 4.5 Results for the size-temperature fit for the heterogeneous morphology of the series of PVCL microgels with different crosslinker amounts, considering the best-fit results of the homogeneous model for the Flory interaction parameters. These results were selected to be in quantitative agreement to the parameters of the homogenous morphology model (Table 4.4) and the heterogeneity showed by ^{1}H NMR transverse relaxation (Table 4.2 and Eq. (4.9)).[c]

	0.04 BIS	0.1 BIS	0.15 BIS	average
ϕ_0^{core}	0.8	0.85	0.85	0.83
ϕ_0^{corona}	0.8	0.85	0.85	0.83
N^{core}	$2.19\text{x}10^4$	$3.9\text{x}10^4$	$1.75\text{x}10^5$	-
N^{corona}	$1.69\text{x}10^4$	$3.2\text{x}10^4$	$1.28\text{x}10^5$	-
ρ	0.51	0.49	0.49	0.5

Figure 4.6 shows the fits of the DLS data for the series of microgels systems with different amount of crosslinker using the modified Flory temperature-induced volume transition theory (Eq. (3.19)). The final results (Table 4.5) show the degree of structural heterogeneity inside the microgel particles. The parameter that reflects the change between the different samples investigated and inside the microgel particle is the number of subchains of core and corona for each microgel system (Fig. 4.7). As expected, the number of subchains in both core and corona increase with the crosslinker amount. The heterogeneity inside the microgel particles is also reflected in the parameter ρ, which describes the ratio between the radius of the core and the hydrodynamic radius. The average value of $\rho \approx 0.5$ means that the volume of the core is only 12% of the total volume of the particle, while the number of subchains in the core and corona are almost equal, which reveals that the subchains density in the core and corona has a bimodal distribution, and the core is much denser.

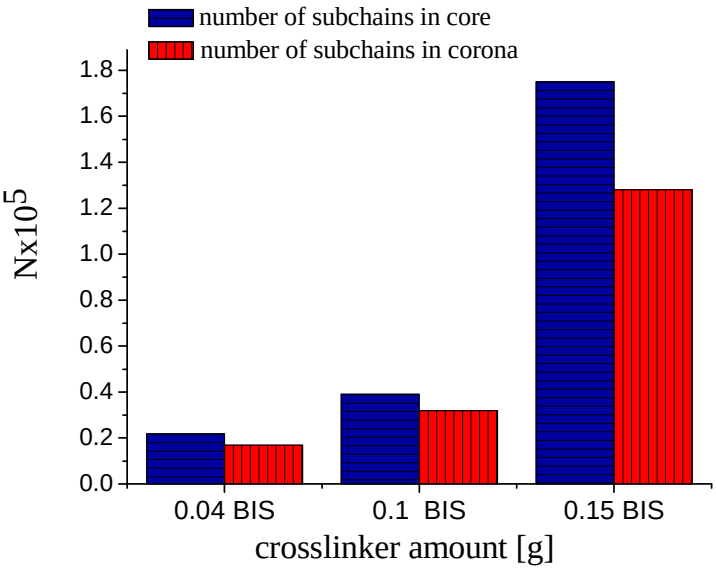

Figure 4.7 Dependence of the number of subchains to the crosslinker amount for the series of PVCL microgels, results obtained in the heterogeneous morphology model.[c]

The results presented in this section were described by Balaceanu *et al.*[c]

4.2 Copolymer PVCL-PNIPAAm and PVCL-PNIPMAAm microgels with heterogeneous morphology

This study[e] is a further generalization of the study presented in section 4.1, which includes the description of the synthesis of a copolymer microgel system. Therefore, I am extending the Flory swelling/deswelling volume transition theory applied to copolymer microgels in order to account for the bimodal internal structural heterogeneities. As discussed previously[c], I am using ^{1}H transverse relaxation NMR measurements to impose additional conditions on the fitting parameters of the Flory swelling state equation for copolymer microgels in this case. This approach allows the quantitative characterisation of the core-corona morphology of PVCL-PNIPAAm and PVCL-PNIPMAAm random copolymer microgels.

The two copolymer microgel systems used for this study have a theoretical molar ratio 1:1 (see Chapter 2, synthesis section 2.1.2), and will be referred to in the text as PVCL-PNIPAAm and PVCL-PNIPMAAm.

4.2.1 Temperature-induced volume transition by dynamic light scattering.

Figure 4.8a shows the temperature-dependent swelling of the two copolymer microgel systems. The measured hydrodynamic radius (R_H) is normalized by the value in the deswollen state (R_{H0} at 40°C). The swelling ratios are different; the PVCL-PNIPAAm microgel is more elastic, because the NIPAAm component is more hydrophilic. There is a minor difference in the volume transition temperature for the two microgel systems, which can be seen in Figure 4.8b of the first-order derivatives of the temperature transition curves. The volume transition temperature is ~30 ^{0}C for PVCL-PNIPAAm and ~33 ^{0}C for PVCL-PNIPMAAm microgel. PVCL and PNIPAAm have a similar volume transition temperature at about 32 and 33°C, respectively, while PNIPMAAm has a volume transition temperature of 45°C.

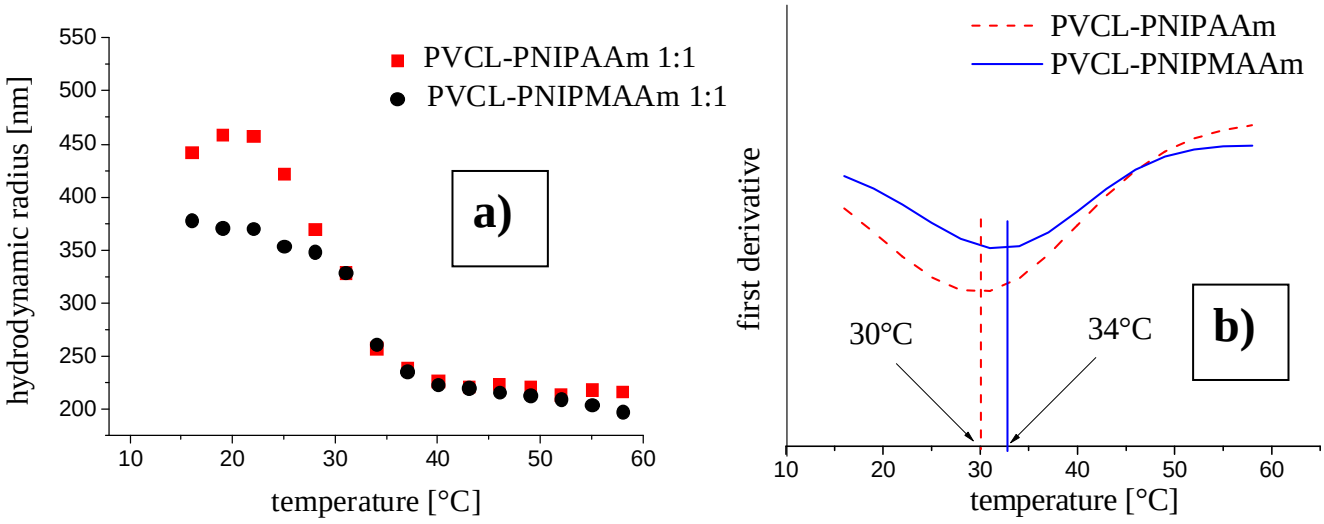

Figure 4.8 a) Normalized hydrodynamic radius of the copolymer microgels PVCL-PNIPAAm and PVCL-PNIPMAAm versus temperature. b) First-order derivatives of the volume size-temperature curves a) showing the volume transition temperature.[e]

4.2.2 Morphology and dynamic heterogeneity of microgels by ^{1}H transverse magnetization relaxation.

To confirm the bimodal heterogeneous structure of the random copolymer microgels of PVCL-PNIPAAm and PNIPMAAm, I performed an NMR study using ^{1}H high-resolution spectroscopy and relaxometry. Proton high-resolution NMR spectra of VCL, NIPAAm, and NIPMAAm monomers measured at 600 MHz are shown in Fig. 4.9. The assignment of these peaks (see Scheme in Fig. 4.9) was made by comparison with simulated NMR spectra obtained using the ChemDraw® and Gaussian03 programs.

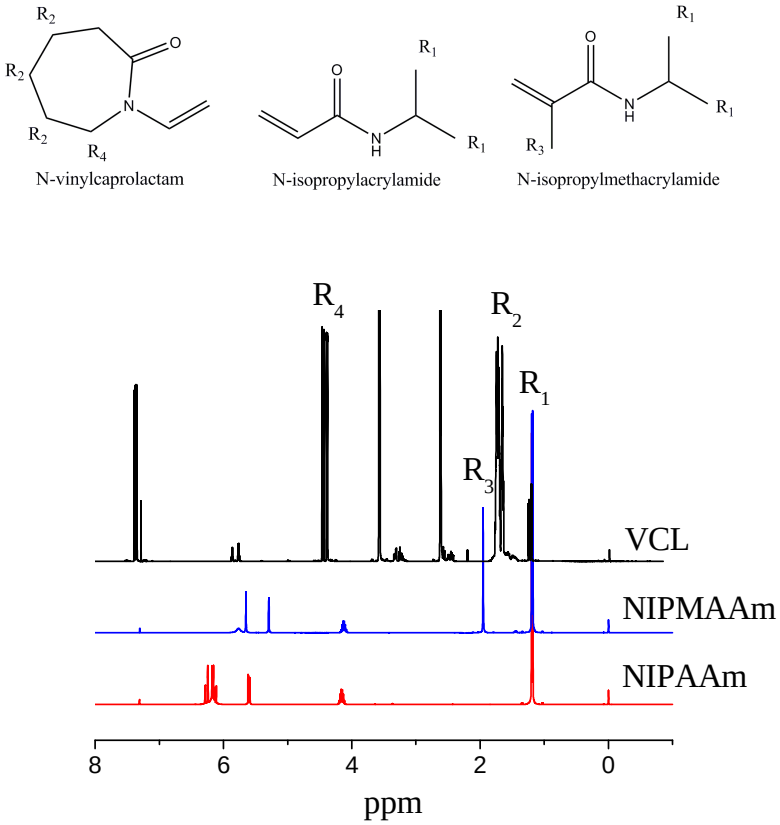

Figure 4.9 Proton high-resolution NMR spectra of VCL, NIPAAm, and NIPMAAm monomers in D_2O measured at 600 MHz. Several resonance assignments are shown in the schemes using NMR spectrum simulations.[e]

Proton high-resolution spectra of PVCL-PNIPAAm and PVCL-PNIPMAAm microgels measured in D_2O at 22 ^{0}C with AV700 Bruker NMR spectrometer under MAS

condition (rotor frequency of 7 kHz) are shown in Fig. 4.10. In the resulting NMR spectrum of PVCL-PNIPAAm two intense resonances with the chemical shifts: R_1 (1.8 ppm) corresponding to CH_3 groups of PNIPAAm and R_2 (2.5 ppm) CH_2 groups of PVCL were identified. The resonance at 4.8 ppm corresponds to HDO. For the PVCL-NIPMAAm microgel the resonances denoted by R_3 (1.8 ppm) belongs to additional CH_3 groups of PNIPMAAm and R_4 (3.3 ppm) corresponds to CH_2 of PVCL (Fig. 4.10).

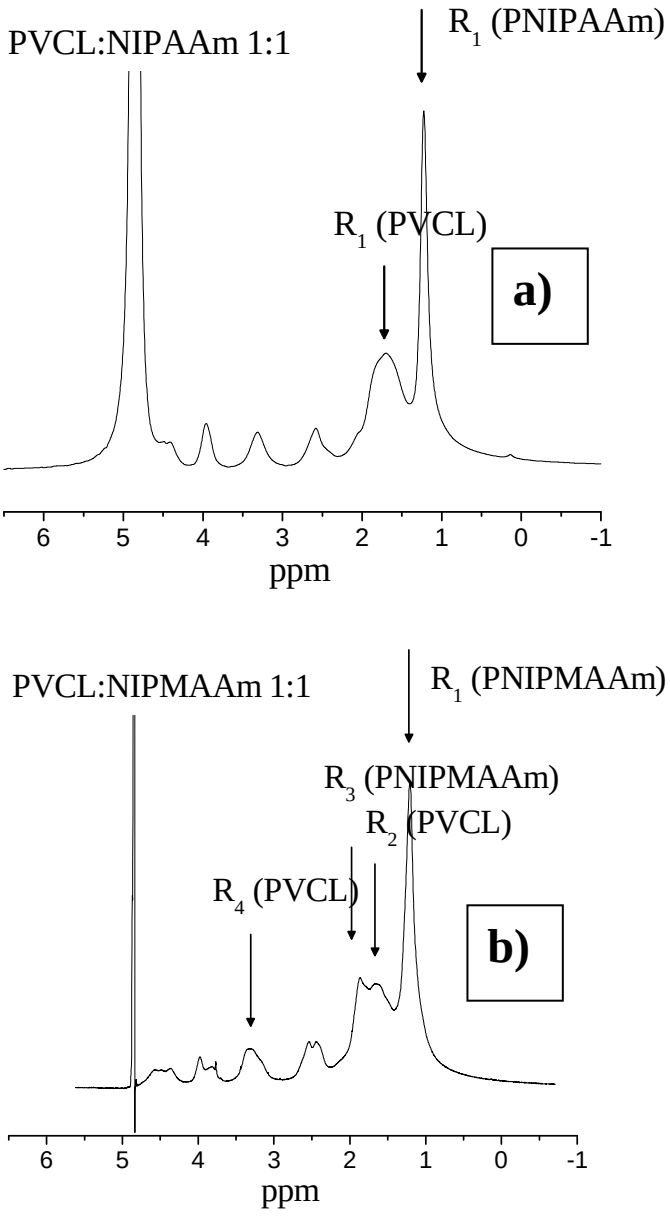

Figure 4.10 Proton high-resolution spectra of a) PVCL-PNIPAAm and b) PVCL-PNIPMAAm copolymer microgels (2% wt. in D_2O) at 22 ^{0}C. The spectra were measured at 700 MHz NMR spectrometer under MAS conditions (ν_R= 7 kHz). The resonance assignments were made using the schemes and spectra shown in Fig. 4.9.[e]

As described in section 4.1.2, the heterogeneity in the microgel particle morphology is reflected in the ^1H transverse magnetization relaxation due to different degree of local molecular motions correlated to the distribution in crosslinking density inside the particle. The investigated microgels are made from random copolymers and because of the pathologic relaxation behaviour of methyl groups due to the fast rotation around the CH_3 axis the Hahn-echo decays were calculated from the total integral intensity of the NMR spectra in the 0-4.5 ppm range (Fig. 4.10). The decay of the integral NMR signals can be well fitted by biexponential decay Eq. (4.1) represented by solid lines in Fig. 4.11. These transverse relaxation times describe the weight average of the relaxation times of each component in the copolymer network. The coefficients C_S and C_L are related to the number of protons in the PVCL-PNIPAAm and PVCL-PNIPMAAm random copolymers. They describe quantitatively the bimodal heterogeneity of the polymer network in the microgels.

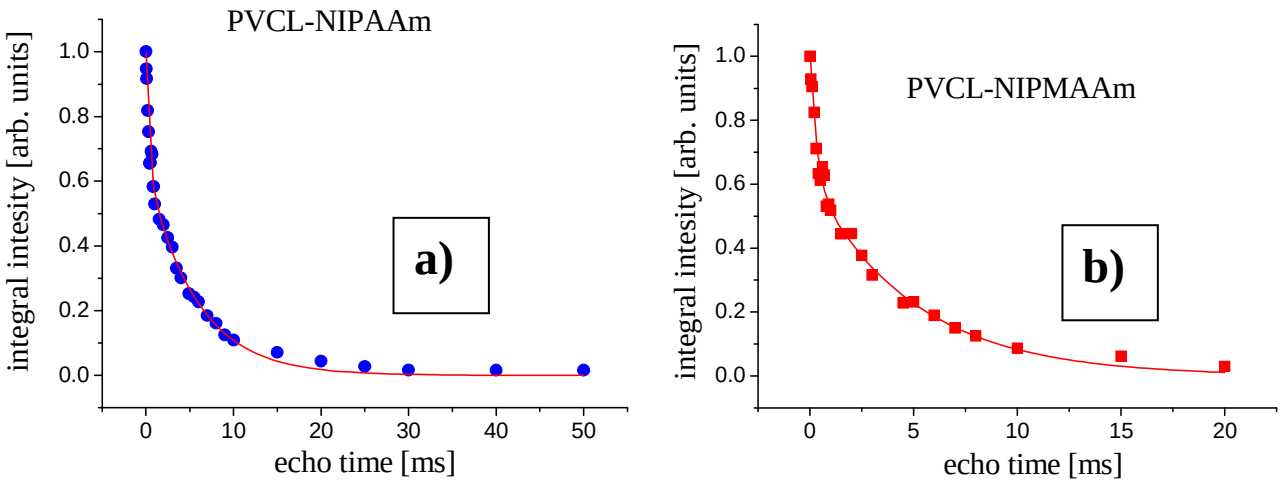

Figure 4.11 Proton NMR transverse relaxation decay by Hahn echo for a) PVCL-PNIPAAm 1:1 and b) PVCL-PNIPMAAm 1:1 copolymer microgels (2% wt. in D_2O) at 22 ^{0}C. The decays were obtained from the total integral intensity of spectra taken in the 0-4.5 ppm range. The fits with two exponential functions (Eq. (5.1)) are shown by solid lines and have Chi^2 ~ 0.0011 and correlation coefficients of R^2 ~ 0.9911.[e]

The values of the ^{1}H transverse relaxation times and the relative concentration of protons given by $C_{S,L}$ coefficients for the PVCL-PNIPAAm and PVCL-PNIPMAAm microgel systems are shown in Table 4.6. The values are similar for the investigated microgel systems having the same molar ratio of NIPAAm and NIPMAAm, which means that the ratio between core and corona in terms of mobility does not change substantially by changing one of the copolymer components. The value of T_{2S} corresponds to a network with a larger value of the crosslinking density as compared to T_{2L}.

The bimodal morphology of PVCL microgel particle is characterised from Eq. (4.4), and the data shown in Table 4.6 by the ratio of the averaged crosslinking density of $CLD^{core}/CLD^{corona} \approx 4.13$ and $CLD^{core}/CLD^{corona} \approx 4.11$ for PVCL-PNIPAAm and PVCL-PNIPMAAm microgels, respectively. The biexponential decays of the total integral intensity of NMR spectra for random copolymer microgels can be interpreted as probing the heterogeneity of crosslinking density in the microgel particles.

Table 4.6 Averaged ^{1}H transverse relaxation rates measured using the total integral intensity of NMR spectra (Fig. 4.11) and relative weights coefficients (C_S and C_L) for PVCL - PNIPAAm 1:1 and PVCL - PNIPMAAm 1:1 microgels.[e]

	PVCL-PNIPAAm	PVCL-PNIPMAAm
T_{2S} [ms]	0.64	0.60
C_S	0.35	0.40
T_{2L} [ms]	10.94	10.16
C_L	0.65	0.56

4.2.3 Microgel structural parameters for homopolymer microgels using the homogeneous Flory model.

The homopolymer microgel systems of the components, PVCL, PNIPAAm and PNIPMAAm were used to obtain the temperature transition parameters that are needed for the copolymer systems investigation. The DLS temperature transition data were fitted with the Flory equation of state for homopolymer microgels Eq. (3.7) presented in Chapter 3, theory section 3.1 (Fig. 4.12). As previously described[4(15),c], since the volume fraction in the deswollen state for this polymeric microgels is unknown, different fits for different values of ϕ_0 were performed, leaving N, A, Θ and χ_1 as free parameters. The condition $N=2N_A V_0 c$ was used again, with c the molar concentration of the crosslinker used in the synthesis process, to determine the best fit parameter. The parameter set that agrees best with this assumption are shown in Table 4.7 for the three homopolymer microgels. Figure 4.12 shows the homogeneous model fit of the DLS data for PVCL, PNIPAAm and PNIPMAAm microgels.

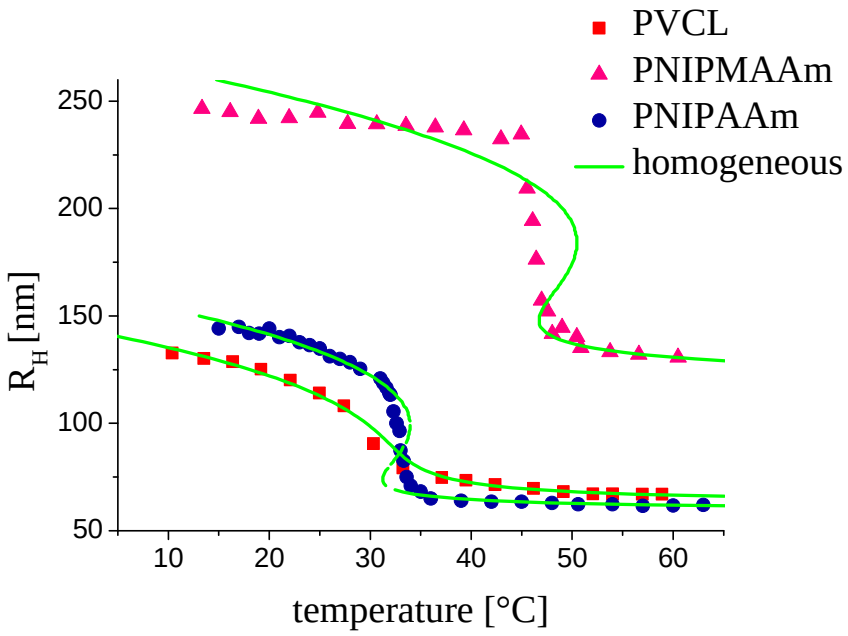

Figure 4.12 Size-temperature data for PVCL, PNIPAAm and PNIPMAAm homopolymer microgels fitted with equation of state (Eq. (3.7)) in the homogeneous morphology approximation (solid line).[e]

Table 4.7 Results from the size-temperature fit by the homogeneous Flory theory morphology approximation for PVCL, PNIPAAm and PNIPMAAm microgels.[e]

	PVCL	PNIPAAm	PNIPMAAm
ϕ_0	0.85	0.9	0.7
N	7.4×10^5	1.86×10^5	1.98×10^6
Θ	309.6	318.05	360.6
A	-7.84	-5.42	-1.56
χ_1	0.56	1.00	0.93

The presence of the α - methyl group interferes with the hydrophobic interactions of the *N*-isopropyl side group, because it provides the chains more flexibility, which explains the fact that PNIPMAAm has a higher LCST than PNIPAAm (and of PVCL).[4(17)] This can be seen in Table 4.7 in the results of the Θ temperatures.

From the experimental size-temperature dependence, Eq. (3.5) and (3.6) can be used together with the values of the fitting parameters (Table 4.7) to obtain the temperature dependence of the Flory parameter for each of the homopolymer microgels (Fig. 4.13).

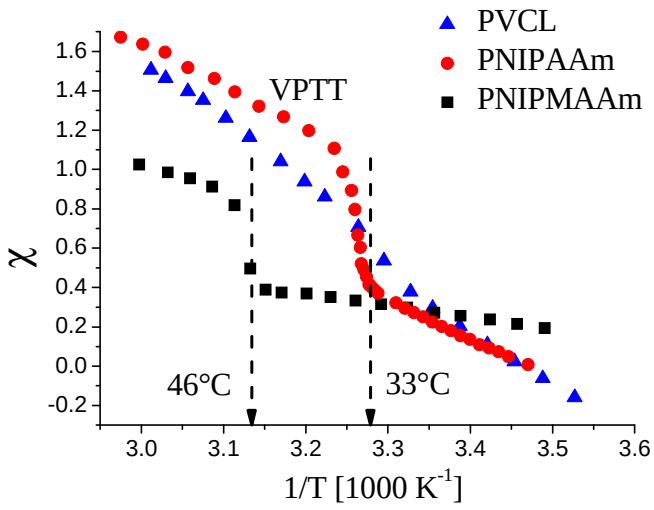

Figure 4.13 Flory interaction parameter temperature dependence for the homopolymer systems, PVCL, PNIPAAm and PNIPMAAm. The arrows indicate the volume phase transition temperatures (VPTT) of the homopolymer microgels.[e]

At low temperatures, the contribution from the polymer fraction ϕ in Eq. (3.5) becomes almost negligible, as the particles are highly swollen and the polymer volume fraction is small. As a result, in this region χ scales linearly with $1/T$ as shown in the right-hand part of Fig. 4.13. For temperatures above the transition temperature, the particle size has appreciably dropped and the ϕ-dependence of the mixing parameter becomes relevant. It is important to note that the dependence on the polymer volume fraction is much more obvious for the isopropyl microgels, than for the PVCL microgel. The temperature dependence of the Flory parameter χ is similar for PVCL and PNIPAAm (Fig. 4.13) and therefore, the volume transition temperature for PVCL-PNIPAAm microgel is close to that of PVCL. This is not expected to take place for the PVCL-PNIPMAAm where $\chi(T)$ is very different for PNIPMAAm compared to PVCL (Fig. 4.13). Nevertheless, the transition temperature is again close to that of PVCL component of random copolymer. A possible explanation could be related to the fact that Eq. (3.8) is only an approximation that neglects the interaction between the copolymers.

These temperature transition parameters are used next to fit the DLS data for the copolymer systems in the homogeneous approximation with Eq (3.10), presented in Chapter 3, theory section 3.2, in order to get the average number of subchains. This will help in selecting the best fit for the heterogeneous approximation.

4.2.4 Morphology characterisation of copolymer microgels using the heterogeneous Flory model.

After having determined the parameters for the homopolymer systems and the parameters for the copolymer systems in the homogeneous approximation, the copolymer system heterogeneity can be investigated.

Eq. (3.20) presented in Chapter 3, theory section 3.4, is used to fit the data obtained by dynamic light scattering with the purpose of finding relevant microgel structural parameters (Fig. 4.14a and b). NMR transverse relaxation results (Table 4.6) were used to select the most physically correct set of fitting parameters. Moreover, some of the microgel parameters obtained above for the homopolymer and copolymer homogeneous models were useful for calculating the structural parameters for the heterogeneous morphology. For instance, the quantities A, Θ and χ_1 (Table 4.7), determined before for each homopolymer system (PVCL, PNIPAAm and PNIPMAAm), are used in good approximation for calculating the structural parameters of the heterogeneous copolymer system. The average number of subchains obtained in the homogeneous approximation of the copolymer system is used to estimate the range of the final heterogeneous model number of subchains. Hence, the free parameters of the final heterogeneous approximation fit are ϕ_0^{core}, ϕ_0^{corona}, N^{core}, N^{corona} and ρ (see Eq. (3.20)). These parameters refer to the polymer volume fractions in the deswollen state for core and corona, the number of subchains for core and corona and the ratio between the radius of the core and the hydrodynamic radius.

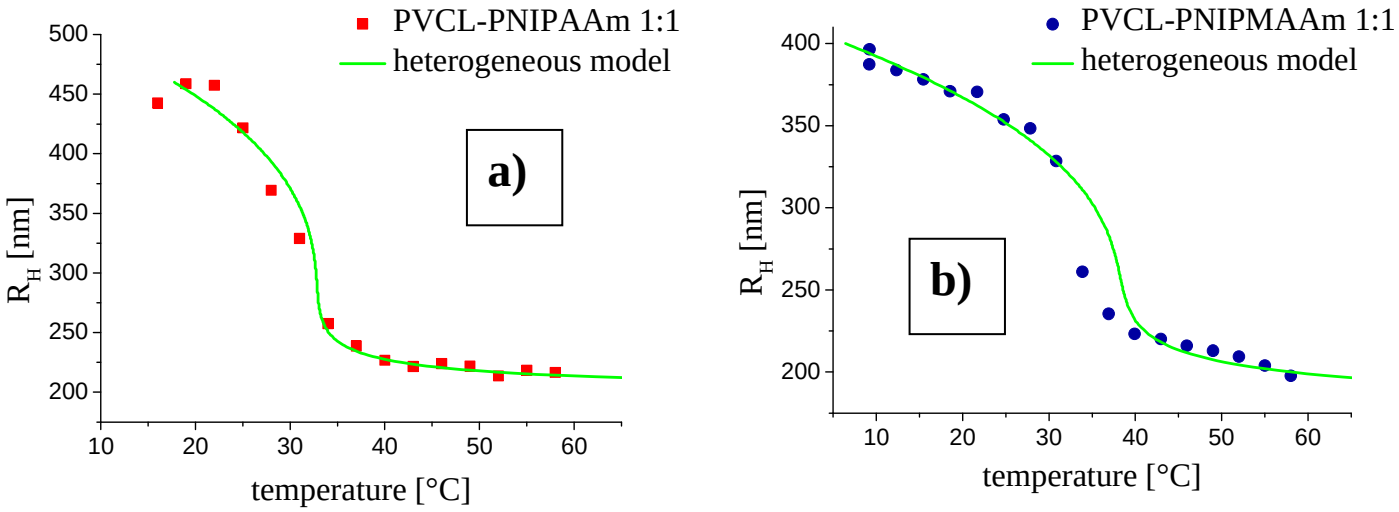

Figure 4.14 Size-temperature data for copolymer microgel a) PVCL-PNIPAAm and b) PVCL-PNIPMAAm fitted with equation of state (Eq. (3.20)) in the bimodal heterogeneous morphology approximation (solid lines).[e]

Furthermore, NMR relaxation results can be used to impose additional constraints and to obtain the best-fit parameter set for the heterogeneous model, as described in section 4.1.2 by Eq. (4.9) and taking the values from Table 4.6. By taking into account all these macroscopic and microscopic constraints the best-fit parameters for the heterogeneous model that describes the structural heterogeneity inside the microgel particles were obtained. The results are shown in Table 4.8 for both copolymer systems. There are no significant differences between the structural heterogeneity results of the two systems. Pearson's product-moment correlation coefficient (R) of the fitting is -0.909 for PVCL-PNIPAAm microgel and -0.943 for the PVCL-PNIPMAAm microgel. The values show that there is a good linear dependence of the calculated and experimental data.

Table 4.8 Results for the size-temperature fits for the heterogeneous morphology of the two microgels systems, considering the best-fit results of the homogeneous model for the Flory interaction parameters. These results were selected to be in quantitative agreement to the parameters of the homogenous morphology model (Table 4.7) and the heterogeneity showed by ^{1}H NMR transverse relaxation (Table 4.6 and Eq. (4.9)).[e]

	PVCL-PNIPAAm	PVCL-PNIPMAAm
ϕ_0^{core}	0.88	0.84
ϕ_0^{corona}	0.88	0.84
N^{core}	$2.9\text{x}10^6$	$3.2\text{x}10^6$
N^{corona}	$1.3\text{x}10^6$	$1.4\text{x}10^6$
ρ	0.49	0.5

It is important to notice that both systems experience a deswelling degree of ½ of the original size (comparing the DLS size at 25°C with the collapsed microgel particle size). The average value of $\rho \approx 0.5$ means that the volume of the core is only 12% of the total volume of the particle, while the number of subchains in the core is higher than the number of

subchains in the corona, which reveals that the subchains density in the core and corona has a bimodal distribution.

4.3 Correlated morphological changes in the volume phase transition of core-shell microgels

The aim of this study[g] is to analyse the correlated changes in the morphology of core-shell microgels during the volume transition temperature by dynamic light scattering (DLS) and Flory-Rehner transition theory. The experimental size-temperature results are fitted by an extended Flory volume transition theory for core-shell microgels, which is able to analyse the individual swelling behaviour of the core and shell regions, and the total effect on the microgel particle. For this purpose I have designed core-shell microgels, which are a new combination of thermoresponsive polymer components, with different lower critical solution temperatures (LCST), 32°C for PVCL and 45°C for PNIPMAAm, and synthesized reverse microgel systems, PVCL-core/ PNIPMAAm-shell and PNIPMAAm-core/ PVCL-shell.

In the previous studies presented above[c,e] I have discussed the temperature swelling behaviour of homopolymer and copolymer microgels, treated as a polymer network with heterogeneous crosslinking morphology. Due to the complexity already introduced by the core-shell morphology, in the case of these microgel systems I am limiting the theoretical treatment to homogeneous crosslinking morphology of each structural component (core and shell), disregarding the intrinsic heterogeneity introduced by the polymerization technique. I am using the previously calculated swelling parameters characteristic for the polymeric microgels of pure PVCL or PNIPMAAm systems.

The synthesised core-shell microgels used in this study (see Chapter 2, synthesis section 2.1.3) will be referred to in the text as PVCL-core/ PNIPMAAm-shell and PNIPMAAm-core/ PVCL-shell.

4.3.1 Volume phase transition temperature by DLS for homopolymer and core-shell microgels.

Dynamic and static light scattering measurements were performed for homopolymer and core-shell microgel systems to determine the monodispersity, the angular dependence of particle size and the change of the hydrodynamic radius with increasing temperature. Figures 4.15a and b show that the size distribution of the core-shell microgel particle is monotonic and narrow, excluding the formation of secondary seeds in the second synthesis step. Figures 4.16a and b show the static light scattering angular dependent measurement, demonstrating no significant change in the size of the particles with changing angle.

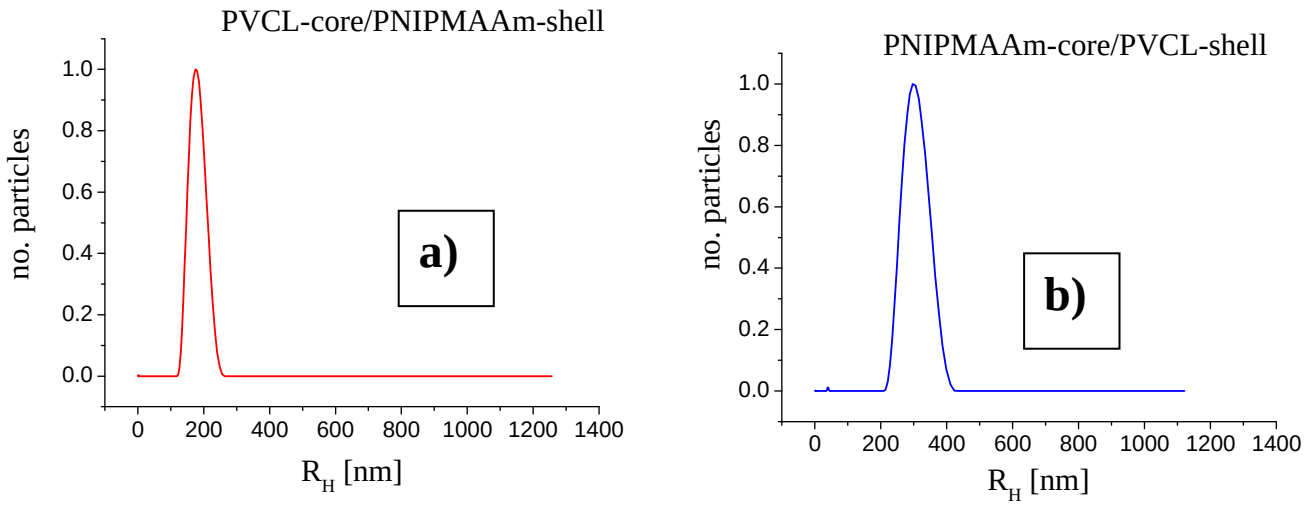

Figure 4.15 Normalized particle size distributions from DLS measurements for a) PVCL-core/ PNIPMAAm-shell and b) PNIPMAAm-core/ PVCL-shell microgels.[g]

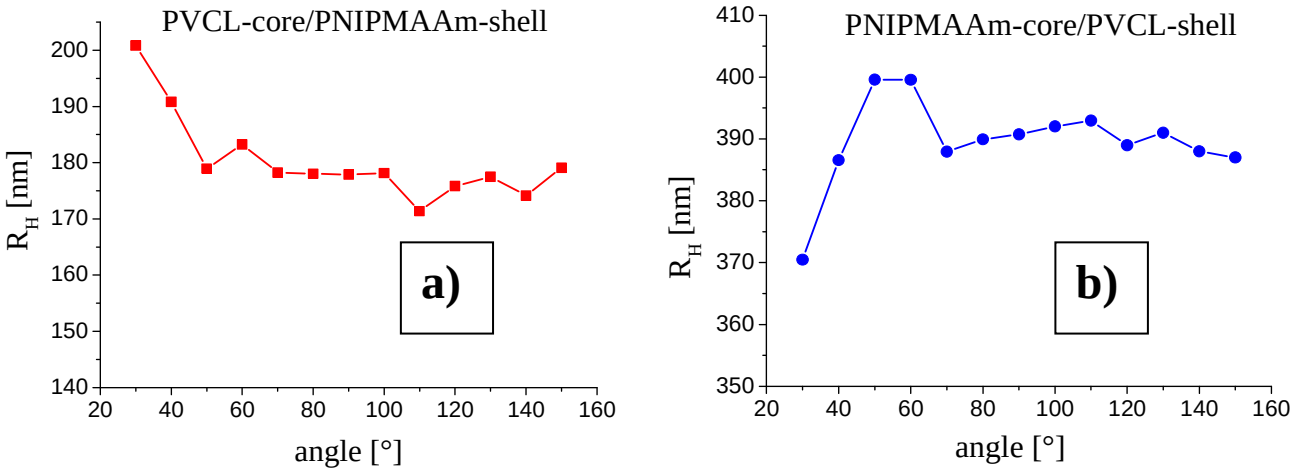

Figure 4.16 Angular dependence from SLS measurements for a) PVCL-core/ PNIPMAAm-shell and b) PNIPMAAm-core/ PVCL-shell microgels.[g]

In Figure 4.17 the volume temperature transitions for homopolymer PVCL (Fig. 4.17a) and PNIPMAAm (Fig. 4.17b) microgels in H_2O are presented, as well as the first derivatives for the transition curves. The derivative was made on the interpolated data, and a smoothing function was subsequently applied in order to minimize the measurement errors. The first derivative provides the possibility of identifying more accurately the volume temperature transition point. From DLS measurements in water, PVCL microgel has a volume transition temperature of 29 °C, while PNIPMAAm microgel has a volume transition temperature of 46 °C.

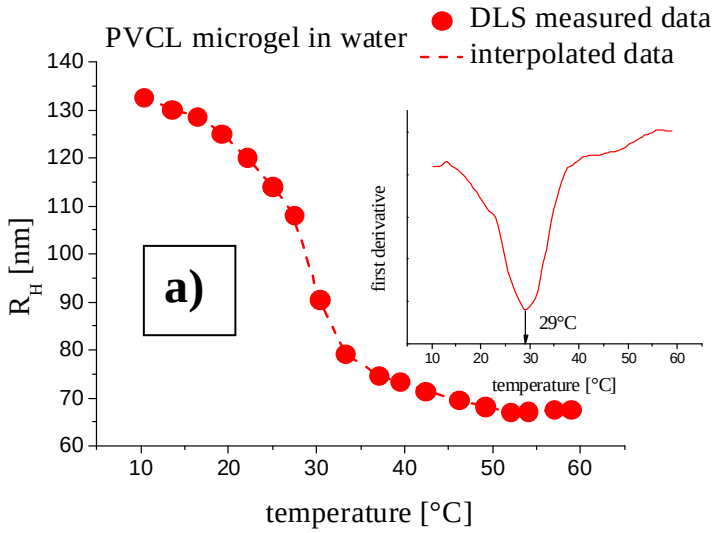

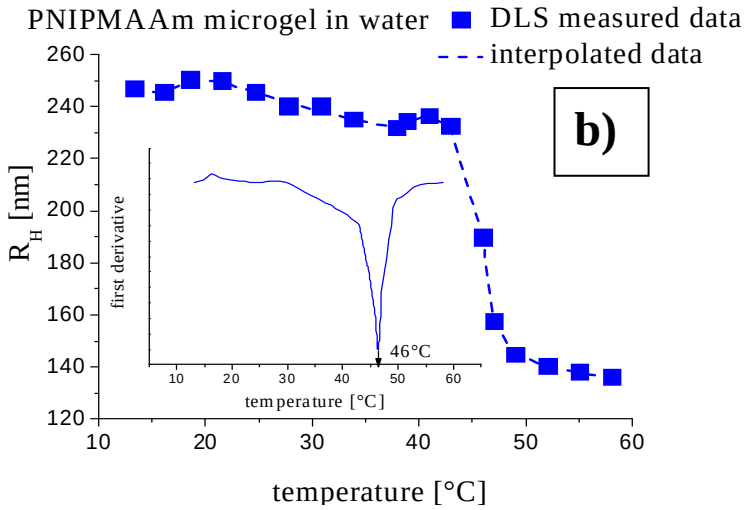

Figure 4.17 Dynamic light scattering measurement of hydrodynamic radius for a) PVCL and b) PNIPMAAm homopolymer microgels in H_2O. The dashed lines represent the interpolations used to obtain the derivatives of the transition curves. The inserts show the first derivatives of the temperature transition curves.[g]

Figures 4.18a and 4.19a show the temperature transition curves determined with DLS measurements in water for PVCL-core/ PNIPMAAm-shell and PNIPMAAm-core/ PVCL-shell microgels, respectively. These figures show the measured data and also the interpolation used later for selecting the temperature intervals. From the first derivatives of the transition curves (Fig. 4.17b and 4.18b) a two steps volume transition can be detected, with two temperature transition points, one corresponding to the PVCL component, and the other one to the PNIPMAAm component. No significant differences between the PVCL-core/ PNIPMAAm-shell and PNIPMAAm-core/ PVCL-shell microgel systems can be detected. Furthermore, the temperature transition of the PNIPMAAm component is much influenced by the presence of the PVCL component, decreasing its transition point with about 4 °C compared to the homopolymer microgel. The volume transition temperatures are given in Table 4.9.

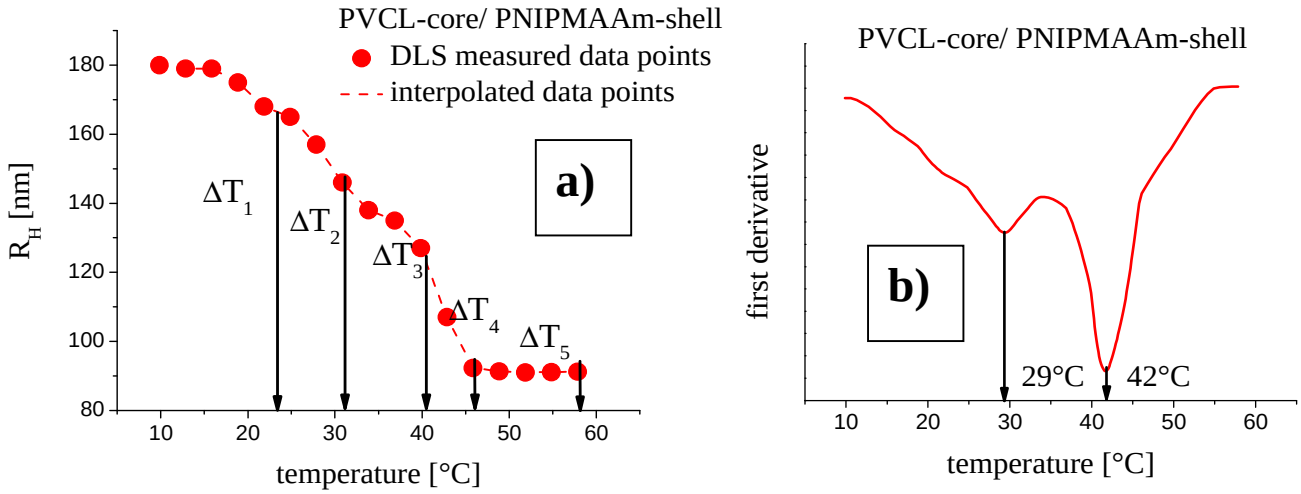

Figure 4.18 a) Dynamic light scattering measurement of PVCL-core/ PNIPMAAm-shell microgel and the temperature intervals for the evaluation of the radius scaling factors ρ_i. The dashed line is the interpolation used to fit the Flory state equation. b) First derivative of the volume temperature transition curve shown in (a), revealing different transition temperatures of the microgel components.[g]

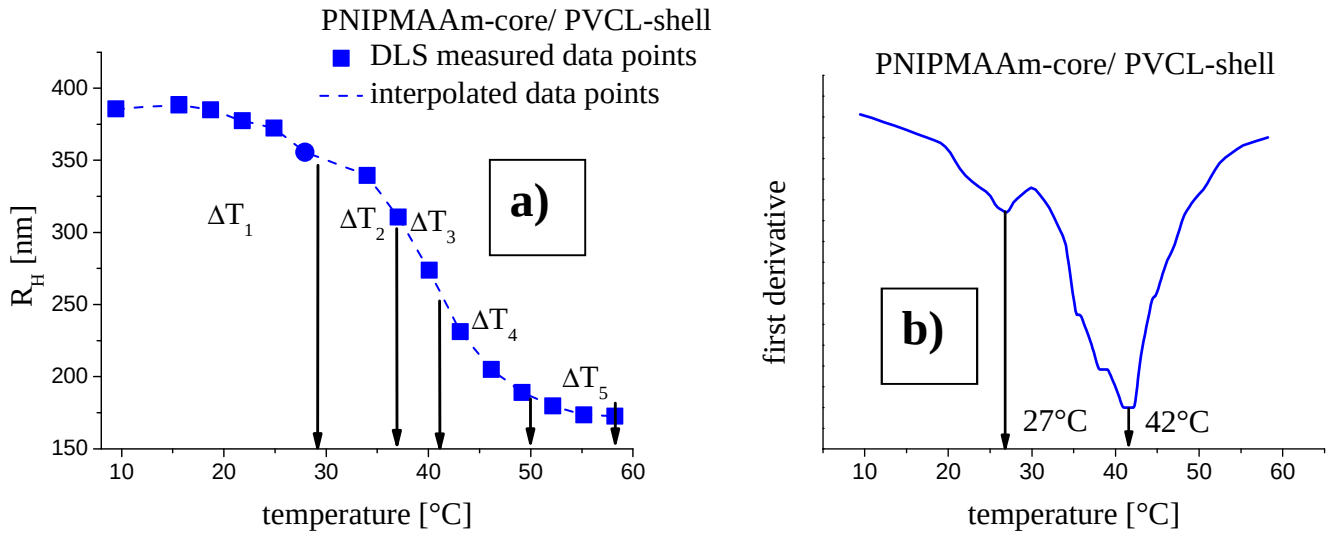

Figure 4.19 a) Dynamic light scattering measurement of PNIPMAAm-core/ PVCL-shell microgel and the temperature intervals for the evaluation of the radius scaling factors ρ_i. The dashed line is the interpolation used to fit the Flory state equation. b) First derivative of the volume temperature transition curve revealing different transition temperatures of the microgel components.[g]

Table 4.9 Transition temperatures of homopolymer and core-shell microgels determined from DLS measurements.[g]

Microgel	T_{c1} [°C]	T_{c2} [°C]
PVCL homopolymer	29	
PNIPMAAm homopolymer		46
PVCL-core/ PNIPMAAm shell	29	42
PNIPMAAm-core/ PVCL-shell	27	42

4.3.2 The temperature dependence of the radial scale factor

The aim is to investigate correlated morphological changes into the process of volume phase transition of the structural components of the core-shell microgel particle by applying the Flory-Rehner swelling theory modified for core-shell morphology as presented in Chapter 3, theory section 3.4. Using the state equation (Eq. (3.31)) to fit the experimental data obtained by dynamic light scattering of the hydrodynamic radius evolution with temperature information related to the individual transition of the structural components can be determined, through the ρ parameter, which is the radial scale factor, the ratio between the radius of the core and the hydrodynamic radius (Eq. (3.25)). In order to have all information needed for the core-shell microgels, I first have to find the characteristic swelling parameters of the homopolymer microgels. For this purpose the dynamic light scattering data was fitted with the Flory-Rehner state equation for homopolymer microgel, described by Eq. (3.7) in theory section 3.1. In this way the characteristic parameters *A*, Θ, χ_1, and ϕ_0, for each homopolymer microgel, are determined and it is assumed that they don't change in the core-shell morphology. In the framework of this approach the number of subchains, *N*, for the core component is also determined. For the shell component I estimate the value of *N* considering that the same amount of subchains will be formed for the same polymeric microgel on the

same volume, in this case a hollow sphere. The values of these parameters are shown in Table 4.10 for PVCL and PNIPMAAm microgels. The number of subchains for the PVCL-core/ PNIPMAAm-shell microgel shell was thus calculated, $N^{shell}(PNIPMAAm) = 3.67x10^5$ and for the PNIPMAAm-core/ PVCL-shell microgel shell, $N^{shell}(PVCL) = 1.473x10^7$.

Table 4.10 Microgel network swelling parameters for homopolymer microgels.[g]

Microgel	A	Θ [K]	χ_1	ϕ_0	N
PVCL homopolymer	-7.84	309.58	0.56	0.85	$7.4x10^5$
PNIPMAAm homopolymer	-1.689	356.43	0.93	0.7	$2.07x10^6$

The radial scale factor, ρ, has an unknown dependence on temperature that can be obtained from the DLS data fitted with the extended Flory-Rehner theory for core-shell microgels. One possible approach to solve this complex problem is to use a coarse-grained approximation by dividing the total temperature interval for $R_H(T)$ in n intervals. For each temperature interval the radial scale factor is considered constant and is denoted by ρ_i for i=1-n.

The next step is to find the interfacial elastic force parameter k and the radial scale factor in the deswollen state, ρ_0, where $\rho_0 \equiv \rho_n$ corresponds to the last temperature interval, ΔT_n. For this purpose an average $\bar{\rho}$ for the entire temperature range is estimated from dynamic light scattering measurements of the core and core-shell microgels, without taking into consideration the correlations of the core and shell swelling behaviour. The values of $\bar{\rho}$ =0.8 and $\bar{\rho}$ =0.7 were used for PVCL-core/ PNIPMAAm-shell and PNIPMAAm-core/ PVCL-shell microgels, respectively. By fitting the experimental data using the core and shell

parameters (Table 4.10) determined from homopolymer fits and considering a constant $\bar{\rho}$ for the whole temperature range, instead of ρ_i in Eq. (3.31), ρ_0 and k are determined. The quality of the fits (Fig. 4.20a and b) in the double transition area is influenced by the disregard of the different swelling behaviour of the components in this approximation. Nevertheless, the fits are good in the deswollen state, which means the radial scale factor in the deswollen state, ρ_0 can be determined, which is our goal. The fitting results for PVCL-core/ PNIPMAAm-shell were $\rho_0 = 0.75$ and $k = 5.33x10^{-11}$ N/K, and for PNIPMAAm-core/PVCL-shell $\rho_0 = 0.75$ and $k = 3.28x10^{-9}$ N/K.

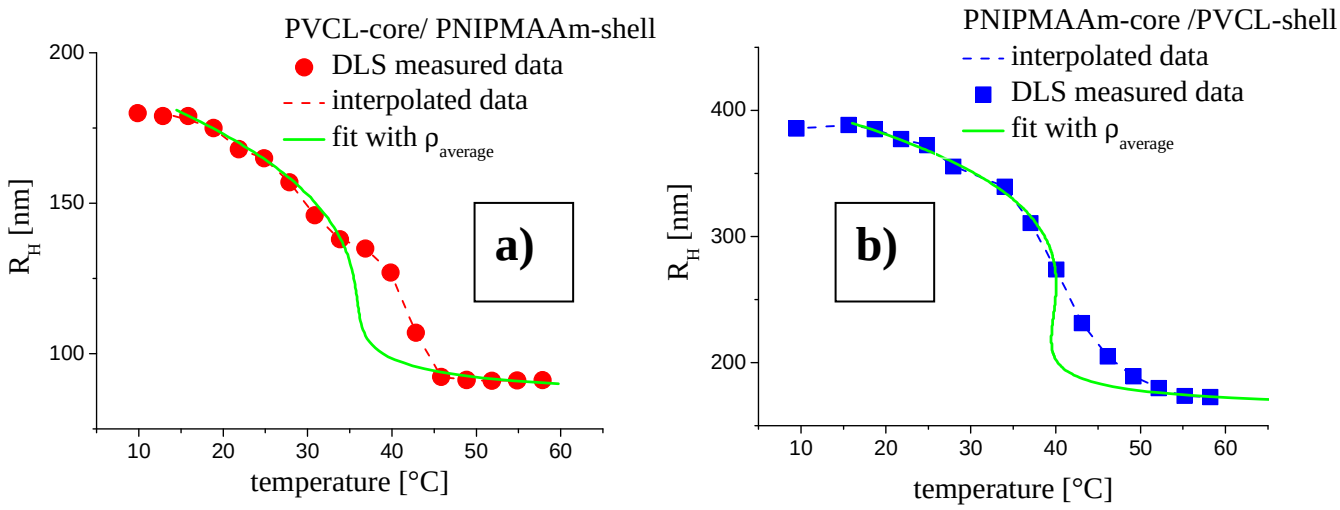

Figure 4.20 Hydrodynamic radius by dynamic light scattering fitted with Flory-Rehner volume transition theory (continuous lines) for core-shell microgels considering an average radial scale factor $\bar{\rho}$: a) PVCL-core/ PNIPMAAm-shell and b) PNIPMAAm-core/ PVCL-shell microgels.[g]

Using the coarse grained approach in order to find the radial scale parameter dependence on temperature, the temperature range has been first divided into five nonequidistant intervals ΔT_i where i=1-5. Figures 4.18a and 4.18a show the temperature intervals on the interpolated data points defined radius by arrows where the radius of the core is considered proportional to the hydrodynamic for PVCL-core/ PNIPMAAm-shell and

PNIPMAAm-core/ PVCL-shell microgels, respectively. These intervals were chosen by considering regions where the profile of the transition curve doesn't change significantly, so that the approximation doesn't introduce significant errors. Furthermore, in order to demonstrate that the final result does not depend essentially on the choice of n=5 intervals, the temperature range was further divided into n=10 intervals. Eq. (3.31), and ρ_0 and k, as previously determined, were used to find ρ_i corresponding to each temperature interval. The quality of the fits (Figures 4.21a and b) on n=5 separate intervals improves considerably from the one considering an average $\overline{\rho}$ (Fig. 4.20), allowing the radius of the core to vary with respect to the hydrodynamic radius, therefore taking into account the differences in the swelling behaviour of the components. Nevertheless, there are still problems in the transition area (for ρ_4). This can be explained by the limitations imposed by the Flory swelling theory itself, and by the modifications introduced in order to account for core-shell morphology.

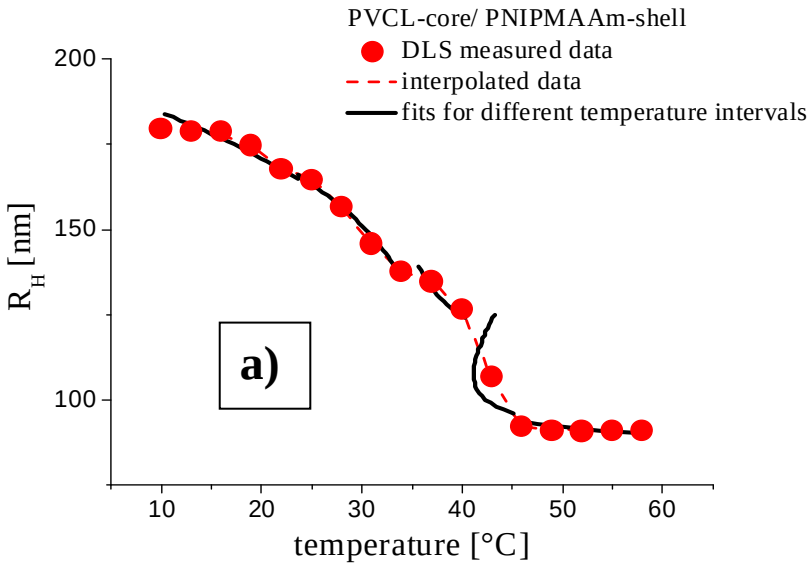

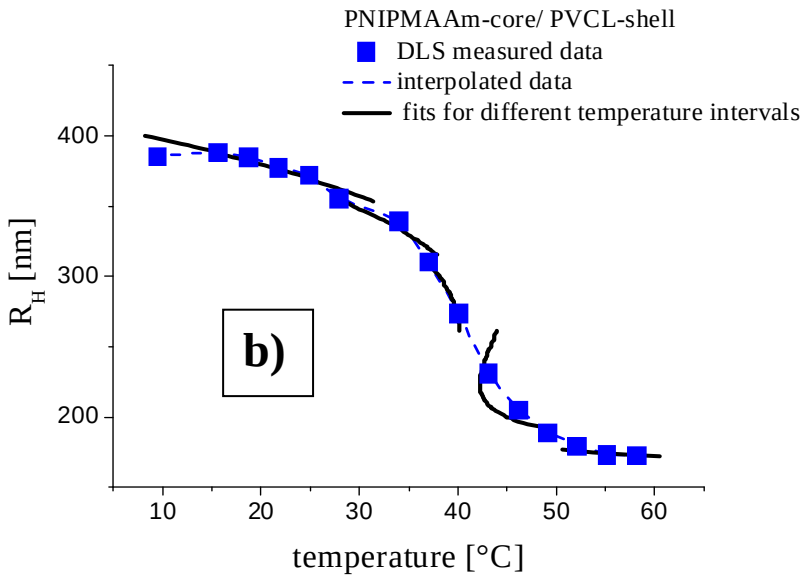

Figure 4.21 Hydrodynamic radius by dynamic light scattering fitted with Flory-Rehner volume transition theory (continuous lines) for core-shell microgels divided into temperature intervals ΔT_i (i=1-5) (see text): a) PVCL-core/ PNIPMAAm-shell and b) PNIPMAAm-core/ PVCL-shell microgels.[g]

4.3.3 Scenarios for the correlated morphological changes of core-shell microgels.

Figures 4.22 and 4.23 show the morphological changes of the core-shell microgel systems, i.e., the individual behaviour of the core-shell components reflected in the change of the radial scale factor with temperature for *n*=5 (Fig. 4.22a and 4.23a) and *n*=10 (Fig. 4.22b and 4.23b) temperature intervals considered in the coarse grained approach. For the PVCL-core/ PNIPMAAm-shell microgel the core component PVCL, shrinks in the first temperature intervals because the volume transition temperature for PVCL begins first. Results show this by a decrease in the ratio of the radius of the core and the hydrodynamic radius (Fig. 4.22a and b). Afterwards, the shell component, PNIPMAAm, undergoes a collapse, and the radial scale factor increases. In the last intervals the shell component, already collapsed makes the radial scale factor continue to increase slowly. Figure 4.22c shows the pictorial diagram of the morphological changes with temperature in the PVCL-core/ PNIPMAAm-shell microgel.

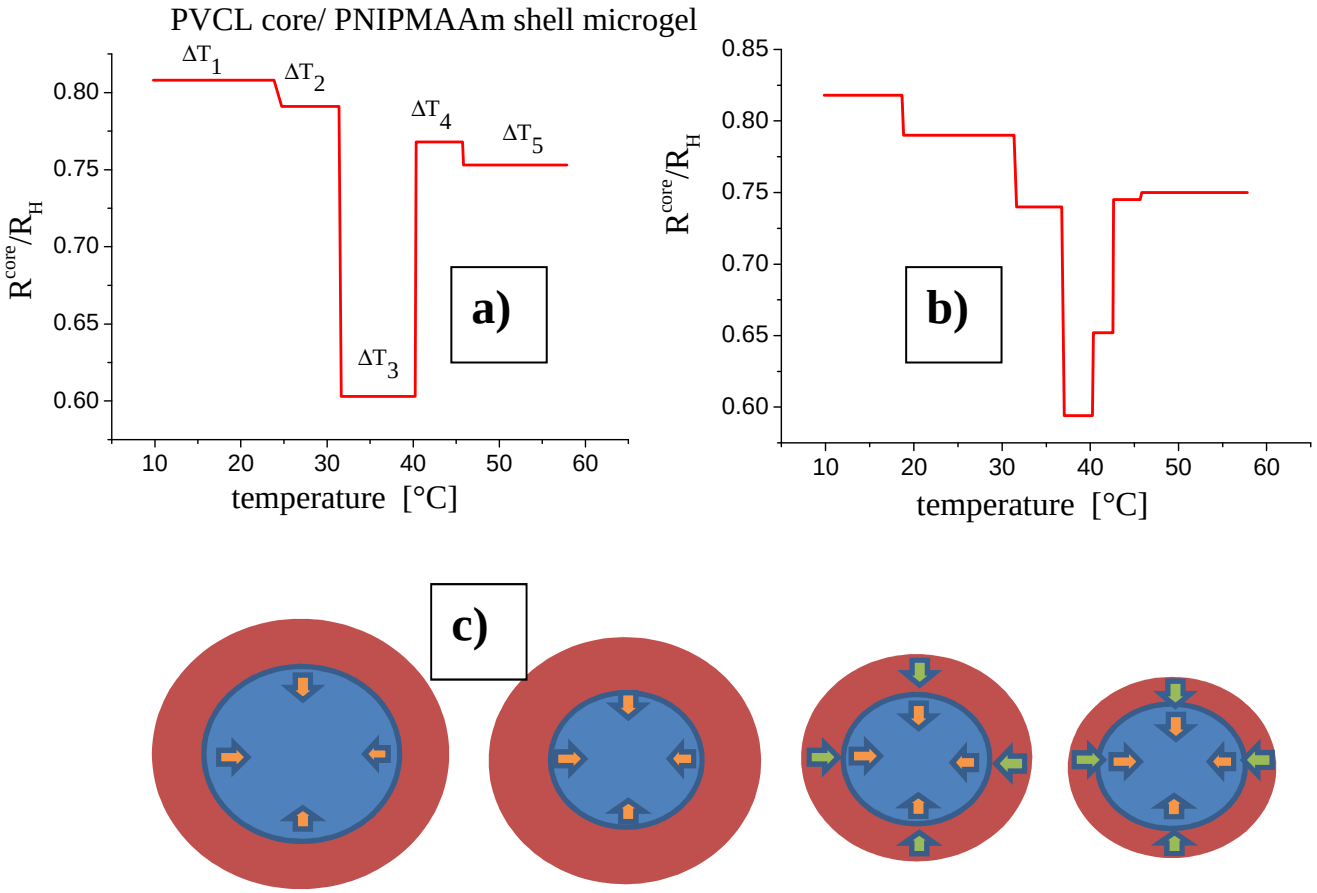

Figure 4.22 a) Variation of the radius scaling parameter R^{core}/R_H with temperature for n=5 intervals and b) for n=10 intervals obtained by dividing in two the n=5 intervals for PVCL-core/ PNIPMAAm-shell microgel. c) Pictorial representation of the evolution of the core and hydrodynamic radius. The arrows in the pictorial diagram of the morphological changes symbolize the collapse processes of the components due to deswelling in different temperature intervals.[g]

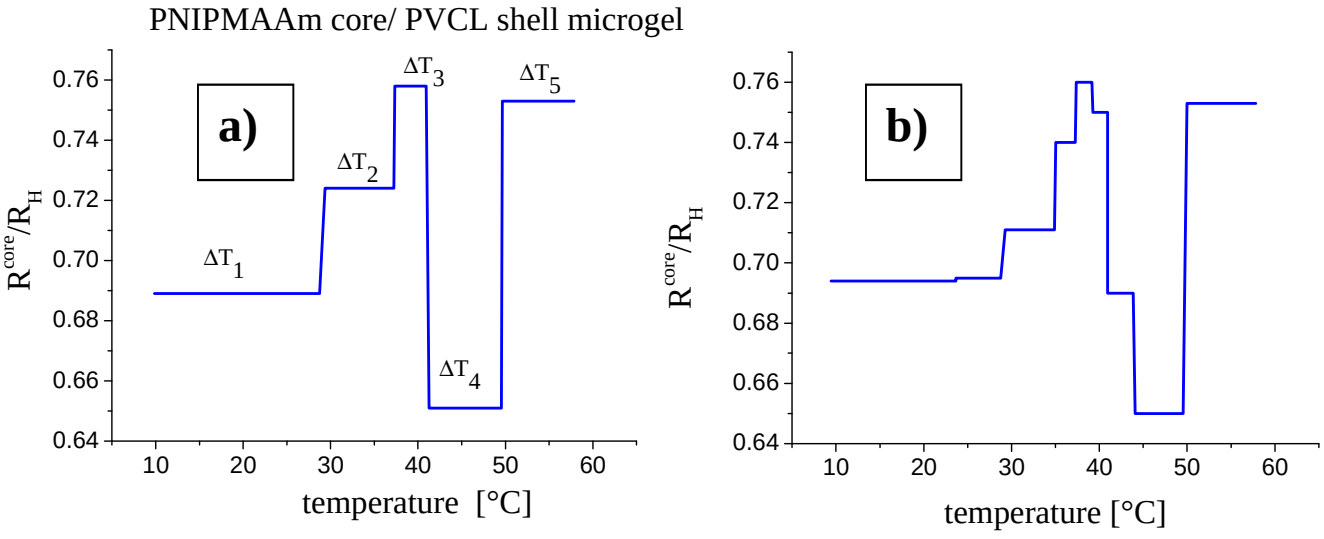

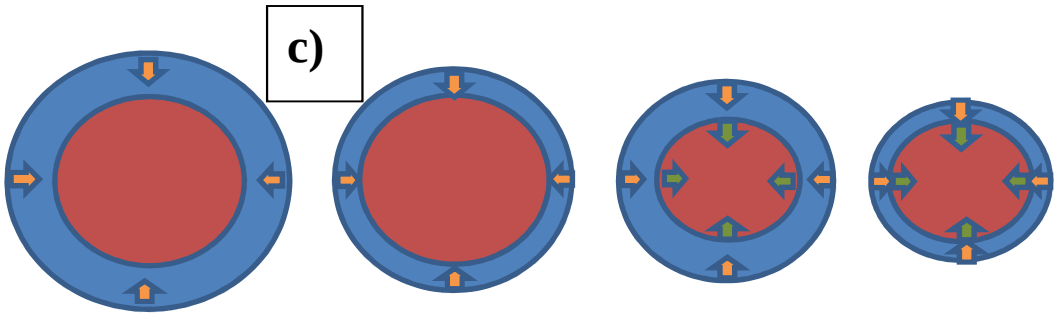

Figure 4.23 a) Variation of the radius scaling parameter R^{core} / R_H with temperature for *n*=5 intervals and b) for *n*=10 intervals in the case of PNIPMAAm-core/ PVCL-shell microgel. c) Pictorial representation of the evolution of the core and hydrodynamic radius. The arrows in the pictorial diagram of the morphological changes symbolize the collapse processes of the components due to deswelling in different temperature intervals.[g]

In the case of PNIPMAAm-core/ PVCL-shell microgel the first changes in the morphology take place in the shell. Hence, the results show that only the shell shrinks in the first temperature intervals, which can be seen from an increase in the ratio of the radius of the core to the hydrodynamic radius in Figure 4.23a and b. Afterwards, the PNIPMAAm core collapses decreasing its radius, and so the ratio between the radius of the core and the hydrodynamic radius decreases. In the last temperature intervals the dramatic decrease in the core stops since the PNIPMAAm component is also collapsed, so the radial scale factor increases again. Figure 4.23c shows the pictorial diagram of the morphological changes with temperature in the PNIPMAAm-core/ PVCL-shell microgel. It is clear from comparing the profile of the radial scale parameter dependence on temperature for *n*=5 and *n*=10 intervals, for both microgel systems, that the trend is very similar. This proves that the choice of the intervals does not affect the radial scale factor dependence on temperature. Moreover, the accuracy of the method increases with more intervals considered.

Under the assumption that some of the parameters characteristic for homopolymer microgels (Table 4.10) have different values in the core-shell morphology, several attempts to improve the quality of the fits were made: (i) the volume fraction in the deswollen state (ϕ_0)

for both components of core-shell was considered a free parameter, but because these parameters appear in Eq. (3.31) at different powers, it is impossible for the function to fit the experimental data; (ii) the values of ϕ_0 for both components were manually changed, but the fits didn't improve, and the values obtained did not have physical meaning; (iii) the interaction parameters χ_1 for core and shell were considered as free fitting parameters, the fits improved, but the physical meaning of the evolution of the radial scale factor with temperature (see Figures 4.22 and 4.23) disappeared. Therefore, I have concluded that to my knowledge the method described above gives the best fits possible, keeping the physical meaning of the resulting parameters, and providing a believable scenario for the evolution of the components of the microgel particle with temperature.

It is obvious from Eq. (3.31) that $R_H(T)$ is an equation of the ninth degree, a multi-valued function, with nine solutions. The value of R_H at equilibrium corresponds to the lowest minimum of free energy. Nevertheless, there are R_H for which there are two or more minima with the same value of free energy, and a discrete volume-transition takes place, which explains the behaviour of the fitting function in the transition area of 40-50 °C (Figures 4.21a and b). Such results were reported previously in literature for weakly ionized gels, (see Ref. 4(18) and references therein).

The results presented in this section were described by Balaceanu *et al.*[g]

5.4 Conclusions

In the first study the effect of the crosslinker amount was investigated using DLS for a series of PVCL microgel systems. The decrease of the swelling degree with crosslinker amount shows that the particles become more compact. The Flory thermodynamic theory for temperature-induced volume transition of microgels was applied in the approximation of a homogenous morphology for the series of homopolymer PVCL microgels with different

amounts of crosslinker in water for the first time. The number of subchains in a microgel particle (N), polymer volume fraction in the deswollen state (ϕ_0) and the parameters A, Θ, and χ_1 of the Flory polymer-water interaction were determined from microgel size-temperature fits measured by DLS. Therefore, the temperature dependence of the Flory interaction parameter χ for PVCL/water system was determined. Moreover, parameters of interest for the temperature phase transition of PVCL microgels were calculated, the entropic and enthalpic energies.

Proton transverse relaxation NMR experiments showed the existence of morphology heterogeneity in PVCL homopolymer microgels. A bimodal dynamic structure was detected with a core and corona components for the crosslinked microgel systems under investigation. Therefore, a generalization of swollen/deswollen Flory theory was proposed based on the two morphology components described by different degree of crosslinking and the assumption of temperature-independent proportionality of the core radius to the hydrodynamic microgel radius. Using this new equation of state the heterogeneity parameters of interest for the PVCL microgel systems are calculated: ϕ_0^{core}, ϕ_0^{corona}, N^{core}, N^{corona} and the ratio (ρ) between the measured microgel radius (R_H) and the radius of the core (R_H^{core}) (Table 4.5). The most probable heterogeneity parameters derived from generalized Flory theory were selected by microscopic constraints imposed by ^{1}H transverse relaxation and thermodynamic constraints derived from the homogeneous equation of state. The number of subchains for core and corona and the ratio between the radius of the core and the hydrodynamic radius reflect the degree of heterogeneity inside the particle.

The proof of validity for the equation of state Eq. (3.19), derived for a heterogeneous morphology stands on several arguments. In the limit when the number of corona subchains goes to zero the generalized equation of state agrees with the classical Flory-Rehner

relationship Eq. (3.7). Moreover, the hydrodynamic radius-temperature data were fitted well with this new equation of state assuming Flory interaction parameters obtained by the homogeneous morphology approach. The weighted average number of subchains and polymer volume fractions obtained from the heterogenous Flory-Rehner theory are in quantitative agreement with the values obtained based on the classical homogenous approach. That proved *a posteriori* the validity of the assumptions made for the derivation of equation of state for a homopolymer microgel showing a heterogeneous morphology.

Some limitations of the NMR relaxation approach and Flory theory are *inter alia*: (i) the coefficients C_i are underestimated because of the NMR spectrometer dead time; (ii) the Eq. (3.19) is valid in the approximation of Gauss distribution of the end-to-end vectors that is valid at low crosslinking densities;[4(14)] (iii) the contribution of the dipolar interaction modulation by the microgel tumbling in the solvent to the transverse relaxation rate is neglected in Eq. (4.3); (iv) the elastic energy is overestimated in the Flory theory because the ideal chain conformation entropy is assumed, and (v) the correlations between monomers along the polymer chain are omitted.[4(19)]

In the second study the morphology of two chemically different copolymer systems was investigated using Flory temperature transition theory in the heterogeneous approximation and NMR transverse relaxation measurements. In spite of several approximations used in the theoretical model a quantitative characterisation of copolymer microgel structural heterogeneity is accomplished. The steps used in this approach are summarised bellow. (i) The Flory thermodynamic theory for temperature-induced volume transition of microgels was applied in the approximation of a homogenous morphology for the homogeneous homopolymer microgels in water. The number of subchains in a microgel particle (N), polymer volume fraction in the deswollen state (ϕ_0) and the parameters A, Θ, and χ_1 of the Flory polymer-water interaction were determined from microgel size-temperature

fits measured by DLS. (ii) The homogeneous approximation was also used for the copolymer systems, by considering a Flory interaction parameter consisting of the two contributions. The results were used to approximate the heterogeneous model parameters. (iii) Proton transverse relaxation NMR experiments showed model free the existence of morphology heterogeneity in the copolymer microgels. A bimodal dynamic structure was detected with a core and corona components for the copolymer microgel systems under investigation. Therefore, a generalisation of the Flory temperature transition theory was proposed based on the two morphology components described by a different degree of crosslinking and the assumption of temperature-independent proportionality of the core radius to the hydrodynamic microgel radius. Using this new equation of state the heterogeneity parameters of interest for the PVCL-PNIPAAm and PVCL-PNIPMAAm microgel systems were calculated: ϕ_0^{core}, ϕ_0^{corona}, N^{core}, N^{corona} and the ratio (ρ) between the measured microgel radius (R_H) and the radius of the core (R_H^{core}) (Table 4.8). The most probable heterogeneity parameters derived from generalized Flory theory were selected by microscopic constraints imposed by ^{1}H transverse relaxation and thermodynamic constraints derived from the homogeneous equations of state. The number of subchains for core and corona and the ratio between the radius of the core and the hydrodynamic radius reflect the degree of heterogeneity inside the particle for the two copolymer systems. The parameters describing the structural heterogeneity are similar but not identical for the two copolymer microgels. The presence of PVCL component at the molar concentration investigated diminishes the expected differences due to the presence of PNIPAAm and PNIPMAAm.

The proof of validity for the equation of state Eq. (3.20), derived for a copolymer heterogeneous morphology stands on several arguments. In the limit of only one component, i.e., w=1 and the number of corona subchains going to zero, the generalized equation of state

agrees with the classical Flory-Rehner relationship Eq. (3.7). Moreover, the hydrodynamic radius-temperature data were fitted well with this new equation of state assuming Flory interaction parameters obtained by the homogeneous morphology approach. That proved *a posteriori* the validity of the assumptions made for the derivation of equation of state for a copolymer microgel showing bimodal heterogeneous crosslink morphology.

In the last study I am investigating newly synthesized reverse core-shell temperature responsive microgel systems, composed of poly(*N*-vinylcaprolactam) and poly(*N*-isopropylmethacrylamide), to gain knowledge regarding the confinement effects on the swelling/deswelling of individual components in the microgel particle. The Flory-Rehner volume temperature transition theory was extended for the core-shell morphology microgels, taking into account the dependence on temperature of the radial scale factor, the ratio between the radius of the core and the hydrodynamic radius. This was done using the coarse-grained approximation, dividing the temperature range of the temperature transition curve into intervals. The newly developed core-shell Flory state equation was used to fit experimental dynamic light scattering data showing the hydrodynamic radius dependence on temperature. Using this simple method access is gained to quantitative information about the swelling behaviour of the confined core compared to the swelling behaviour of the entire particle. Furthermore, the theory developed allows an estimation of the force of confinement that influences the transition of the core due to the transition of the shell.

The swelling/deswelling behaviour of the individual components of core-shell microgels with temperature can be investigated directly by performing small-angle neutron scattering (SANS) measurements at different temperatures. Such investigations were performed on core-shell microgels[4(20)] and on homopolymer microgels with heterogeneous core-corona crosslinking[4(3)]. In the first reference the core-shell particles are investigated at three different temperatures, but a profile of the swelling behaviour of the components is not

reported. The second reference reports the differences between the swelling behaviours of the differently crosslinked morphological components, and even if the microgel is a homopoylmer the authors find significant profile swelling differences between components. The major drawback of SANS is the necessity to use predeuterated polymers that is not the case for the DLS, NMR or DSC techniques.

I introduced in this work an indirect method of analysing the swelling profile of the differently thermosensitive components of core-shell microgel particles, by means of dynamic light scattering data fitted with the generalized core-shell Flory-Rehner transition theory. The results of the radial scale parameter dependence on temperature show a predictable temperature behaviour, which proves *a posteriori* the model used and the theoretical treatment. The novelty and the value of developing the core-shell Flory swelling theory is that it gives semiquantitative information about the individual temperature behaviour of the components. The temperature interval where the components undergo temperature transition, which is influenced by the restrains and interactions imposed by the core-shell morphology, can be estimated. The theoretical treatment also allows determination of the size of the core relative to the total hydrodynamic radius at different temperatures. The interaction force between the two morphological components can also be determined. Nevertheless, from Fig. 4.21 it is evident that the modified Flory-Rehner theory is not able to describe accurately the dependence of hydrodynamic ratio on temperature in the temperature range of 40 °C – 50 °C, which is dominated by the volume transition of PNIPMAAm. The theoretical method has limitations because it is based on several assumptions, such as from the Flory-Rehner theory itself, and the coarse-grained approach used for the dependence of the radial scale factor on temperature. Nevertheless, the availability of the method and the relevant semiquantitative morphological information that can be obtained recommend it for stimuli responsive core-shell microgel systems.

References

4(1) Wu, X.; Pelton, R.H.; Hamielec, A.E.; Woods D.R.; McPhee W. *Colloid Polym. Sci.* **1994**, *272*, 467.

4(2) Varga, I.; Gilanyi, T.; Meszaros, R.; Filipcsei, G.; Zrinyi, M. *J. Phys. Chem. B,* **2001**, *105*, 9071.

4(3) Fernández-Barbero A.; Fernández-Nieves A.; Grillo I.; López-Cabarcos E. *Phys. Rev. E***2002**, *66*, 051803.

4(4) Saunders, B.R. *Langmuir,* **2004**,*20*, 3925.

4(5) Mason, T.G.; Lin, M.Y. *Phys Rev E,* **2005**, *71*, 040801 (R).

4(6) Stieger, M.; Richtering, W.; Pedersen, J.S.; Linder, P. *J. Chem. Phys.* **2004**, *120*, 6197.

4(7) Guillermo, A.; Cohen Addad, P.J.; Bazile, J.P.; Duracher, D.; Elaissari, A.; Pichot,C. *J. Polym. Sci.: Part B: Polym. Phys.* **1999**, *38*, 889.

4(8) Ru, G.; Wang, N.; Huang, S.; Feng, J. *Macromolecules,* **2009**, *42*, 2074.

4(9) Senff, H.; Richtering, W. *Colloid Polym. Sci.* **2000**, *278*, 830-840.

4(10) Inomata, H.; Wada, N.; Yagi, Y.; Goto, S.; Saito, S. *Polymer*, **1995**, *36*, 875.

4(11) Cohen Addad, J.P. *NMR and Fractal Properties of Polymeric Liquids and Gels*, in *Prog.Nucl.Magn.Reson.Spec*. **1993**, *25*, 1.

4(12) Demco, D.E.; Hafner, S.; Spiess, H.W. in *Handbook of Spectroscopy of Rubbery Materials*, Repra Technology Ltd., Shawbury, UK, 2002.

4(13) Sotta, P.; Fülber, C.; Demco, D.E.; Blümich, B.; Spiess, H.W. *Macromolecules,* **1996**, *29*, 6222.

4(14) Fechete, R.; Demco, D.E.; Blümich, B. *J. Chem. Phys*. **2003**, *118*, 2411.

4(15) Lietor-Santos, J.J. ; Sierra-Martin, B.; Vavrin, R.; Hu, Z.; Gasser, U.; Fernandez-Nieves, A. *Macromolecules*, **2009**, *42*, 6225.

4(16) Ilavsky, M.; Mamytbekov, G.; Sedalkova, Z.; Hanykova, L.; Dušek, K. *Polym. Bull.* **2001**, *46*, 99.

4(17) Tirumala, V. R.; Ilavsky J.; Ilavsky, M. J. *Chem. Phys.* **2006**, *124*, 234911.

4(18) Quesada-Perez, M.; Maroto-Centeno, J.A.; Forcada, J.; Hidalgo-Alvarez, R. *Soft Matter*, **2011**, *7*, 10538-10547.

4(19) Rubinstein, M.; Colby, R.H. *Polymer Physics*, Oxford University Press, New York 2003.

4(20) Berndt, I.; Pedersen, J.S.; Lindner, P.; Richtering, W. *Langmuir*, **2006**, *22*, 459-468.

5 Microgel characterisation studies

Different characterisation studies on microgel systems with different morphologies are presented in this chapter. Some of the studies are preliminary investigations, and more effort should be made in order to fully understand the implications of the results presented. Nevertheless, all the studies have value and introduce novel ideas and results.

5.1 Copolymer microgels of *N*-vinylcaprolactam and *N*-isopropylacrylamides

For this study[f] I designed copolymer microgels by copolymerization of *N*-vinylcaprolactam (VCL) in combination with (*N*-isopropylacrylamide (NIPAAm) or *N*-isopropylmethacrylamide (NIPMAAm)) under precipitation conditions in water. The molar ratio between the monomers in the synthesis mixture was varied from 1:5 to 5:1. Using NMR and Raman spectroscopy I determined the chemical composition of PVCL-PNIPAAm and PVCL-PNIPMAAm copolymer microgels reflecting the initial monomer ratio in the reaction mixture. ^{1}H transverse magnetization relaxation NMR was used to investigate the heterogeneity of the microgel structure in terms of the distribution of the monomer units, showing that VCL, NIPAAm or NIPMAAm monomers are randomly distributed in the polymer networks. The investigation of the volume phase transition temperature (VPTT) for copolymer microgels was performed by dynamic light scattering, liquid and solid-state NMR and differential scanning calorimetry.

The synthesis procedure of the copolymer microgels is presented in Chapter 2, synthesis section 2.1.2. The different microgel samples will be referred to in text according to the theoretical molar ratio between the monomers, for example PVCL-PNIPAAm 1:1.

Some of the results and the descriptions in this chapter were presented by Balaceanu *et al.*[f]

5.1.1 Chemical composition of microgels determined by ^{1}H NMR and Raman-Spectroscopy

The ^{1}H NMR spectra for the microgel sample PVCL-PNIPAAm 1:1 is presented in Figure 5.1. By integrating the peaks corresponding to a specific functional group in each monomer, namely CH_2 protons in PVCL (assigned as R_2) and CH_3 protons in PNIPAAm (assigned as R_1), I have obtained the real molar ratio of VCL and NIPAAm in the copolymer structure (Table 5.1).

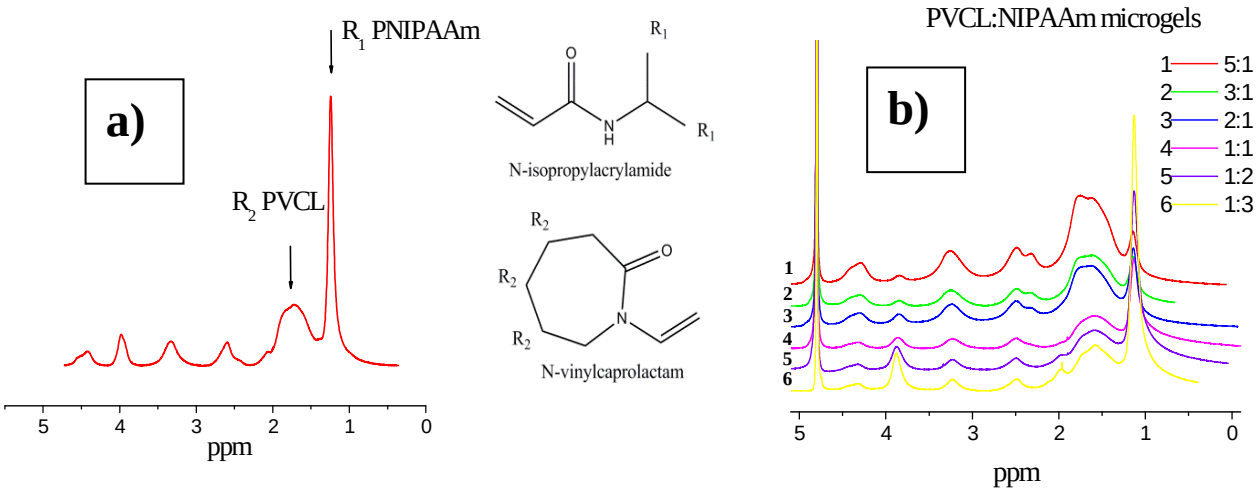

Figure 5.1 Proton MAS NMR spectra: a) PVCL-PNIPAAm 1:1 microgel and b) PVCL-PNIPAAm microgels with different molar ratios (T=22°C).[f]

Due to the overlap of the peaks corresponding to CH_2 protons in PVCL (assigned as R_2) and CH_3 protons close to the vinyl bond in PNIPMAAm (assigned as R_3) (Figure 5.2) the determination of the copolymer composition by ^{1}H NMR for this system was hindered. Therefore, I have used Raman spectroscopy to evaluate the chemical composition of PVCL-PNIPMAAm microgels. The intensities of characteristic peaks for VCL and NIPMAAm at 689-703 cm^{-1} and 950 cm^{-1}, respectively, were used for the calculation of the chemical composition (Figure 5.3).

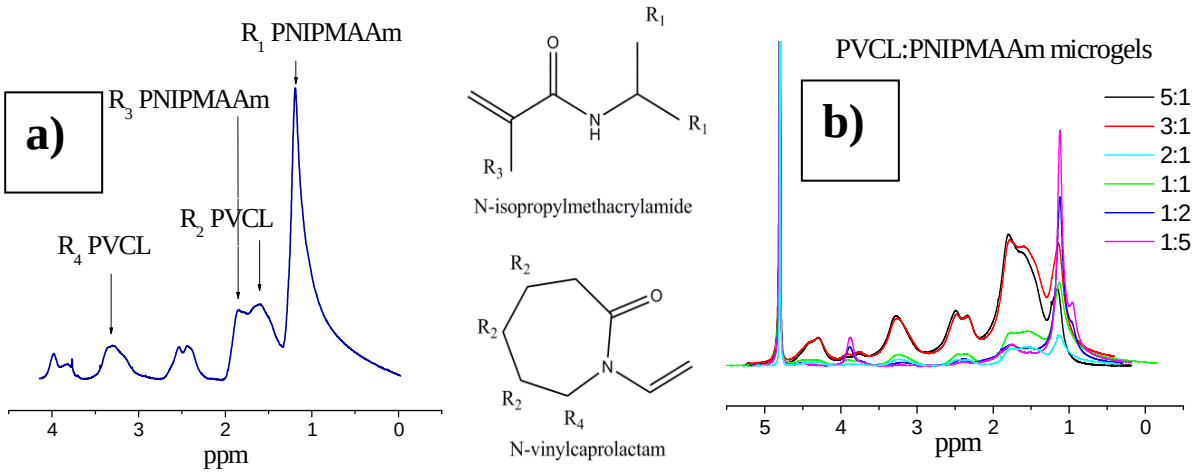

Figure 5.2 Proton MAS NMR spectra: a) PVCL-PNIPMAAm 1:1 microgel and b) PVCL-PNIPMAAm microgels with different molar ratios (T=22°C).[f]

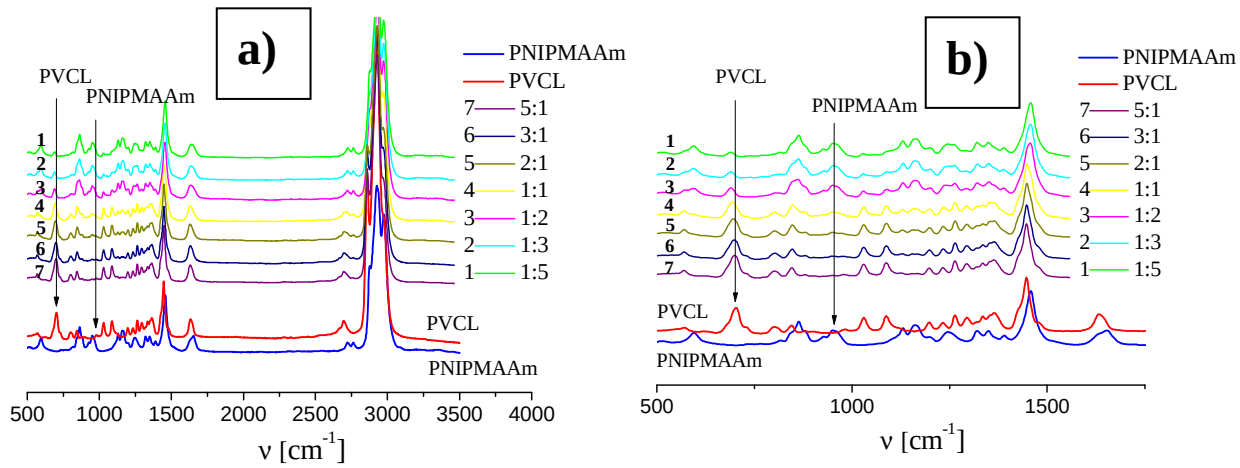

Figure 5.3 Raman spectra of PVCL-PNIPMAAm microgels and PVCL and PNIPMAAm homopolymer microgels, a) entire frequency region; b) region of interest.[f]

The summary of the experimental results from NMR and Raman Spectroscopy are given in Table 5.1 and Figure 5.4. It is obvious that the chemical composition of the copolymer microgels agrees very well with the initial monomer composition in the reaction mixture. This shows a possibility of flexible variation of the microgel chemical structure by adjustment of the monomer ratio in the polymerization process.

Table 5.1 Measured monomer composition in PVCL-PNIPAAm and PVCL-PNIPMAAm microgels.[f]

Sample	VCL/NIPMAAm/NIPMAAm [mol:mol]^{theor}	VCL/NIPAAm [mol:mol]^{meas}	VCL/NIPMAAm [mol:mol]^{meas}
1	5	4.6	5.04
2	3	2.9	3.04
3	2	2.3	1.87
4	1	1.01	1.08
5	0.5	0.55	0.48
6	0.33	0.4	0.33
7	0.2	0.3	0.2

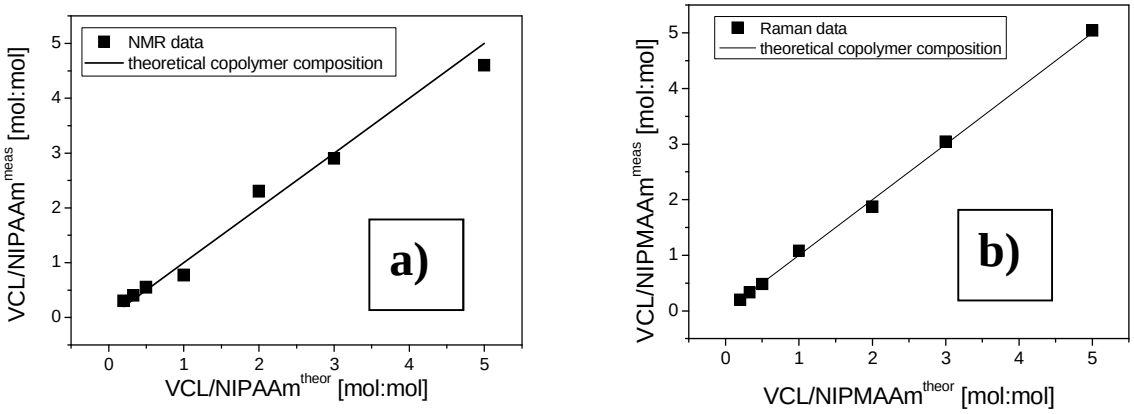

Figure 5.4 Correlation between the monomer ratio in reaction mixture and in copolymer structure for PVCL-PNIPAAm a) and PVCL-PNIPMAAm b) microgels. Solid lines represent theoretical correlation between monomer ratio in reaction mixture and in copolymer structure.[f]

To address the question of the copolymerisation process in the present system I performed a kinetic experiment for the PVCL-PNIPAAm 1:1 system. Samples of the solution were taken from the reactor at different time intervals after the addition of the initiator. The solid content was measured after freeze drying (gravimetrical analysis), and the samples were analysed with quantitative ^{1}H NMR to determine the chemical composition. The experimental data presented in Figure 5.4 suggest that the copolymerization process is fast and the monomer conversion of 85% is achieved after 20 min reaction time. Then the conversion increases slowly and reaches 90% after 120 min.

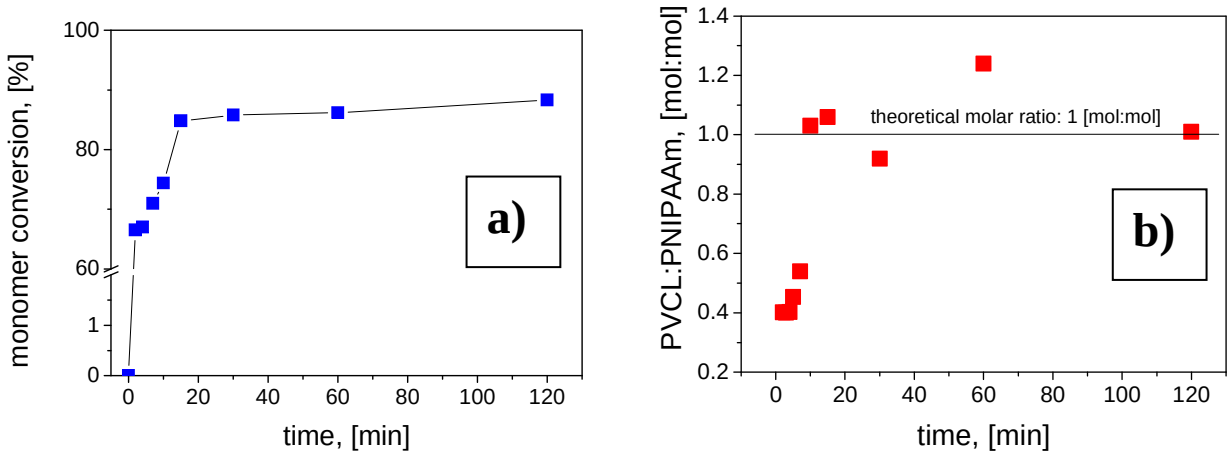

Figure 5.4 Monomer conversion (a) and chemical composition (b) as a function of reaction time for PVCL-PNIPAAm 1:1 microgel[f]

Interestingly, the evolution of the chemical composition of the formed copolymers (Figure 5.4b) shows a very similar trend to the conversion time curve. The VCL-NIPAAm molar ratio increases with polymerization time and reaches the final value (close to 1) after 20 min of reaction time. This indicates that NIPAAm is the more reactive monomer and that it dominates in the copolymer structure at low conversions. Nevertheless, this gives little information concerning the internal 3D structure of the microgel particle, since entangled polymer chains create the network. For this reason I will subsequently perform a transverse relaxation NMR study to determine the monomer heterogeneity inside the microgel particle. Due to the low monomer concentration in the reaction mixture it was not possible to detect more experimental points at shorter polymerization times.

5.1.2 Structural heterogeneity of the microgels by NMR

To investigate the internal microgel structure in terms of the distribution of the VCL and acrylamide units in the copolymer microgel I performed a detailed NMR study similar to the one presented in Chapter 4, results section 4.1[b,c]. To study the polymer network structure and

dynamics heterogeneities, ^{1}H NMR relaxometry, diffusometry and measurements of the residual dipolar couplings were used in the past[5(1)-5(3)]. The structural inhomogeneities inside microgel particles of PNIPMAAm were studied by ^{1}H transverse magnetization relaxation[5(4)] without any ^{1}H resolution. The chain mobility for three different types of PNIPMAAm hydrogels (normal cross-linked, comb-type grafted gel, and comb-type grafted gel with styrene-modified comb chains) has also been investigated by ^{1}H transverse magnetization relaxation (T_2)[5(5)].

The synthesis procedure of microgels leads to structural inhomogeneities (a more crosslinked core and a looser corona)[b,5(6)] that provide two different structural dynamics regions to be probed by the high-resolution site selective NMR method. To study the distribution of monomer units in microgel by NMR, the PVCL-PNIPAAm and PVCL-PNIPMAAm samples prepared at equimolar monomer ratios were used. Proton high-resolution NMR MAS spectrum of these samples were recorded (see Figures 5.1 and 5.2) and the resonance assignments were made using the ^{1}H simulated spectra obtained with Gaussian03® Simulation Package and ^{1}H liquid-state spectra of monomers measured at 400 MHz Bruker NMR spectrometer. The functional groups corresponding to each resonance can be identified in Figure 5.5. The MAS spectra show improved spectral resolution as compared to the ones measured under the static conditions.

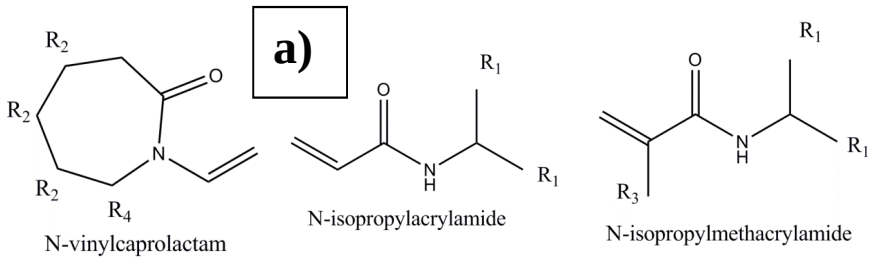

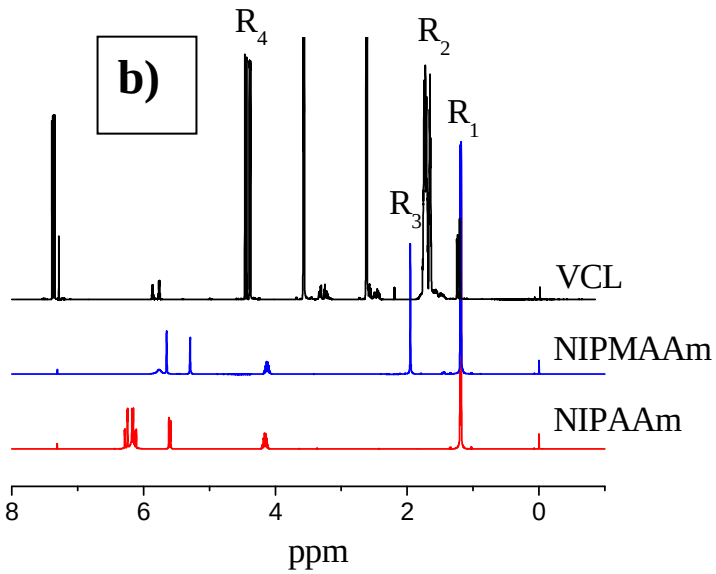

Figure 5.5 Proton NMR spectra for VCL, NIPAAm and NIPMAAm monomers.[f]

The proton Hahn-echo decays measured chemically site selective for the NMR lines of PVCL, PNIPAAm and PNIPMAAm are shown in Figure 5.6 for the PVCL-PNIPAAm 1:1 system and in Figure 5.7 for PVCL-PNIPMAAm 1:1 system. A biexponential decay for all the resonances is assumed, i.e.,

$$\frac{S(t)}{S(0)} = c_1 \exp\left\{-\frac{t}{T_{2s}}\right\} + c_2 \exp\left\{-\frac{t}{T_{2l}}\right\}, \qquad (5.1)$$

where $S(t)/S(0)$ is the normalized NMR signal integral as a function of spin-echo time t, c_i (i=s and l) are the relative contribution of the decays characterized by short (T_{2s}) and long (T_{2l}) transverse relaxation times. The errors of the fits are below 5%.

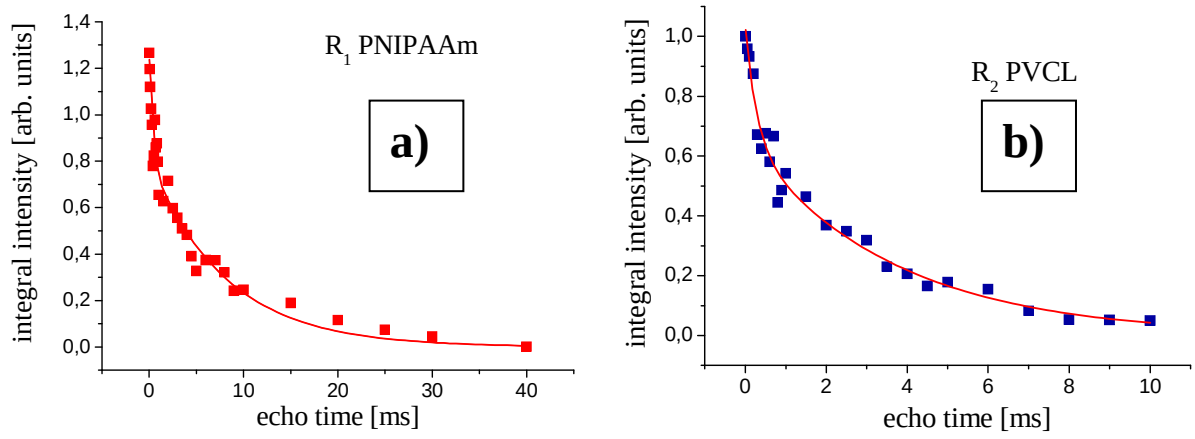

Figure 5.6 Hahn-echo decay curves for PVCL-PNIPAAm 1:1 microgel (R_1 NIPAAm spectrum line; R_2 VCL spectrum line).[f]

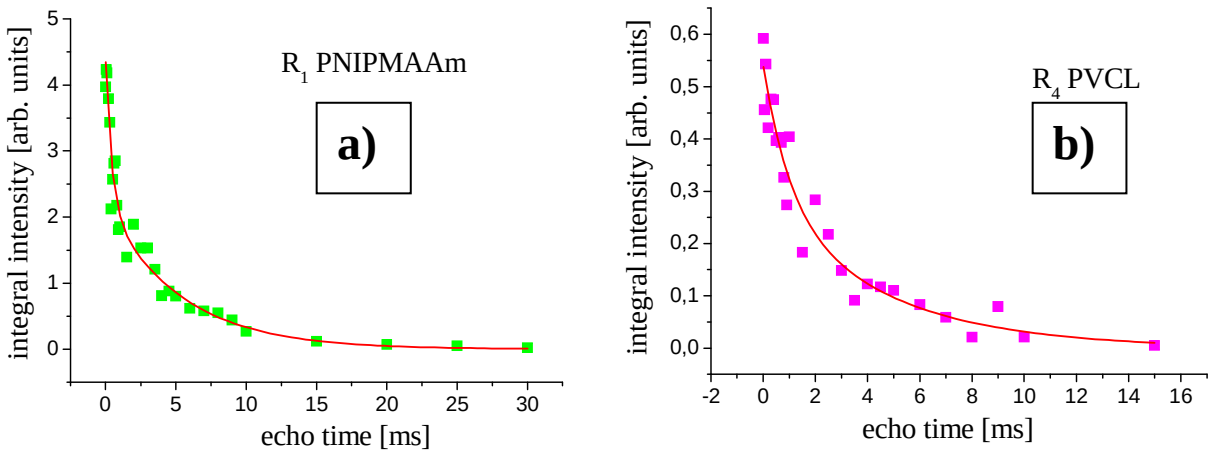

Figure 5.7 Hahn-echo decay curves for PVCL-PNIPMAAm 1:1 microgel (R_1 PNIPMAAm spectrum line; R_4 VCL spectrum line).[f]

The values of the ^{1}H transverse relaxation times and coefficients for all resonances are shown in Table 5.2. In the below analysis I assume that the transverse relaxation is dominated by the polymer network fluctuation as compared to the microgel tumbling and translation mechanisms. It is well known from the NMR relaxometry of polymer networks[5(2),5(7)] that the transverse relaxation is strongly affected by the degree of the crosslink density via residual dipolar couplings and their fluctuations. The value of T_{2s} corresponds to a network with a

larger value of the crosslink density (core of microgel particle) as compared to T_{2l} which corresponds to a loose network (corona of microgel particle). Local functional groups dynamics and the fluctuation of dipolar network contribute together to the T_2 values. Since all the decay curves can be fitted best with a biexponential fitting curve, it can be concluded that the different monomers are located both in the core and in the shell of the microgel particle. By analysing the fitting coefficients, which are proportional to the number of protons in the microgel (Table 5.2) the morphological distribution of monomers in core and corona can be found[5(2),5(3)]. Results summarized in Table 5.2 show that the number of PVCL, PNIPAAm and PNIPMAAm protons in core and corona are similar within experimental errors. From this I can conclude that the distribution of different component monomers in the PVCL-PNIPAAm and PVCL-PNIPMAAm microgels is uniform.

Table 5.2 Transverse relaxation times for PVCL-PNIPAAm 1:1 and PVCL-PNIPMAAm 1:1 microgels.[f]

Microgel	PVCL-PNIPAAm 1:1		PVCL-PNIPMAAm 1:1	
Signal	R_1 (PNIPAAm)	R_2 (PVCL)	R_1 (PNIPMAAm)	R_4 (PVCL)
T_{2S} [ms]	0.72	0.56	0.86	1.98
C_S [%]	40	38	51	45
T_{2L} [ms]	16.08	7.32	10.56	9.04
C_L [%]	60	62	49	55

Based on the experimental data presented above I can conclude that the copolymerisation of VCL and NIPAAm or NIPMAAm under precipitation conditions in aqueous phase yields microgel particles with variable copolymer compositions that can be easily adjusted by the variation of the monomer amount in the reaction mixture. The second important conclusion is that the final distribution of the monomer units in the polymer colloidal network is random

and no chemical heterogeneities or formation of core-shell structures could be detected. This means that in both PVCL-PNIPAAm and PVCL-PNIPMAAm microgels, *N*-vinylcaprolactam and acrylamide monomer units form random copolymers chemically crosslinked due to the presence of crosslinking agent in the reaction mixture.

5.1.3 Microgel size and morphology

Figure 5.8 shows hydrodynamic radii of microgels determined with dynamic light scattering at 25°C. For dynamic light scattering measurements, the polydispersity index of the sample is given by the higher orders of the cumulant method fitting of the intensity correlation function. For the systems investigated, DLS measurements give a polydispersity index of below 0.1, which shows a monodisperse particle size distribution. For the first system, PVCL-PNIPAAm the size of the microgel particle does not change significantly when the molar ratio between VCL and NIPAAm changes. This macroscopic result suggests that the interplay of interactions between water – monomer and monomer – monomer is similar for VCL and NIPAAm, leading to the same degree of swelling for microgels of different monomer ratios at room temperature. The result is in accordance with studies made on PNIPAAm and PVCL that show similar temperature dependence, with a LCST of the two polymers in the physiological range of 32 – 34 °C[5(8)-5(11)]. The fact that these two polymers have the same LCST is also due to the similarity in hydrophilic and hydrophobic interactions.

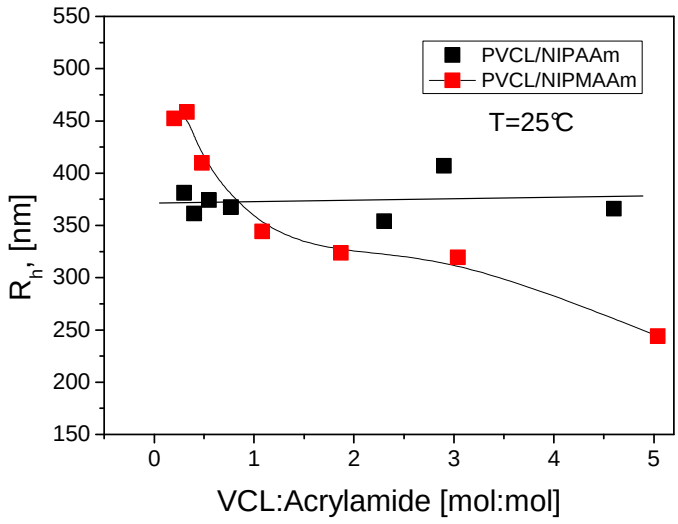

Figure 5.8 Hydrodynamic radii of PVCL-PNIPAAm and PVCL-PNIPMAAm microgels (DLS data; temperature of 25°C).[f]

On the other hand, for the PVCL-PNIPMAAm system the size of the particle increases with the relative increase of the NIPMAAm monomer from 230 nm to 470 nm. This result would suggest that the microgel particle becomes more hydrophilic with the increase of the NIPMAAm component, i.e. the NIPMAAm monomer makes the overall particle swell more in water. The result is not surprising when considering the chemical structure differences between NIPAAm and NIPMAAm. The α-methyl group in PNIPMAAm interferes with the hydrophobic interactions of the *N*-isopropyl side group, because it provides the chains more flexibility [5(12)].This is also the explanation for the fact that PNIPMAAm has a higher LCST than PNIPAAm and PVCL.

I have used AFM and TEM to investigate the microgel morphology in the dry state. Figure 5.9 shows a comparison of PVCL-PNIPAAm and PVCL-PNIPMAAm microgel samples prepared at molar ratios VCL/acrylamide 1:3 (mol:mol). PVCL-PNIPMAAm 1:3 microgels appear smaller in microscopy images with an average radius of 125 nm (the average radius of PVCL-PNIPAAm 1:3 microgels was 160 nm). The difference in size

between selected microgel samples is in a good agreement with DLS results reported in Figure 5.8. However, because the microscopy measurements are performed on dried microgel samples, the absolute values of the microgel dimensions derived from the microscopy images are much smaller compared to the light scattering results. Microscopy images show that spherical microgel particles with narrow size distribution were prepared, which is also supported by the polydispersity values of DLS measurements.

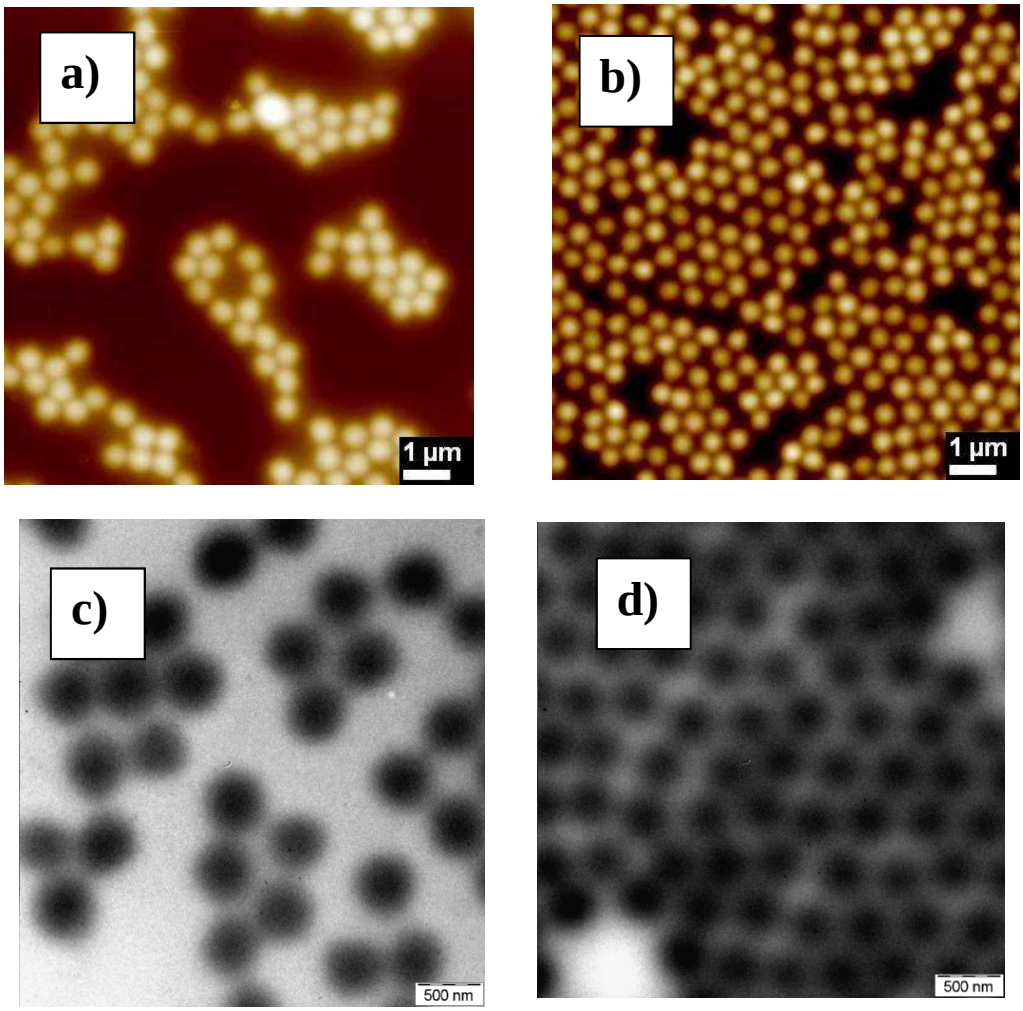

Figure 5.9 AFM images (top) a) with Δh=280 nm, b) with Δh=150 nm) and TEM images (bottom) of PVCL-PNIPAAm 1:3 a),c) and PVCL-PNIPMAAm 1:3 b),d) microgels. The average particle radii in dry state are 160 nm and 125 nm for samples a),c) and b),d), respectively).[f]

5.1.4 Volume phase transition of microgels in water

Figures 5.10a and c show the hydrodynamic radii of the microgels at different temperatures upon heating determined by dynamic light scattering. The homopolymer microgel particles of PVCL, PNIPAAm and PNIPMAAm that are shown in this graph as reference systems, are smaller than the heteropolymer ones. One reason for this is that surfactant was used for their synthesis in order to provide stability in dispersion. The increase of the temperature induces the volume phase transition for both PVCL-PNIPAAm and PVCL-PNIPMAAm microgels and results in microgel collapse. As an exception, the microgel sample PVCL-PNIPMAAm with VCL/NIPMAAm experimental molar ratio 2:1 shows some aggregation in the transition region. It can be seen that for the PVCL-PNIPAAm system, the volume phase transition temperature does not change significantly with the chemical composition and it is quite similar to the homopolymer PVCL and PNIPAAm microgels.

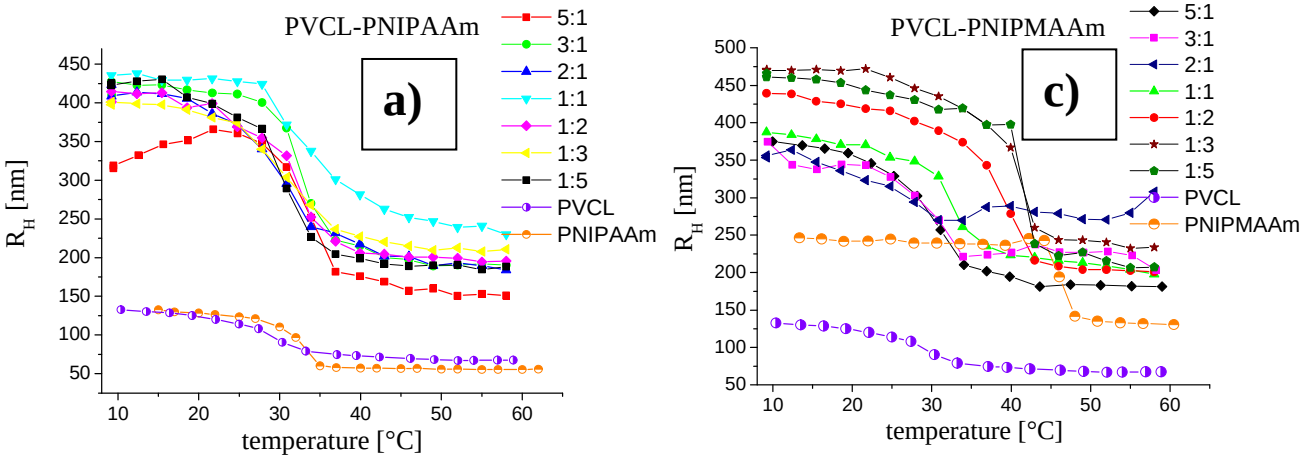

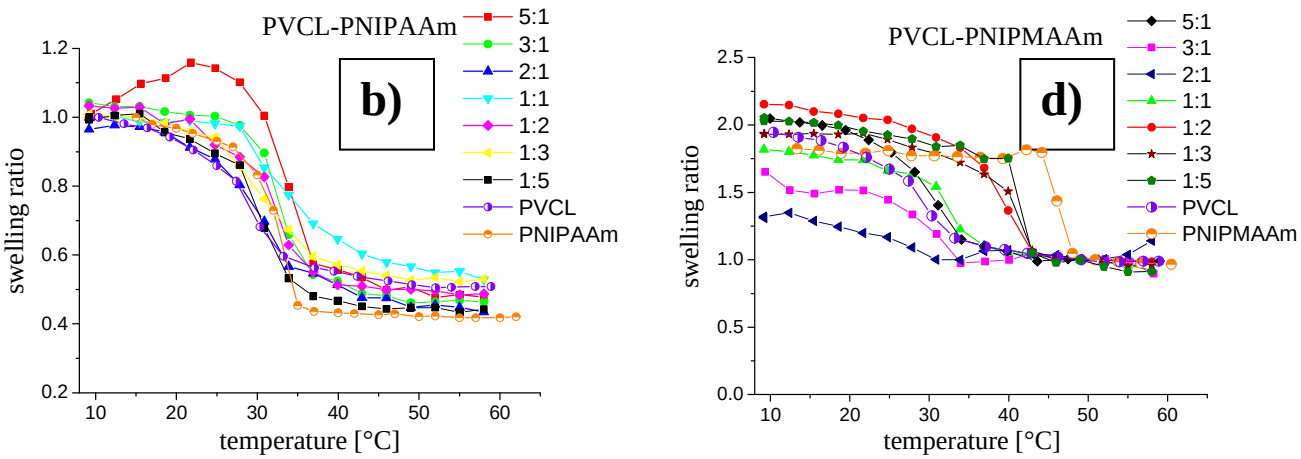

Figure 5.10 Variation of the hydrodynamic radius and swelling ratio with temperature: a),b) PVCL-PNIPAAm and c),d) PVCL-PNIPMAAm. The swelling ratio is defined as $(R_h^M/R_h^{DSW})^3$ where R_h^M = measured hydrodynamic radius at different temperatures; R_h^{DSW} = measured hydrodynamic radius for deswollen nanogels at temperature of 50 °C. Numbers in the legends indicate VCL/NIPAAm and VCL/NIPMAAm experimental molar ratios in microgels.[f]

Contrary, for the PVCL-PNIPMAAm system, the VPTT increases with increase of PNIPMAAm content. The microgels PVCL-PNIPMAAm 1:3 and 1:5 exhibit VPTT similar to PNIPMAAm sample. This is an expected result, because PNIPMAAm has a LCST of approx. 45 °C. Aqueous microgels of PVCL, PNIPAAm or PNIPMAAm form hydrogen bonds with water, which swells the particles at temperatures bellow the VPTT. At the same time these polymers have hydrophobic regions that promote the polymer-polymer interaction. Due to temperature increase, the thermal fluctuations in the polymer chains increase, the hydrogen bonds with water break and the water-polymer interactions are replaced by polymer-polymer interactions. The volume collapse of the particles for temperature sensitive microgels is an entropy driven endothermic process. The difference in PNIPAAm and PNIPMAAm is an additional α-methyl group, which has the propriety of relaxing the thermal energy of the polymer chain, providing improved flexibility. Therefore, PNIPMAAm microgels can maintain the hydrogen bonds with water to higher temperatures before seeking entropic

compensation by undergoing phase transition[5(12),5(13)]. The experimental data shown in Figure 5.10c and d suggest the increase of VPTT with increase of PNIPMAAm content in microgels.

The calculated swelling ratios for different microgel samples presented in Figure 5.10b,d suggest that the chemical composition is not influencing the swelling degree of microgels. This indicates that the hydrophilic/hydrophobic balance in polymer network is not influenced by the nature of monomer units that can reversibly form hydrogen bonds with water molecules. The swelling degree of PVCL-PNIPAAm and PVCL-PNIPMAAm microgels suggests that there is no strong influence of the acrylamide type on the microgel behaviour. Nevertheless, the swelling behaviour of PVCL-PNIPMAAm as a function of temperature is strongly influenced by the monomer composition, therefore the change in LCST.

The temperature transition in microgels can also be investigated using high-resolution NMR spectroscopy and relaxometry by following the response of each chemical component in the microgel particle. The accepted explanation in literature[5(1)] is that the NMR temperature transition behaviour is generated by the increasingly restricted motions of the gel network chains as the temperature rises. The correlation times of the functional groups motions (correlation time of the microgel network) are inversely proportional with the transverse relaxation time, i.e.,

$$\frac{1}{T_2} \propto \tau_c \quad . \qquad (5.2)$$

The transverse relaxation time is inversely proportional to the half width at half height of the NMR spectrum line,

$$\Delta\nu_{1/2} \propto \frac{1}{T_2} \quad , \qquad (5.3)$$

therefore, at low temperature the microgel is swollen, the spaces between polymer chains are large, the correlation time is small (the time between rotations), the transverse relaxation time

is long, making the resonance lines in the NMR spectrum narrow and well resolved. When the temperature increases the microgel particle shrinks, the correlation time becomes larger, the transverse relaxation time decreases, the lines broaden to a degree that they are not anymore detected in the NMR spectrum[5(2)]. The NMR temperature transition investigation is an indirect one, through the change in mobility of the microgel particle. Figure 5.11 shows the NMR temperature transition behaviour for the two components of the copolymer microgels, VCL and NIPMAAm, respectively. Here I selected the samples PVCL-PNIPMAAm 1:1 and 1:2 microgels.

For the PVCL-PNIPMAAm 1:1 microgel samples the signals intensities for both VCL and NIPMAAm signals decrease with temperature and the transition temperature is detected around 35.6°C. For the PVCL-PNIPMAAm 1:2 microgel samples the transition temperature is shifted to 45°C for both VCL and NIPMAAm. These results are in a good agreement with dynamic light scattering data presented in Figure 5.10c,d.

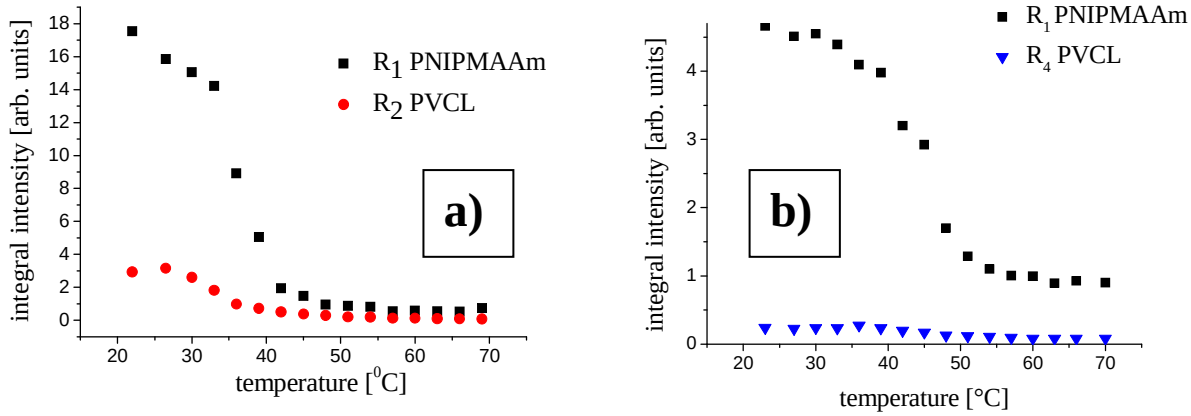

Figure 5.11 Mobility temperature transition for a) PVCL-PNIPMAAm 1:1 and b) PVCL-PNIPMAAm 1:2 by NMR spectroscopy.[f]

The NMR results suggest that in the copolymers with equimolar ratio of monomer units the mobility temperature transition is dominated by VCL. Only if the NIPMAAm segments start to dominate in the copolymer structure the thermal transition is governed by acrylamide and shifted to higher temperatures. Interestingly, there is no two-step transition

observed in this case and according to NMR data the intensity of the PVCL signals follows a similar trend as compared with PNIPMAAm.

DSC was further used to characterize the temperature-induced volume phase transition of microgel samples of different chemical compositions. DSC experiments indicate that in the case of all samples one transition can be observed. The experiments include heating, cooling and again heating of the samples, and no difference in the VPTT upon heating and cooling was observed. The transition temperatures calculated from DSC spectra for PVCL-PNIPMAAm microgels are shown in Figure 5.12. The increase of the NIPMAAm content in the copolymer structure induces a shift of the transition temperature to higher values, but the transition is still cooperative, therefore in all microgel samples only one transition has been observed.

A summary of transition temperatures determined for PVCL-PNIPAAm and PVCL-PNIPMAAm microgels is shown in Figure 5.12 and Table 5.3. For PVCL-PNIPAAm microgels the VPTT is around 35-36°C and not dependent on the chemical composition. Interestingly, the VPTT of PVCL-PNIPAAm copolymer microgels is considerably higher compared with homopolymer PVCL and PNIPAAm microgels.

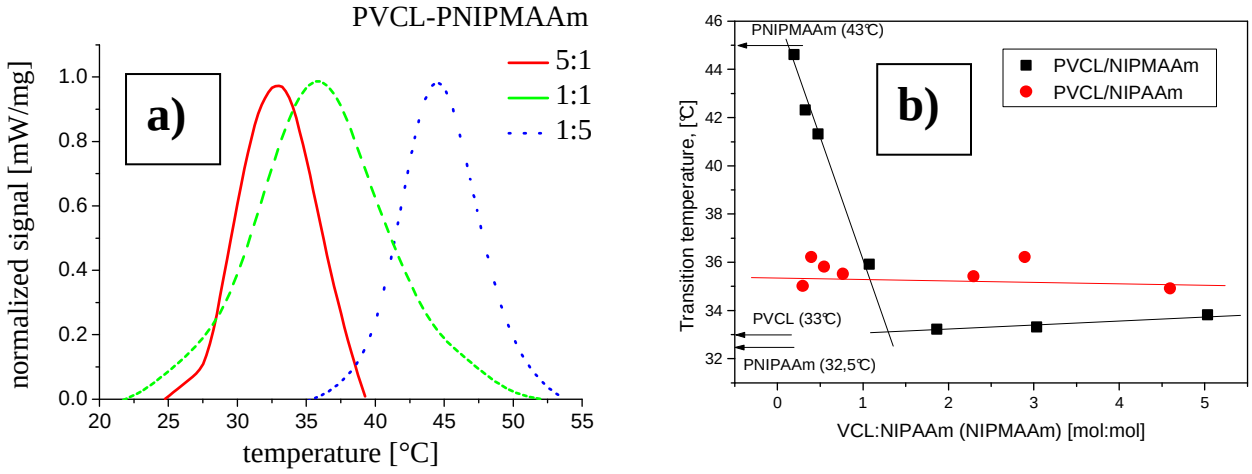

Figure 5.12 a)Normalized DSC thermograms of PVCL-PNIPMAAm microgels having different chemical composition; b) transition temperatures calculated from DSC spectra.[f]

Table 5.3 Transition temperatures and calorimetric heats of copolymer microgels.[f]

Sample	T, [°C]	ΔH, [kJ/mol]
PVCL	33	-
PNIPAAm	32.5	5.38
PNIPMAAm	43.0	5.04
PVCL-PNIPAAm		
5:1	34.9	0.355
3:1	36.2	0.196
2:1	35.4	0.483
1:1	35.5	0.365
1:2	35.8	0.520
1:3	36.2	0.676
1:5	35.0	0.963
PVCL-PNIPMAAm		
5:1	33.8	0.406
3:1	33.3	1.359
2:1	33.2	2.131
1:1	35.9	3.075
1:2	41.3	3.35
1:3	42.3	2.87
1:5	44.6	3.09

Poly(*N*-vinylcaprolactam) has a syndiotactic structure of the main chain[5(14)]. This architecture can be understood after consideration of the sterical effects due to the bulky caprolactam rings. In this situation the syndiotactic microstructure of the PVCL chains provides minimal repulsion between caprolactam rings. The incorporation of the NIPAAm units in PVCL chains increases the rotational freedom of monomer units and leads ultimately to the increase of the chain flexibility. This provokes more effective solvatation of the polymer chains within the microgel and consequently increases VPTT. For PVCL-PNIPMAAm microgels the VPTT is changing in a non-linear fashion from 33°C (VCL-rich copolymers) to 45°C (NIPMAAm-rich copolymers). The PVCL-PNIPMAAm microgels with VCL/NIPMAAm ratios 2:1, 3:1 and 5:1 behave very similar to PVCL homopolymer microgel showing the VPTT around 33°C. If the VCL/NIPMAAm ratio decreases from 1:1 to 1:5 the VPTT increases rapidly to 45°C (VPTT of homopolymer PNIPMAm microgel). These data

show that the behaviour of copolymers with VCL/NIPMAAm ratios higher or lower than one is dominated by VCL or NIPMAAm respectively.

The results of this study are presented by Balaceanu *et al.*[f].

5.2 Core-shell microgels of *N*-vinylcaprolactam and *N*-isopropylacrylamides

Doubly thermoresponsive microgels made of PVCL and PNIPAAm/PNIPMAAm with core-shell structure were synthesised and analysed. Selected samples with theoretical molar ratio 1:1 of PVCL-core/ PNIPMAAm-shell and PNIPMAAm-core/ PVCL-shell were characterised using the Flory swelling theory in Chapter 3, section 3.3. In this study I discuss the characterisation of a series of core-shell systems composed of PVCL, PNIPAAm and PNIPMAAm with different molar ratios. The synthesis method was optimised, microgels with different shell thickness were constructed, and the systems were characterised with DLS, DSC and AFM.

This is a preliminary study and further investigation of the systems is needed to fully understand their properties. Nevertheless, the study has value because of the novelty of the microgel systems. To the best of my knowledge a combination of these monomers was not developed into core-shell structures before. Furthermore, these systems pave the way to complex microgel morphology investigations.

The synthesis procedure of the core-shell microgels was described in Chapter 2, synthesis section 2.1.3, and the different samples will be referred to in the text by citing the core-shell monomer composition and the monomer theoretical molar ratio, as example: PVCL-core/ PNIPMAAm-shell 1:3.

5.2.1 Dependence of the shell thickness on the monomer composition

Dynamic light scattering measurements were made on different core-shell microgel samples with increasing amount of the shell monomer, in order to observe the increase in the thickness of the shell. The results are presented in Figure 5.13 for all investigated core-shell microgel samples. The first point in each graph corresponds to the core of the microgels alone taken as reference, and since two different samples for each core microgel were prepared, there are two values for the starting cores (see Chapter 2, synthesis section 2.1.3 for a detailed description of the synthesis procedure).

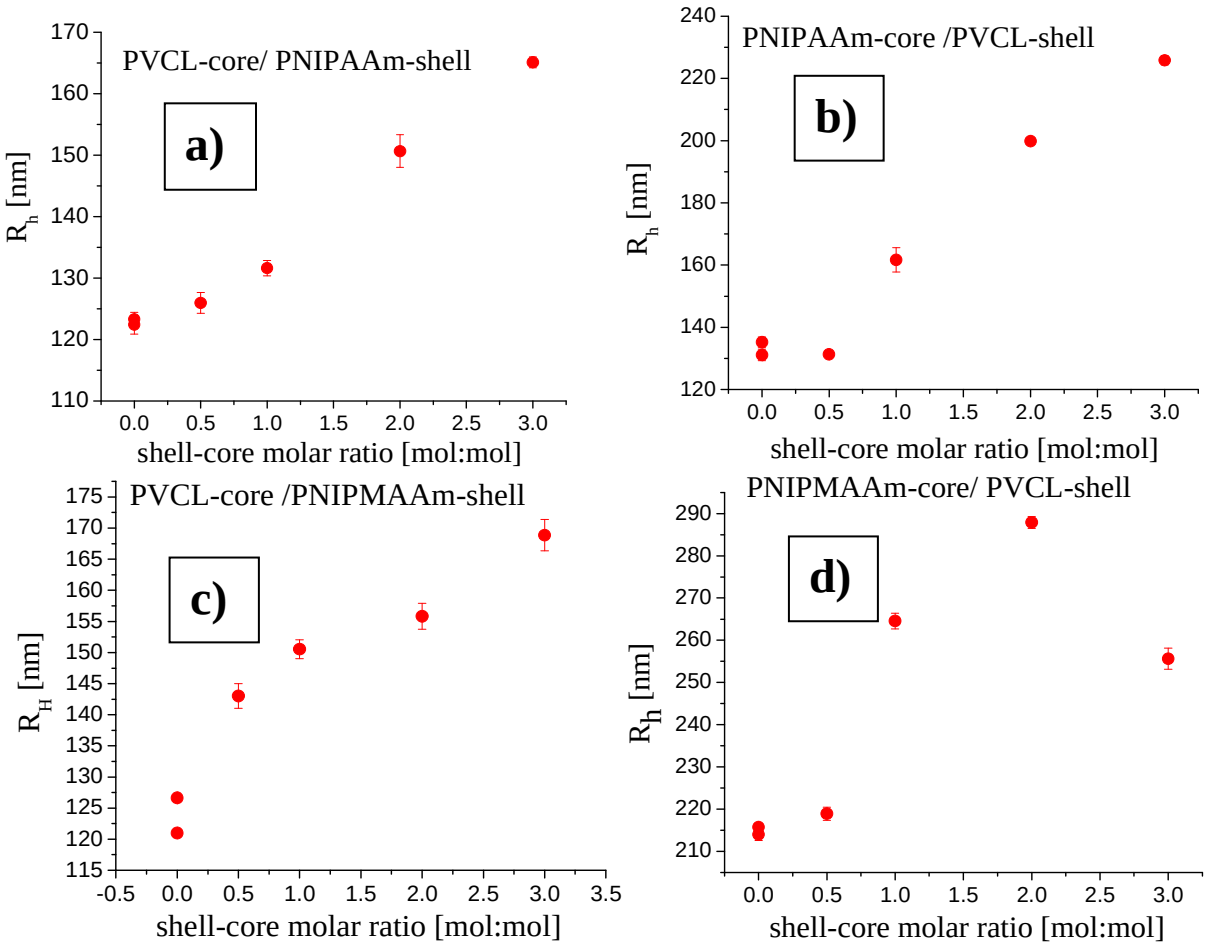

Figure 5.13 Dependence of the particle size on the shell monomer content for a) PVCL-core/ PNIPAAm-shell; b) PNIPAAm-core/ PVCL-shell; c) PVCL-core/ PNIPMAAm-shell and c) PNIPMAAm-core/ PVCL-shell microgels

An almost linear increase of the size of the particles with increasing amount of shell monomer is observed for most of the microgel systems. The PNIPMAAm-core/ PVCL-shell system behaves atypical; the increase in the shell thickness reaches a limit for the system with 1:2 core-shell molar ratio, after which the size of the particle decreases with more shell monomer added. I have encountered problems in the synthesis of this system (as can be seen also in Chapter 2, synthesis section 2.1.3) and further optimisation of the synthesis method is required, thus the following investigations are focused on the previous three reliable microgel systems. The results show that the morphology of the core-shell microgel systems can be controlled, designing microgels with different shell thickness. For all dynamic light scattering data, the PDI index is bellow 0.1.

AFM images show the quality and the size distribution of microgel particles of selected samples (Figure 5.14). It can be seen that the samples are spherical particles, with a uniform distribution. The samples analysed were in high concentration and have some tendency to agglomerate on the AFM grid.

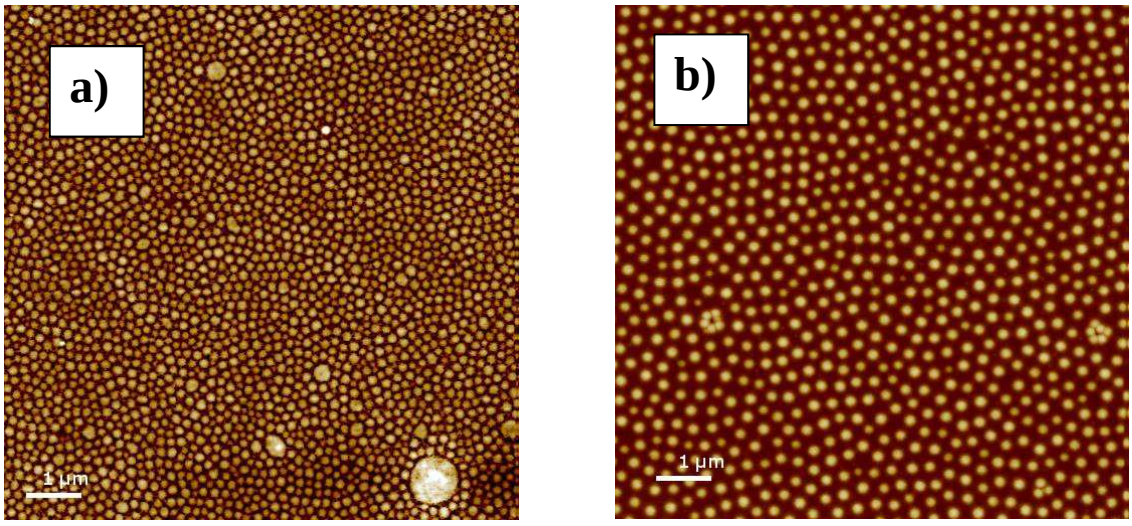

Figure 5.14 AFM pictures of a) PVCL-core/ PNIPAAm-shell 1:3 (height of the image is 50nm), and b) PNIPAAm-core/ PVCL-shell 1:3 (height of the image is 130nm).

5.2.2 Temperature transition of core-shell microgel systems

The temperature transition of the different core-shell microgel systems was investigated using two different techniques, dynamic light scattering and differential scanning calorimetry. In Figure 5.15 I am presenting the temperature transition of core-shell microgel samples determined with DLS. Because of the difference in LCST of PVCL and PNIPMAAm, it can be observed that the values of the transition temperature increases systematically with increasing shell content in the PVCL-core/ PNIPMAAm-shell microgels (Fig. 5.15c). For the systems containing PVCL and PNIPAAm, the transition temperature doesn't change significantly with monomer ratio.

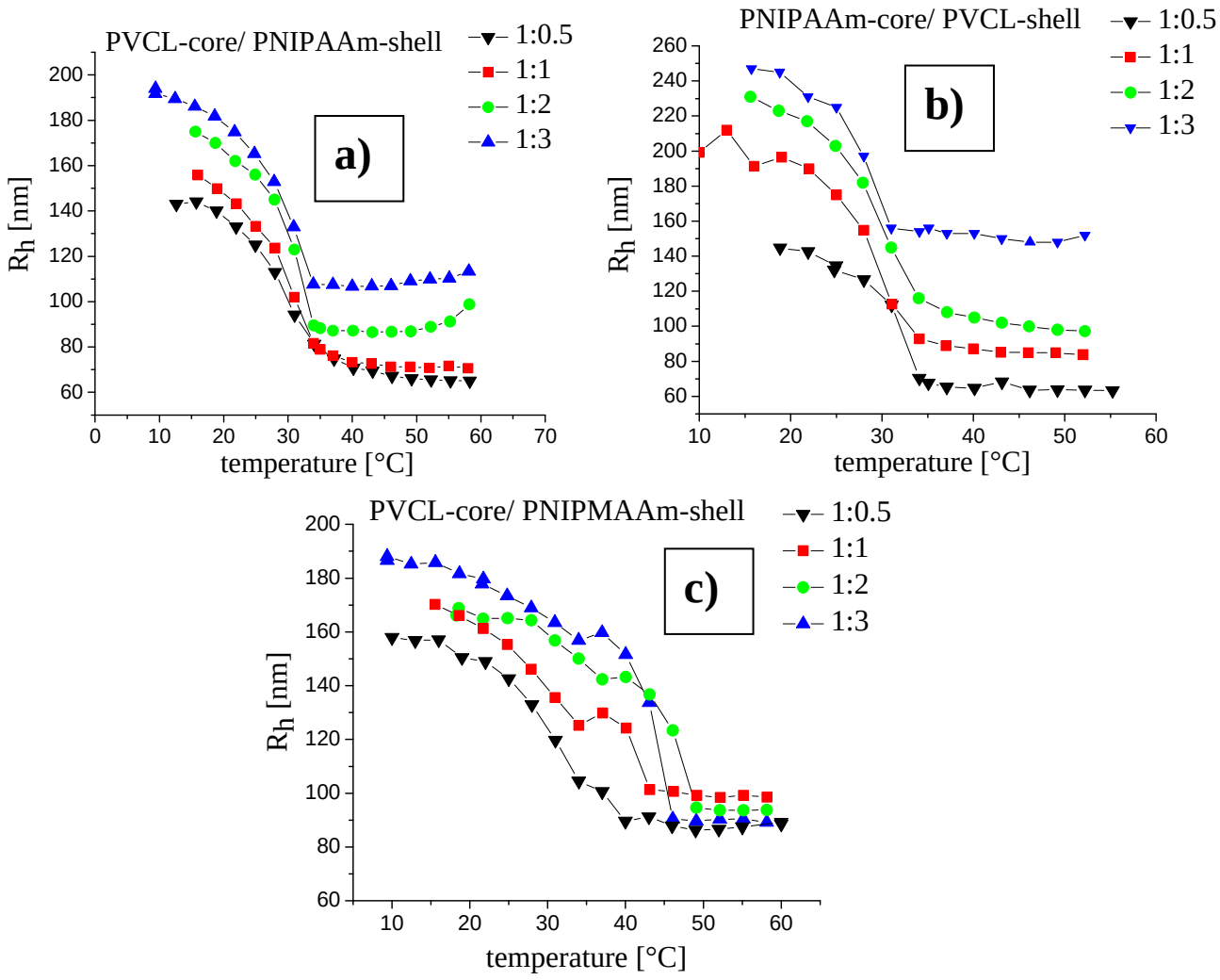

Figure 5.15 Temperature transition measured with DLS for a) PVCL-core/ PNIPAAm-shell, b) PNIPAAm-core/ PVCL-shell and c) PVCL-core/ PNIPMAAm-shell microgels.

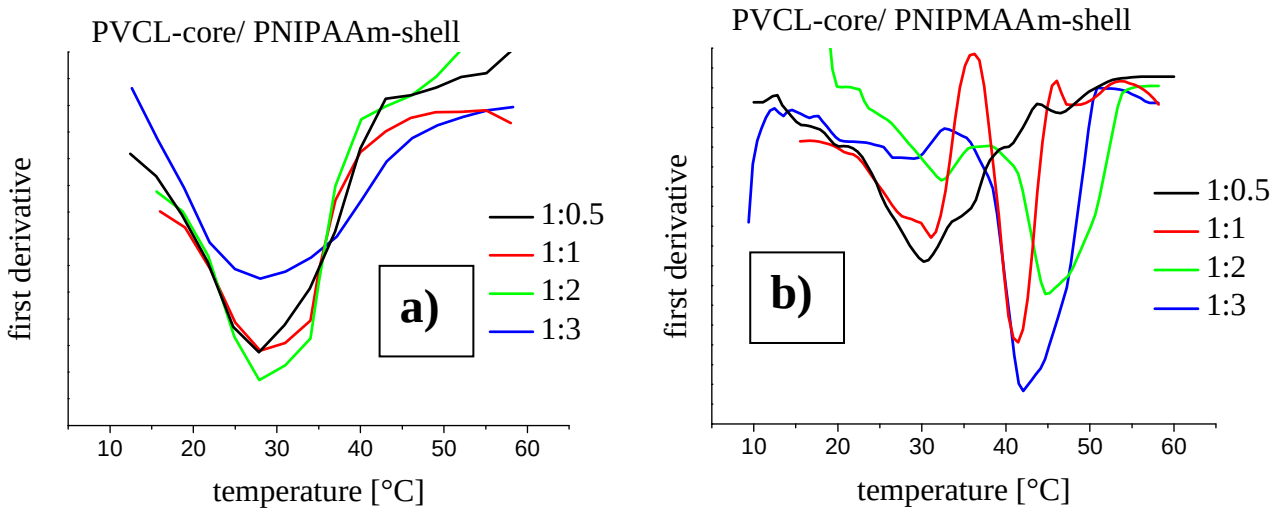

Figure 5.16 First derivative of the transition curve measured by DLS, for a) PVCL-core/ PNIPAAm-shell and b) PVCL-core/ PNIPMAAm-shell microgels. Experimental data were first interpolated, derivated and in the end smoothed.

A comparison of the transition temperature of PVCL-core/ PNIPAAm-shell and PVCL-core/ PNIPMAAm-shell microgels is made in Figure 5.16. For the PVCL-core/ PNIPAAm-shell microgel (Fig. 5.16a) the transition temperature is very similar for all core-shell monomer ratios. On the other hand for the PVCL-core/ PNIPMAAm-shell (Fig. 5.16b), the transition temperature changes from dominated by the PVCL core, to a two-step transition for core-shell ratios 1:1 and 1:2, and further to a transition dominated in principal by the PNIPMAAm shell.

Differential scanning calorimetry measurements were performed on PVCL-core/ PNIPAAm-shell, PNIPAAm-shell/ PVCL-core and PVCL-core/ PNIPMAAm-shell microgel systems (Figure 5.17). For systems containing PVCL and PNIPAAm, the transition temperature doesn't change significantly, which is accordance with DLS results, and a unimodal transition can be observed. For the PVCL-core/ PNIPMAAm-shell, a double transition for the 1:0.5 molar ratio can be seen, but not for further samples with increasing shell monomer content, where the single transition is dominated by the PNIPMAAm

component. This is different from the DLS results, and the explanation lies in the differences between the two methods of investigation used. The thermodynamic phenomenon observed in the energy change in the DSC measurement is different from the size measurements at thermal equilibrium performed by the DSC device.

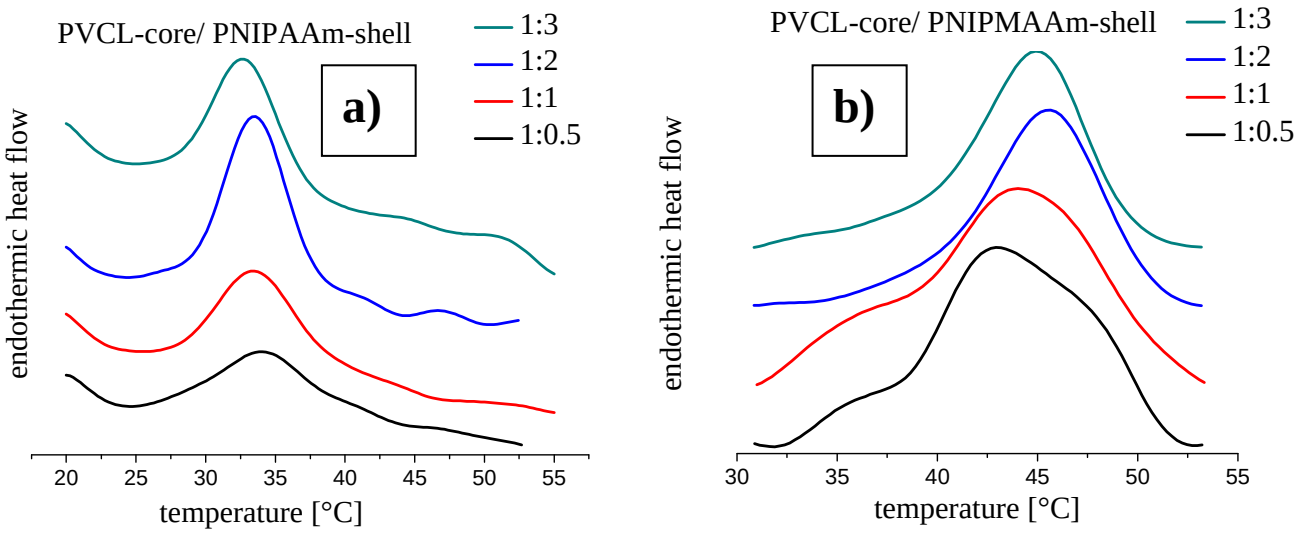

Figure 5.17 DSC transition curves for a) PVCL-core/ PNIPAAm-shell and b) PVCL-core/ PNIPMAAm-shell microgels

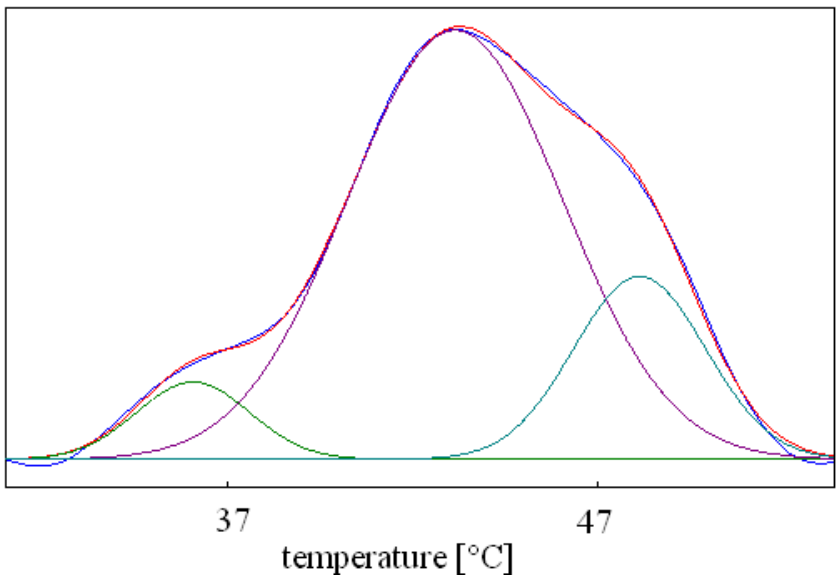

Figure 5.18 Deconvolution of DSC transition curve for PVCL-core/ PNIPMAAm-shell 1:0.5 microgel using the DMFIT program.

The transition curve of the PVCL-core/ PNIPMAAm-shell 1:0.5 microgel can be further analysed by deconvolution using the DMFIT program in order to separate the transition peaks for each component (Figure 5.18). The deconvolution reveals three contributions to the transition, one corresponding to the PVCL transition temperature (around 35°C), one to PNIPMAAm (48 °C) and an intermediate contribution (42 °C), corresponding probably to an interface between the core and shell, a region where the chains interpenetrate and influence each-other.

5.3 Cononsolvency effect for PVCL based microgels

The phenomenon of cononsolvency is defined as the phenomenon that allows for certain solvent mixtures to be bad solvents for a polymer depending on composition, while the pure solvents are good solvents for the same polymer [5(15)]. It can be seen as another stimuli responsive property of the polymers, and therefore of microgels, exhibiting a change in volume at certain solvent mixture compositions. The cononsolvency behaviour of linear polymers[5(15),5(16)], gels[5(17),5(18)] and also microgels[5(19)] received some attention in recent years because of the increasing interest in the applications of stimuli responsive materials. Different polymers[5(20),5(21)], the most studied being poly(*N*-isopropylacrylamide) (PINPAAm)[5(15),5(16)], and different solvent-solvent systems, mostly water/alcohol[5(15),5(19),5(22)-5(27)] were examined using a variety of methods. It was found that beside the thermoresponsive behaviour, PNIPAAm polymers and microgels also exhibit a change in solubility and volume by addition of a cononsolvent to the aqueous solution. While linear polymers might form aggregates in the two phase region due to the reduced hydrophilic character of the chains, microgels form colloidally stable dispersions, and therefore don’t aggregate if the quality of the solvent changes, they exhibit a volume phase

transition[5(28),5(29)]. A schematic representation of the cononsolvency effect is presented in Figure 5.19.

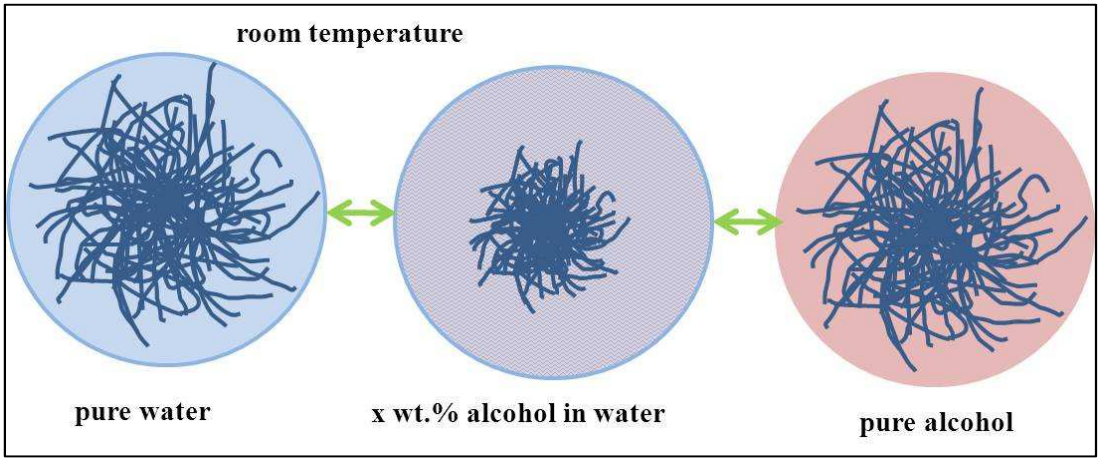

Figure 5.19 Schematic representation of the cononsolvency effect

In this study I am investigating homopolymer PVCL and PNIPMAAm microgels in water/methanol mixtures in order to determine the cononsolvency point and to see the influence of the cononsolvency effect on the temperature transition of the microgels. For this purpose I am using DLS to determine the swelling of the microgel particles at 20°C and the volume temperature transition of the microgels at different concentrations of methanol in water mixtures. Copolymer PVCL-PNIPMAAm microgels were also studied in order to determine the cononsolvency point and to investigate the influence of the monomer content on the good solvent – bad solvent transition in water/methanol and ethanol mixtures. These investigations were made using DLS and ^{1}H NMR spectroscopy.

The samples used are presented in Chapter 2, synthesis section 2.1.1 for homopolymer microgels and section 2.1.2 for copolymer systems , and will be referred to in the text considering the theoretical molar ratio of the monomers, for example PVCL-PNIPMAAm 1:1. The microgel samples are dissolved in water/methanol or water/ethanol mixtures, which were prepared in weight per cent concentrations. This is a preliminary study, and further research should be undertaken in order to elucidate the reasons behind the findings.

5.3.1 PVCL and PNIPMAAm homopolymer microgels cononsolvency behaviour

The swelling of microgels at constant temperature below the volume phase transition temperature is affected by the concentration of the water/alcohol mixture. The point at which the swelling has a minimum is defined as the cononsolvency point in this case. This phenomenon was theoretically explained by Tanaka *et al.*[5(30)] i.e., the total coverage function of the polymer chain has a minimum at the critical composition, where the competition to form hydrogen bonds between the two solvents and chain is highest.

Figure 5.20 shows the size decrease of homopolymer microgel particles of PVCL and PNIPMAAm in solvent mixtures with increasing alcohol at the fixed temperature of 20°C. The cononsolvency minimum is for both microgels and in mixtures of both alcohols at a concentration of 30 wt.% of methanol and ethanol in water (Fig. 5.20a and b). The hydrodynamic radius was normalized to the value in pure water solvent (R_h^0). For both alcohol mixtures, the transition of PNIPMAAm microgel is sharper than that of the PVCL microgel.

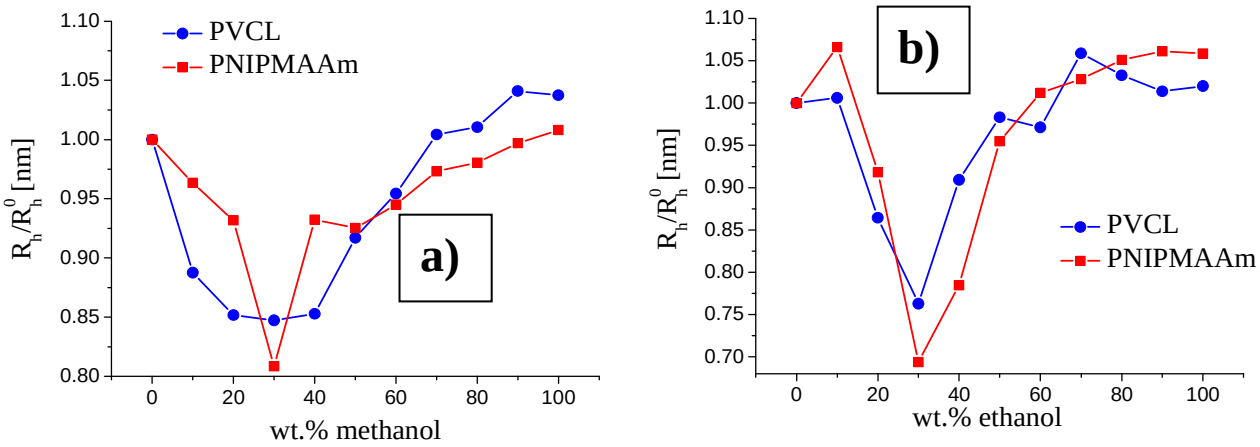

Figure 5.20 a) DLS measurements of homopolymer microgels in methanol-water mixtures; b) DLS measurements of homopolymer microgels in ethanol-water mixtures. Measurements made at 20°C.

Cononsolvency was also defined as an enhancement on the temperature phase transition in mixed good solvents[5(31)] for PNIPAAm polymers and gels. To investigate this effect, DLS was further used to determine the temperature phase transition behaviour of the homopolymer microgels PVCL and PNIPMAAm at different methanol in water concentrations. Figures 5.21a and 5.22a show the transition curves for PVCL and respectively PNIPMAAm microgels at different wt.% methanol in water. Figures 5.21b and 5.22b show the dependence of the volume phase transition temperatures (VPTT) on the methanol concentration for both microgels. The volume phase transition temperatures were determined from the first derivatives of the size-temperature transition curves obtained by DLS.

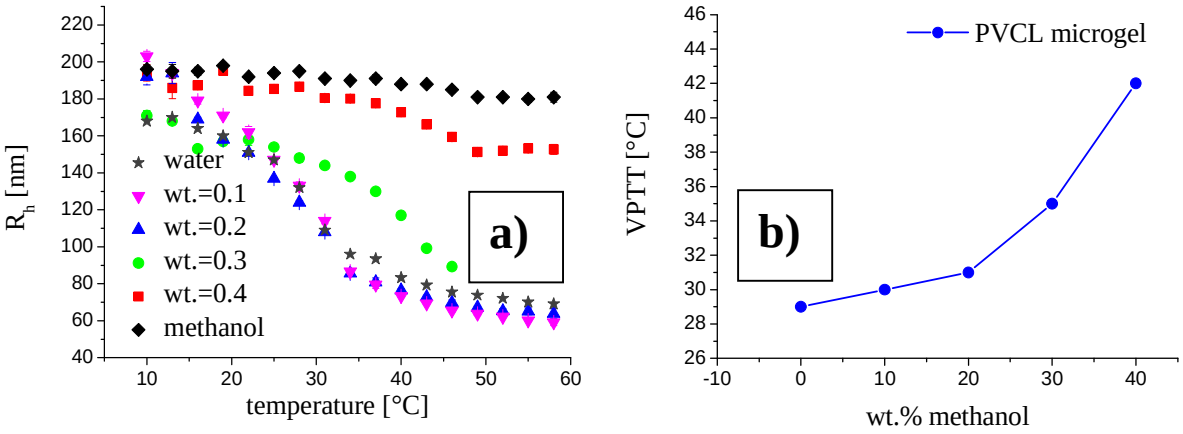

Figure 5.21 a) DLS size-temperature measurements in water/methanol wt. % mixtures; b) dependence of the VPTT on the methanol amount for PVCL microgel.

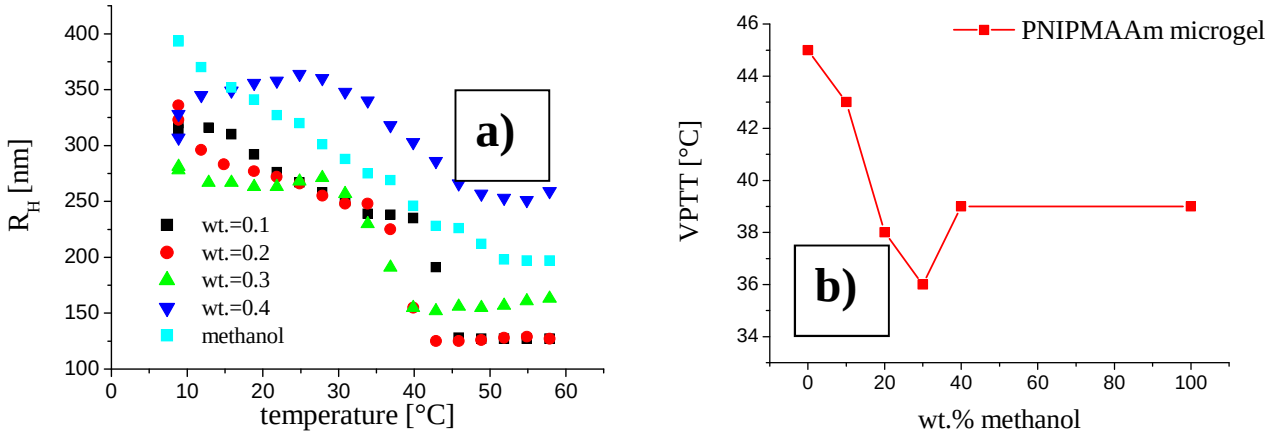

Figure 5.22 a) DLS size-temperature measurements in water/methanol wt. % mixtures; b) dependence of the VPTT on the methanol amount for PNIPMAAm microgel.

It is clear that PVCL and PNIPMAAm homopolymer microgels have different temperature transition behaviours in solvent mixtures of water/methanol. For PVCL the volume phase transition temperature (Fig. 5.21b) increases with more methanol content, while for PNIPMAAm the volume phase transition temperature decreases to a minimum, and afterwards increases to a plateau (Fig. 5.22b). The results show that the PVCL microgel does not experience a cononsolvency point in the sense of an enhancement of the phase transition. The temperature transition behaviour of the PNIPMAAm microgel is very similar to the previously reported behaviour of PNIPAAm microgel[5(32)]. The minimum of the VPTT dependence on methanol for PNIPMAAm is at 30 wt.% methanol in water, exactly the same concentration previously marking the minimum of swelling at low temperature for the same microgel (see Figure 5.20a).

In order to explain the difference in the temperature transition behaviour in different solvent mixtures for PVCL and PNIPMAAm microgels, we can consider the monomer structures (Figure 5.23), and their abilities to build hydrogen bonds. It has been argued that the ability to build hydrogen bonds has the key influence on the cononsolvency behaviour,[5(32)-5(34)] although this is still a controversial idea[5(34),5(35)]. The NIPMAAm monomer is different from the VCL monomer in the fact that it has both donor (the amide hydrogen) and acceptor (carbonyl oxygen) functions in the hydrogen bond formation. VCL only has a donor function. This gives PNIPMAAm the ability of forming both intra and intermolecular hydrogen bonds, while PVCL can only form intermolecular hydrogen bonds.

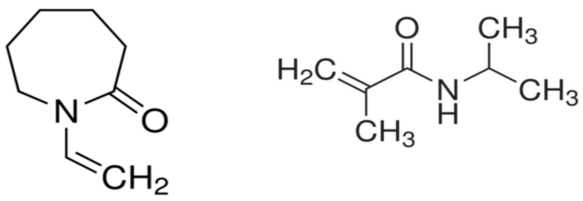

Figure 5.23 *N*-vinylcaprolactam and *N*-isopropylmethacrylamide monomer structures.

Considering the difference in H-bond capability, I suggest as possible explanation for the differences observed in PVCL and PNIPMAAm microgels in different water/alcohol mixtures, two ways of manifestation of the cononsolvency effect: (i) at temperatures bellow the temperature transition, the particles' size has a minimum at a certain alcohol concentration, which occurs because the two solvent molecules compete to interact with the polymer chains, and at a certain concentration neither of the solvents swells the microgel at maximum capacity; (ii) additionally, for monomers that have both hydrogen bond donor and acceptor groups, such as PNIPAAm and PNIPMAAm, there is a second effect present. A decrease of the VPTT at certain alcohol concentrations can be observed, because the interactions with the solvent are exchanged for both inter and intramolecular hydrogen bonds, promoting the polymer-polymer interactions and decreasing the stability of the particles swollen in the solvent mixture. The collapse of the particles is enhanced, it occurs at lower temperatures, when the concurrence between water and alcohol is high, because the interactions with water are exchanged faster for polymer-polymer interactions. On the other hand for PVCL and other H-bond donor only polymers, the interaction with water could be exchanged mostly for interaction with the alcohol, which is a better solvent, making the particles stable in the solvent mixture until higher temperatures.

To verify this explanation we are further conducting 2D NMR experiments to investigate directly the different interactions at different temperatures and different alcohol concentration. Moreover, investigation of other polymer microgels in needed.

5.3.2 Copolymer microgels cononsolvency investigation in different alcohols

Copolymer microgels PVCL-PNIPMAAm with different molar ratios were investigated in water/methanol and water/ethanol wt.% mixtures. The influence of the monomer molar ratio in relation to the different alcohols and their concentrations was investigated.

Figure 5.24 shows DLS measurements of the hydrodynamic radius of PVCL-PNIPMAAm copolymer microgels at different molar compositions of monomers (2:1, 1:1, 1:2) in water/methanol and water/ethanol mixtures. The interesting result is that in water/methanol, the cononsolvency minimum increases with increase of PNIPMAAm monomer ratio, whereas in water/ethanol, the minimum has the same value for all monomer ratios. This is a surprising result since the cononsolvency minima for homopolymer microgels PVCL and PNIPMAAm have the same value both in methanol-water and ethanol-water (Figure 5.24).

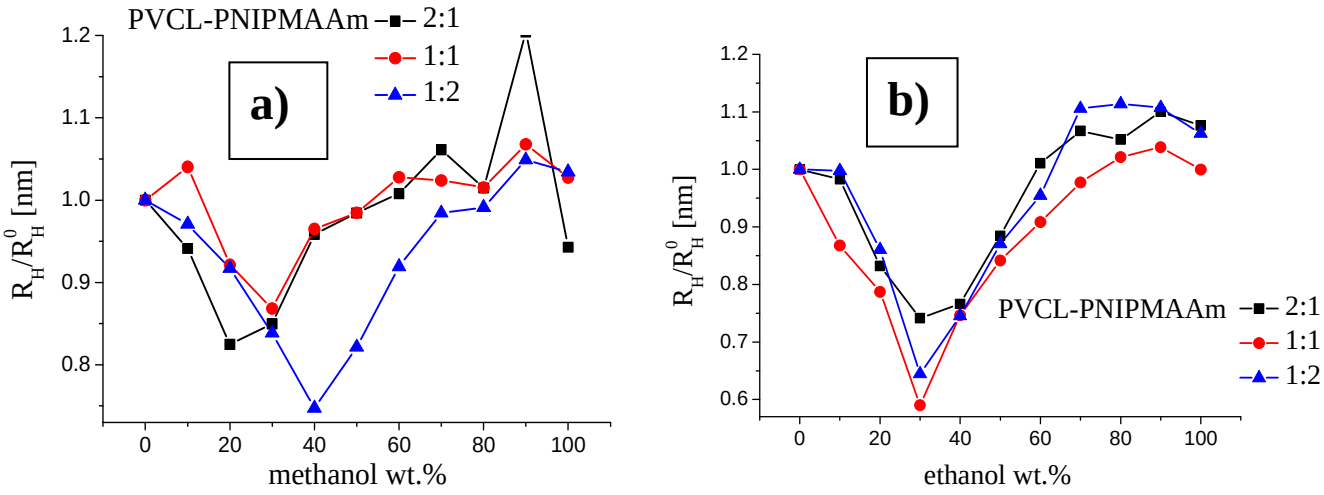

Figure 5.24 a) DLS measurements of copolymer PVCL-PNIPMAAm microgels in water/methanol mixtures; b) DLS measurements of copolymer PVCL-PNIPMAAm microgels in water/ethanol mixtures.

In order to investigate the cononsolvancy phenomenon with nuclear magnetic resonance, I measured ^{1}H NMR spectra for the copolymer microgel systems PVCL-PNIPMAAm (2:1, 1:1, and 1:2) in different deuterated water/deuterated methanol wt.% concentration mixtures. In order to compare the spectra between each other I used the same amount of dried microgel in solution. The behaviour of the two components in the NMR

spectrum was followed, by measuring the integral intensity of the line corresponding to PVCL, and PNIPMAAm respectively (Figure 5.25).

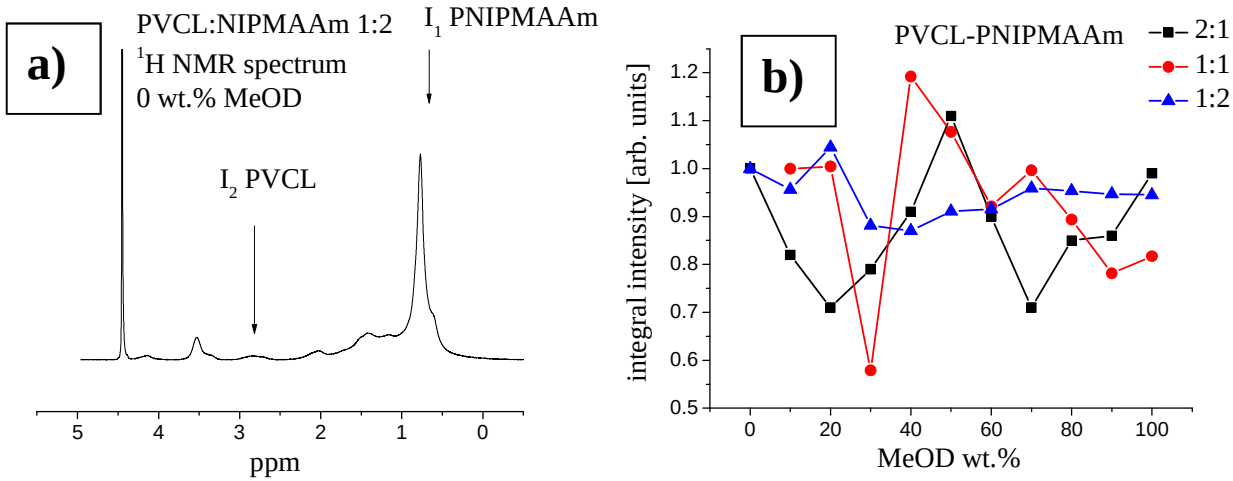

Figure 5.25 a) Proton NMR spectrum of PVCL-PNIPMAAm 1:2 copolymer microgel; b) Integral intensity measurements of the ^{1}H NMR spectrum lines for PVCL-PNIPMAAm copolymer microgel systems in D_2O/MeOD mixtures.

From DLS experiments it can be observed that the radius of the microgel particle decreases at certain alcohol concentrations, giving the cononsolvency point. It is expected to see the same trend in the NMR measurements because the integral intensity of the NMR spectrum line can reflect the mobility of the NMR species, and when the particle deswells the motions of the spins are hindered. The NMR results are in agreement with the DLS results (Figure 5.24a), obtaining the same cononsolvency points for the three different monomer ratio systems in deuterated water/deuterated methanol mixtures (Figure 5.25b). It can be observed that the cononsolvency minimum increases with increase of PNIPMAAm monomer.

5.4 Temperature volume phase transition of microgels by Hahn-Echo ^{1}H measurements

For this study I have used PVCL-core/ PNIPMAAm-shell 1:1 and PNIPMAAm-core/ PVCL-shell 1:1 microgels, synthesis described in Chapter 2, synthesis section 2.1.3, as well as PVCL and PNIPMAAm homopolymer microgels for reference (synthesis section 2.1.1). The aim is to analyse the temperature transition of microgels using temperature dependent nuclear magnetic resonance spectroscopy. The explanation found in literature[5(1),5(14),f] regarding the observation of the temperature transition of polymer, gels and microgels with NMR spectroscopy is that during the temperature transition, because of the collapse of the particle, the spaces between the polymer chains become smaller, the motions become hindered and the corresponding lines of functional groups in the NMR spectrum become too broad (transverse relaxation times of respective protons become too short) to be detected. This mechanism was also used as explanation in this thesis in Chapter 5, results section 5.1.4[f], for the temperature transition observed by NMR spectroscopy of copolymer microgels. Until now no theoretical model was supplemented to this qualitative picture. In this study I am making the first steps to explaining this effect, by taking into account all the possible mechanisms of collapse of spectrum lines with increasing temperature.

5.4.1 Temperature transition of microgels by NMR spectroscopy

Nuclear magnetic resonance spectroscopy allows the examination of the individual behaviour of the components in copolymer[f] and core-shell microgel structures. In order to investigate the temperature transition of core-shell microgels, I have used a new approach, which relies on Hahn-Echo temperature dependent measurements. Usually the transverse relaxation time is calculated through this type of experiment, but I have also used the NMR spectrum obtained

after the first echo time to get the temperature dependence of the integral intensity of the components spectrum lines. This type of measurement ensures that the results are not affected by the magnetic field inhomogeneities and also are not affected by the spectrometer dead time that cuts the fast decaying part of the NMR signal. Figure 5.26 shows a schematic representation of the Hahn-Echo NMR experiment used to determine the transverse relaxation time.

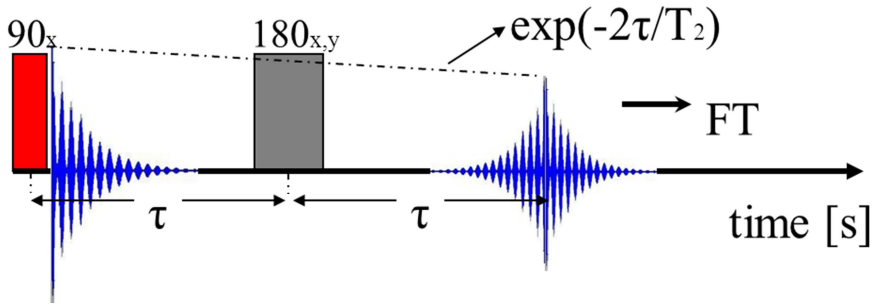

Figure 5.26 Scheme of a Hahn-Echo NMR experiment.

Figure 5.27 shows the NMR temperature transition Hahn-Echo experiments on the homopolymer microgels. The temperature transitions measured by NMR are higher than the ones measured by DLS (see results section 5.1.4[f]).

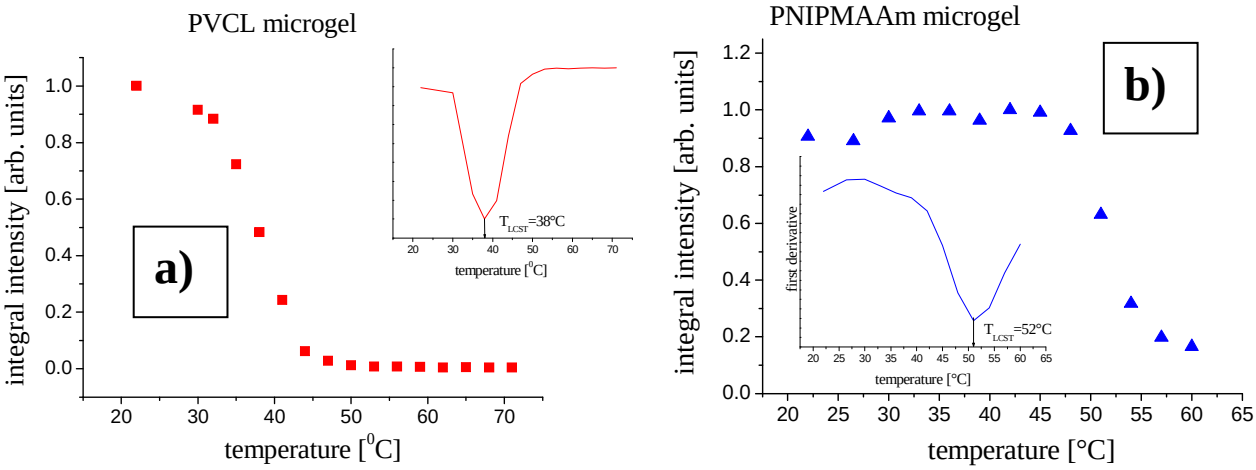

Figure 5.27 Temperature transition of homopolymer microgels a) PVCL and b) PNIPMAAm measured after the first echo time using a Hahn-Echo NMR experiment. The inserts show the first derivatives of the transition curves.

For core-shell microgels, I have calculated the integral intensity of the entire NMR spectrum (I_{total}) and the integral intensities of functional groups of PVCL (I_{PVCL}) and PNIPMAAm ($I_{PNIPMAAm}$) from the NMR spectrum obtained after the first echo time (Figure 5.28) at different temperatures. By analysing the integral intensity variation with temperature of the high resolution spectrum lines, the behaviour of the core can be separated from the one of the shell. Figure 5.28 shows that for the PVCL-core/ PNIPMAAm-shell system, the core has a transition temperature in D_2O at 35°C and the shell at 48°C. The temperature transition points of both PVCL and PNIPMAAm are lower in the core-shell morphology than in the homopolymer microgel. This can be explained by taking into account that the promoters of the transitions, i.e. the interactions between polymer-polymer and polymer-water molecules are different, and the polymer chains lose some of their stability and collapse faster in the case of core-shell morphology.

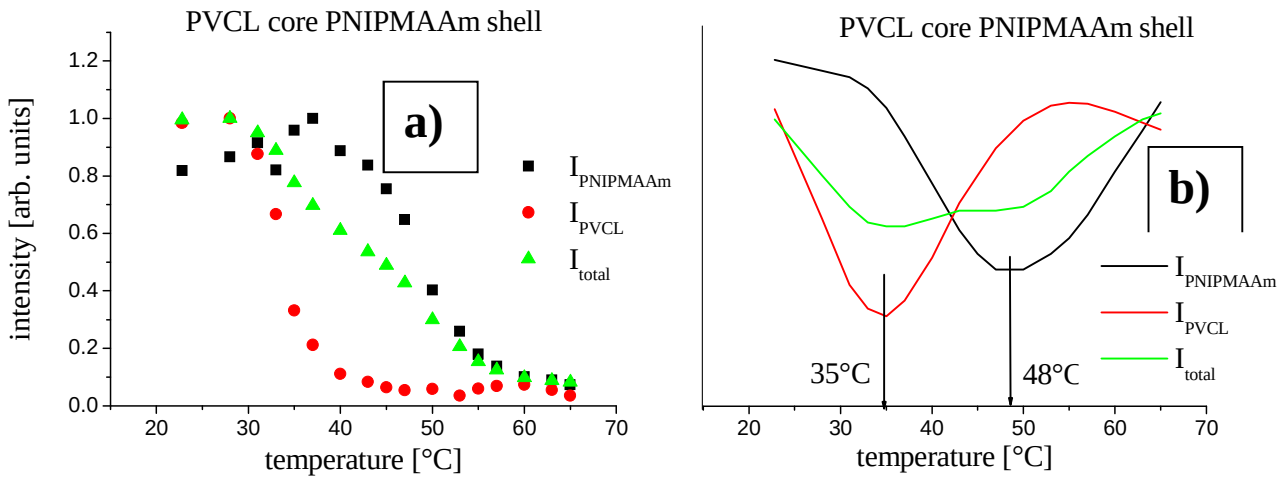

Figure 5.28 a) NMR temperature transition measured for the entire spectrum and for individual components resonance lines, and b) derivatives of temperature transition curves measured with NMR for PVCL-core/ PNIPMAAm-shell 1:1 microgel.

In the case of the reverse system, Figure 5.29, PNIPMAAm-core/ PVCL-shell, the transition temperature of the core is now 46.5°C and the transition of the shell is 35°C. It can be observed that when PNIPMAAm is located in the core, its temperature transition is lower.

This is because of the influence of the shell, mainly the PVCL shell has a lower transition temperature so it forces the PNIPMAAm core to collapse sooner.

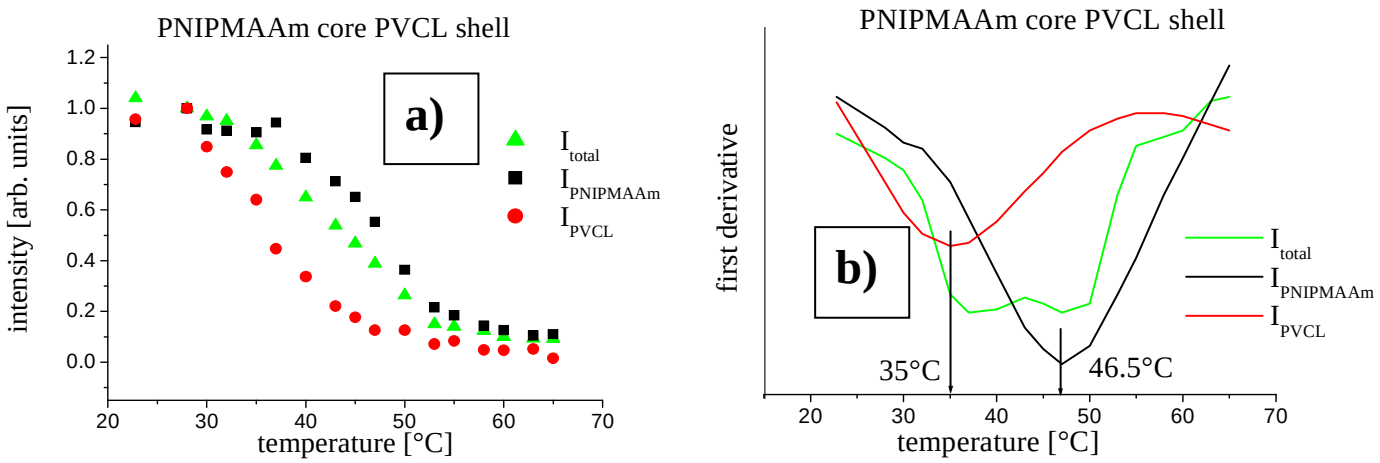

Figure 5.29 a) NMR temperature transition measured for the entire spectrum and for individual components resonance lines, and b) derivatives of temperature transition curves measured with NMR for PNIPMAAm-core/ PVCL-shell 1:1 microgel

The main reason why the integral intensity of a particular resonances is sensitive to the changes in temperature is thought to be related[5(1)] to the dependence of the linewidth at half height $(\Delta\nu)_{1/2}$ on this parameter. Because $(\Delta\nu)_{1/2}$ is proportional with $1/T_2$ the temperature dependence of the T_2 could be governing the changes in integral intensities of the resonances. However, the transverse relaxation rate is complex in microgels being related to the following mechanisms of dipolar interaction modulation by: (i) rotational diffusion of microgel (tumbling), (ii) translational diffusion of microgels, (iii) fast rotational isomerization transition of functional groups around the polymer backbone, and (iv) slow segmental motions of the network chains. The relative weights in which these mechanisms contribute to the dependence of the transverse relaxation time dependence on temperature is actually unknown. In previous literature [5(1) and references therein] it was supposed that the T_2 dependence on temperature is dominated by the slow segmental motions of the network.

Another concept is to consider that the disappearance of the spectrum lines is related to a decrease in the intensity of the spectrum lines, and not affecting the line width at half height. If the shrinking of the lines is dependent on the longitudinal relaxation time (T_1), when the recycle delay is not long enough so the longitudinal magnetization can recover to equilibrium for higher temperatures, the shrinking of the NMR spectrum could come from a decrease in the intensity rather that a broadening.

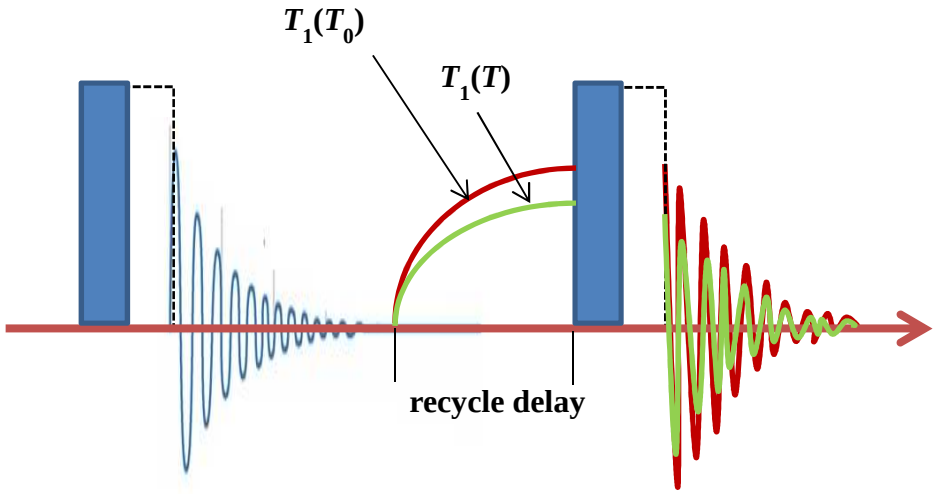

Figure 5.32 Partial recovery of the longitudinal magnetization in an NMR experiment.

I am currently working on temperature dependent measurements of the two transverse relaxation times (T_2 and T_1), which are the main contributors to the observation of the temperature transition of microgels in the NMR spectra. The possible contribution of tumbling to the transverse relaxation time can be supressed by increasing the concentration in the measured microgel sample to the point that the rotational diffusion is drastically reduced. I will also explore the possibility that the longitudinal relaxation time is responsible for the collapse of the spectrum lines by performing T_1 temperature dependent measurements. The aim of this study and of the discussion is to show that the observation of the temperature phase transition of microgels in the NMR spectrum is a complex phenomenon, which should

be investigated with a rigorous theory that takes into account all possible relaxation mechanisms. At the moment I am trying to develop such an approach.

5.5 Conclusions

Different morphologies of microgel systems based on PVCL were characterized. PVCL-PNIPAAm and PVCL-PNIPMAAm copolymers with different molar ratios of monomers were investigated using DLS, DSC, NMR and TEM, optimizing methods of controlling the size, the temperature transition behaviour and the inner structure of the particles. Core-shell PVCL/PNIPAAm and PNIPMAAm microgels with different shell monomer content were also synthesized and analysed using DLS, DSC and AFM. The purpose of the study was to control the shell thickness of different morphological particles and the influence on the transition temperature, by obtaining a double temperature transition curve.

The cononsolvency effect was highlighted for PVCL and PNIPMAAm homopolymers and for copolymers based on them. The influence of the alcohol content in water/alcohol mixtures on the temperature transition of homopolymers was investigated by DLS. The influence of the monomer ratio on the cononsolvency transition point was investigated by DLS and ^{1}H NMR spectroscopy.

The temperature transition of microgels can also be investigated by NMR spectroscopy. The advantage is that the contribution of different functional groups or structural components can be separated and followed individually. The complexity of the temperature transition observed by NMR spectroscopy of microgels is discussed. New ideas were introduced regarding the temperature dependence of the relaxation times that are responsible for the disappearance of the NMR spectrum lines.

References

5(1) Spěváček, J. *Curr. Opin.Colloid & Interf. Sci*., **2009**, *14*, 184-191.

5(2) Demco, D.E.; Hafner, S.; Spiess, H.W. *Handbook of Spectroscopy of Rubbery Materials*, Repra Technology Ltd., Shawbury, UK, 202.

5(3) Demco, D.E.; Blümich, B. *Encyclopedia of Polymer Science and Technology*, **2004**, *10*, 637.

5(4) Guillermo, A.; Cohen Addad, P.J.; Bazile, J.P.; Duracher, D.; Elaissari, A.; Pichot, C. *J. Polym. Sci.: Part B: Polym. Phys.* **1999**, *38*, 889.

5(5) Ru, G.; Wang, N.; Huang, S.; Feng, J. *Macromolecules*, **2009**, *42*, 2074.

5(6) Stieger, M.; Richtering, W.; Pedersen, J.S.; Linder, P. *J. Chem. Phys.* **2004**, *120*, 6197.

5(7) Sotta, P.; Fülber, C.; Demco, D.E.; Blümich, B.; Spiess, H.W. *Macromolecules*, **1996**, *29*, 6222.

5(8) Shostakovski, M. F.; Sydelkovskaya, F.P. *Vesnik Akad.Nauk.SSSR* **1957**, *7*, 127.

5(9) Makhaeva, E.E.; Thang, L.T.M.; Starodubzev, S.G.; Khohlov, A.R. *Macromol.Chem. Phys.* **1996**, *197*, 1973.

5(10) Heskins, M.; Guillet, J.E. *J Macromol.Sci. Chem.* **1968**, *2*, 1441.

5(11) Shibayama, M.; Tanaka, T. *Adv. Polym Sci*. **1993**, *109*, 1.

5(12) Tirumala, V. R.; Ilavsky, J.; Ilavsky, M. *J. Chem. Phys.* **2006**, *124*, 234911.

5(13) Kano, M.; Kokufuta, E. *Langmuir*, **2009**, *25*(15), 8649–8655.

5(14) Kirsh, E.Y. *Prog. Polym.Sci.* **1993**, *18*, 519.

5(15) Winnik, F.M.; Ringsdorf, H.; Venzmer, J. *Macromol.Communic.***1990**, *23*, 2415.

5(16) Maeda, Y.; Sakamoto, J.; Wang, S.-y.; Mizuno, Y. *J. Phys. Chem. B.* **2009**, *113*, 12456.

5(17) Amiya, T.; Hirokawa, Y.; Hirose,Y.; Li, Y.; Tanaka, T. *J. Chem. Phys.* **1987**, *86*, 2375.

5(18) Walter, J.; Sehet, J.; Vrabec, J.; Hasse, H. *J. Phys. Chem. B.* **2012**, *116*, 5251.

5(19) Crowther, H.M.; Vincent, B. *Colloid and Polymer Science* **1998**, *276*, 46.

5(20) Pagonis, K.; Bokias, G. *Polymer*, **2004**, *45*, 2149.

5(21) Orakdogen, N.; Okay, O. *Polymer,* **2006**, *47*, 561.

5(22) Zhu, P.W.; Napper, D. *Chem. Phys. Lett.***1996**, *256*, 51.

5(23) Zhu, P.W.; Napper, D. *Macromol.Chem. and Phys.***1999**, 200, 1950.

5(24) Dalkas, G.; Pagonis, K.; Bokias, G. *Polymer*, **2006**, *47*, 243.

5(25) Edmondson, S. ; Nguyen, N.T. ; Iewis, A.L. ; Armes, S.P. *Langmuir,* **2010**, *26*, 7216.

5(26) Zhang, G.; Wu, C. *J. Am. Chem. Soc.* **2001**, *123*, 1376

5(27) Tao, C.T.; Young, T.H. *Polymer*, **2005**, *46*, 10077.

5(28) Baltes, T.; Garret-Flaudy, F.; Freitag, R. *J. Polym. Sci.: Part A: Polym. Chem.* **2000**, *37*, 2977.

5(29) Pelton, R. *Adv. Colloid Interf. Sci.* **2000**, *85*, 1.

5(30) Schild, H.G.; Muthukumar, M.; Tirrel, D.A., *Macromolecules*, **1991**, *24*, 948.

5(31) Tanaka, F.; Koga, T.; Winnik, F.M. *Physical Review Letters,* **2008**, *101*, 028302.

5(32) Kojima, H.; Tanaka, F.; Scherzinger, C.; Richtering, W. *Journal of Polymer Science: Polymer Physics*, **2013**, *51*(14), 1100-1111.

5(33) Kojima, H.; Tanaka, F. *Macromolecules*, **2010**, *43*, 5103.

5(34) Tanaka, F.; Koga, T.; Kojima, H.; Xue, N.; Winnik, F.M. *Macromolecules,* **2011**, *44*, 2978.

5(35) Walter, J.; Sehet, J.; Vrabec, J.; Hasse, H. *J. Phys. Chem. B*, **2012**, *116*, 5251.

6 General conclusions

The studies presented in this thesis contain novelty elements related to the synthesis of new microgel systems, new experiments designed to characterise the samples and new theoretical description of the phase transition theory.

- ✓ Combinations of *N*-vinylcaprolactam and *N*-isoproplyacrylamides monomers were used for the first time to form different morphologies of microgels, such as random copolymer and core-shell structures. The differences in monomer-monomer and monomer-solvent interactions that provide the temperature and solvent composition sensitivity of the polymers give the microgel systems formed versatility in possible applications.
- ✓ The Flory-Rehner swelling theory was for the first time extended to include crosslink heterogeneous morphology of the microgel particle. The NMR transverse relaxation results that provide information on the crosslink density heterogeneity were for the first time used as a fitting condition for the Flory temperature transition state equation of microgels. The crosslink heterogeneity introduced into the Flory swelling theory was used to describe homopolymer and copolymer microgel systems. The core-shell morphology of microgels was also described using a generalised Flory swelling theory for the first time. This approach provides access to parameters describing the internal structure of the microgel particle and the correlations in the temperature transition of the core and shell structural components.
- ✓ Copolymer microgels were for the first time analysed by high resolution selective NMR relaxometry in oder to determine the morphology of the particles. The results showed a random distribution of the monomers in the microgel particles.
- ✓ The monomer-monomer and monomer-solvent interactions were studied for the first time using homopolymer and copolymer microgels in water/alcohol mixtures. Differences in

the behaviour of the different homopolymer microgels and in the copolymer microgels with different monomer molar ratios in different alcohol mixtures show the complexity of the interplay of interactions.

- ✓ A closer look at the explanation behind the observation of the microgel volume phase temperature transition in ^{1}H NMR spectra was attempted. Possible theoretical principles behind the disappearance of the spectrum lines were described and debated for the first time.

List of published papers

a. Claudiu Melian, Dan E. Demco, Monica Istrate, **Andreea Balaceanu**, Dumitrita Moldovan, Radu Fechete, Crisan Popescu, Martin Möller, 'Morphology and side-chain dynamics in hydrated hard α-keratin fibres by ^{1}H solid-state NMR', *Chem. Phys. Lett.* **2009**, *480,* 300–304.
b. Susann Schachschal, **Andreea Balaceanu**, Claudiu Melian, Dan E. Demco, Thomas Eckert, Walter Richtering, Andrij Pich, 'Polyampholyte Microgels with Anionic Core and Cationic Shell', *Macromolecules,* **2010**, *43*, 4331–4339.
c. **Andreea Balaceanu**, Dan E. Demco, Martin Möller, Andrij Pich, 'Microgel Heterogeneous Morphology Reflected in Temperature-Induced Volume Transition and ^{1}H High-Resolution Transverse Relaxation NMR. The Case of Poly(N-vinylcaprolactam) Microgel', *Macromolecules*, **2011**, *44*, 2161–2169.
d. Stephanie Hiltl, Marco-Philipp Schürings, **Andreea Balaceanu**, Veronica Mayorga, Clemens Liedel, Andrij Pich, Alexander Böker, 'Guided self-assembly of microgels: from particle arrays to anisotropic nanostructures', *Soft Matter*, **2011**, *7*, 8231.
e. **Andreea Balaceanu**, Dan E. Demco, Martin Möller, Andrij Pich, 'Heterogeneous morphology of random copolymer microgels as reflected in temperature-induced volume transition and ^{1}H high-resolution transverse relaxation NMR', *Macromol. Chem. Phys.* **2011**, *212*, 2467-2477.
f. **Andreea Balaceanu**, Veronica Mayorga, Wanjuan Lin, Marco-Philipp Schürings, Dan E. Demco, Alexander Böker, Mitchell A. Winnik, Andrij Pich, 'Copolymer microgels by precipitation polymerisation of N-vinylcaprolactam and N-isopropylacrylamides in aqueous medium', *Colloid Polym Sci*, **2013**, *291*, 21-31.
g. **Andreea Balaceanu**, Dan E. Demco, Martin Möller, Andrij Pich, 'Correlated morphological changes in the volume temperature transition of core-shell microgels', *Macromolecules,* **2013**, *46* (12), 4882.